Room 14-0551
77 Massachusetts Avenue
Cambridge, MA 02139
Ph: 617.253.5668 Fax: 617.253.1690
Email: docs@mit.edu
http://libraries.mit.edu/docs

LAMINAR CONDENSATION INSIDE HORIZONTAL

AND INCLINED TUBES

by

John C. Chato

M.E., University of Cincinnati
(1954)

M.S., University of Illinois
(1955)

SUBMITTED IN PARTIAL FULFILLMENT OF THE

REQUIREMENTS FOR THE DEGREE OF

DOCTOR OF PHILOSOPHY

at the

MASSACHUSETTS INSTITUTE OF TECHNOLOGY

June 1960

Signature of Author. . . . .
Department of Mechanical Engineering, May 14, 1960

Certified by . . . .
Thesis Supervisor

Accepted by. . . . .
Chairman, Departmental Committee on Graduate Students

TO THE MEMORY OF MY FATHER

AND

THE LOVE OF MY ENTIRE FAMILY

BIOGRAPHICAL SKETCH

The author was born in Budapest, Hungary on December 28, 1929. After finishing high school, he attended the Hungarian Institute of Technology for a short while before emigrating to the United States in 1948. He went to his parents and brother in Dayton, Ohio, where he attended the University of Dayton. In 1949 he entered the University of Cincinnati in Ohio, where he graduated in 1954 as the outstanding engineering senior, receiving the degree of Mechanical Engineer. In August of 1954 he married Elizabeth Owens, also a graduate of the University of Cincinnati and a Canadian by birth. They then moved to the University of Illinois where the author held a Visking Corporation Fellowship. In 1955 he received the Master of Science degree there. The same year they came to M.I.T. to accept a Whitney Fellowship. The author started his teaching career as an assistant in 1956. He was promoted to Instructor in 1957 and to Assistant Professor in 1958. During the summers he worked in industry as engineer and consultant. At present their family consists of a daughter, Christine, and a son, David.

LAMINAR CONDENSATION INSIDE HORIZONTAL AND INCLINED TUBES

by

John C. Chato

Submitted to the Department of Mechanical Engineering on May 14, 1960 in partial fulfillment of the requirements for the degree of Doctor of Philosophy.

ABSTRACT

The fluid mechanics and heat transfer phenomena occurring during condensation inside single-pass, horizontal and slightly inclined condenser tubes were investigated analytically and experimentally.

Two independent analyses were developed for the condensate forming on the wall. One was the development of the boundary layer equations for a class of curved surfaces for which similarity solutions exist. These equations could be solved for a circular tube only approximately. The second method was the derivation of approximate solutions from the momentum-energy relations. Both methods yielded similar results indicating that for ordinary refrigerants under normal operating conditions the complete solution does not differ significantly from the simplest approximation which is identical to the one developed by Nusselt. For liquid metals, however, both of these methods indicate a significant reduction of heat transfer rates as compared to the simplified solution. There is a discrepancy between the results of the two methods as to the actual magnitudes; however, the boundary conditions for the second method are more reasonable, and consequently, its results can be considered more reliable.

The momentum equation was developed for the bottom condensate flow and certain depth criteria were established. It was shown that a relatively slight downward inclination will significantly increase the heat transfer rates. Beyond a certain slope, however, heat transfer will be reduced again due to the changing flow pattern of the wall condensate. A simple optimization procedure was developed for determining the slope for the highest heat transfer rate.

A fluid mechanics analogy setup was used with water for the horizontal position, and a condensation apparatus was built for the investigation of both fluid mechanics and heat transfer in horizontal and inclined tubes, using Refrigerant-113. These results check the analyses well within the experimental errors.

Thesis Supervisor: Warren M. Rohsenow

Title: Professor of Mechanical Engineering

ACKNOWLEDGEMENTS

The author wishes to thank the following people for their help, advice, discussion, or encouragement during this work:

The members of the thesis committee, Professors A. L. Hesselschwerdt, Jr., W. M. Rohsenow, and A. H. Shapiro.

Professor P. Griffith, Messrs. M. M. Chen, and E. M. Dimond.

Miss Alice Seelinger for an excellent typing job.

Last, but not least, my entire family and especially my wife, Beth, whose moral support was indispensable.

The project was sponsored in part by the A.S.R.E., now called A.S.H.R.A.E., and by the Whirlpool Corporation.

The experimental work was done at the MIT Refrigeration and Air Conditioning Laboratories, which are under the direction of Professor A. L. Hesselschwerdt, Jr.

Part of the work was performed at the MIT Computation Center.

TABLE OF CONTENTS

Page

Page

CHAPTER I

INTRODUCTION

Definition of the Problem

The basic mechanism of condensation inside a horizontal tube is the same as that occurring on the outside of a tube; but the geometrical restrictions imposed upon the former make the problem considerably more complex. The easiest way to analyze the process is to follow the "life history" of the medium as it passes through the tube. Thus, the following phenomena can be found as distinct but interrelated phases of the overall picture:

1. The flow of vapor in the tube
2. The mass and heat transfer at the vapor-condensate interface
3. The flow of condensate on the side walls of the tube
4. The heat transfer through this condensate layer
5. The axial flow of the liquid on the bottom of the tube discharging at the outlet
6. The heat transfer through this layer
7. The interactions between these various phenomena.

Each of the above items can be studied separately at first, but it is obvious that the problem has to be solved ultimately by interrelating all of them.

A qualitative examination of the above phenomena immediately reveals that the most profound difference between condensation on the outside and on the inside of a tube results from the simple geometrical restriction forced upon the latter case. This is that all the vapor to be condensed has to enter at the inlet, while all the liquid condensed in the tube and any vapor to be condensed subsequently has to leave through the outlet. In other words, the total mass flow has to pass through the relatively confined volume created by the tube itself. This condition creates relatively strong interactions between the various phenomena described above which usually do not exist when the vapor condenses on the outside of a tube.

Although in most cases it is more advantageous to condense on the outside of the tube, there are certain applications where condensation on the inside is inherently required. Two outstanding examples of this latter condition are the air cooled condensers, used primarily in air conditioning and refrigeration, and the radiation cooled condensers, employed primarily in vehicles for outer space. These two applications, however, have a very basic difference between them, namely the influence of gravity. For an orbiting space vehicle the terms horizontal and vertical have no real significance and gravity, unless it is artificially created, plays no part at all. In the case of the "earth-bound" condensers, gravity exerts an all important influence on the phenomena occurring. In the following chapters this latter problem will be investigated almost exclusively, first because of its commercial importance and second because of its greater complexity.

The method of investigation will follow essentially the outline given previously; that is, the "life history" of the medium will be traced along the tube. For the purpose of analysis it will be assumed that film-wise condensation occurs, which is the usual case.

In order to define the problem more precisely, the flow will be investigated primarily for the case of a single pass condenser tube. Thus the end conditions will be that only vapor enters and only condensate leaves the tube. As it will be seen later such a narrowing of the scope is necessary in order to eliminate some variables from a very complex process.

Superheated vapor introduces some problems of physical chemistry not yet fully understood. Consequently this investigation will be restricted to the case of the pure saturated vapor.

Historical Background

The classical work of Nusselt (37)* forms the basis of most subsequent analyses of film condensation. A number of investigators elaborated on this theory and used it for comparison to experimental results. An excellent and exhaustive review of references is given by McAdams (34) who also summarizes the experimental results. The measured values of the heat transfer coefficients run from about 36% below to 70% above the predicted values for condensation of pure saturated vapors on the outside of single horizontal tubes.

Until recently the analytical investigations were based essentially on an improvement of the original Nusselt theory. Peck and Reddie (38) included an acceleration term, but their formulation of the equation was incorrect. Bromley, et al (8) investigated the effect of temperature variation around the tube, then Bromley (7) and later Rohsenow (40) examined the problem of subcooling of the condensate and suggested correction factors. These results indicated that for the usual operating conditions all these effects are negligible for pure saturated vapors. Recently Sparrow and Gregg (46,47) presented solutions of boundary-layer type equations developed for the condensate layer. Their results indicate that although for the usual fluids, with relatively high Prandtl Numbers, there is no significant change from the Nusselt solution; the heat transfer rates are significantly lowered for liquid metals with very low Prandtl numbers.

Analysis of the condensation inside horizontal tubes was made by Chaddock (10) who used the Nusselt analysis together with an empirical relation for the depth of the bottom condensate.

---

* Numbers in parentheses refer to numbers in the Bibliography.

Experimental investigations of condensation inside horizontal, or nearly horizontal, tubes were relatively few until recently. Jakob, et al (26) and Jakob (24, 25) condensed steam and found good agreement with the Nusselt theory even though the effect of the axially flowing bottom condensate was ignored. Trapp (50, 51) found heat transfer coefficients for ammonia and alcohol vapors which were generally lower than the theory predicted. Chaddock's (10) and Dixon's (15) experiments indicated that the variation of the depth of the bottom condensate is small in tubes up to a length-diameter ratio of about 30.

A number of experiments were done with relatively high vapor velocities existing in the tubes. Under such circumstances the vapor shear has greater importance and the results show marked deviation from the Nusselt theory. Tepe and Mueller (49) condensing benzene and methanol inside a tube inclined at 15° from horizontal found coefficients 1.5 times higher than the Nusselt results. Akers, et al (2, 3) correlated a great number of local heat transfer data as a function of a density-corrected local Reynolds Number, and his points fall for the most part above the Nusselt values, particularly at high flow rates. Hakimi's (18) results with Refrigerant 12 agreed well with Akers' correlation and were about 30% above theoretical values. None of these results, however, cover the situation that was to be investigated in this work; namely, where the condensate layer on the bottom is deep enough to seriously influence the heat transfer rates, and the vapor shear is relatively low for most part of a relatively long condenser tube.

Misra and Bonilla (36) did condensation experiments with liquid metals. Their results were markedly below the theoretical values predicted by any of the analyses and the scatter was very large. This was due primarily to the lack of control of the vapor shear conditions at the interface. Consequently this data is good only for qualitative comparison.

Recent investigations have thrown some light on the phenomenon observed quite a long time ago, among others by Jakob (24), that when superheated vapor is condensed the liquid interface temperature is lower than that corresponding to thermodynamic equilibrium. Schrage (45) did basic analyses on this problem, and Balekjian and Katz (5) used some of his results to correlate their data. This field is still quite unexplored and more investigations will be needed. Until then, heat transfer correlations with superheated vapor have to be treated very carefully.

The problem of condensation on an inclined tube was investigated by Hassan and Jakob (19), who found analytically that for a long tube the heat transfer rate varies as the one-fourth power of the cosine of the inclination.

CHAPTER II

THE VAPOR PHASE

In the usual case where the specific volume of the vapor is considerably greater than that of the liquid, the medium enters at a relatively high velocity. As more and more is condensed along the tube, the vapor slows down. In the case of single-pass condenser tubes the vapor velocity becomes essentially zero at the outlet end. It is clear that both entrance and exit conditions have to be considered for the complete definition of the problem. The most profound aspects of such a process as condensation inside a tube are that there is no fully developed flow, it is constantly changing spatially; and that the flow cannot get far enough from end effects to escape their influence. As a matter of fact end effects exert all important control on the entire process.

Since in a horizontal tube condensate collects at the bottom, the cross-section of the vapor flow is asymmetric. There is not much information available on such flows. Analyses are practically non-existent and experimental data are rather scarce. The most complete and detailed work is that of Gazley (16) whose experiments were done on two-phase mixtures without change of phase. For lack of better information it may be assumed that the friction factors found in this reference can be applied to the constantly varying vapor flow in a condenser tube. In the horizontal tube the flow pattern is further complicated by the fact that, with the exception of the very lowest of flow rates, there are always surface waves generated on the bottom condensate. In the confined space available these waves have very pronounced effect on the vapor flow. In particular, they increase the energy loss from the flow and, correspondingly, cause a greater pressure drop. The asymmetric configuration and the surface waves generated on the bottom condensate indicate that the equivalent friction losses are not uniformly distributed around the circumference of the flow. Compared to the wavy surface of the bottom condensate, the liquid on the walls is smooth if the condensation is film-wise, as is the usual case. Consequently, the friction losses at the wall are probably lower than at the bottom of the tube. If the tube is inclined, most of these surface waves disappear and the friction losses become more uniform around the periphery. For the purpose of calculations the concept of friction factor will be used with the numerical values taken primarily from Gazley's (16) data.

As was mentioned earlier, there is a rather important difference between the condensation of a saturated vapor and that of a superheated vapor. In the former case the surface of the condensate in contact with the vapor may be considered to be very nearly in thermodynamic equilibrium with the vapor; that is, the temperature of this surface may be taken as the saturation temperature, the same as that of the vapor. Thus, essentially no heat transfer occurs in the vapor. However, there is a slow outward movement towards the condensing surfaces. Under such circumstances it is reasonable to consider the vapor as uniform in temperature and in pressure at any cross-section; and, if the pressure drop is small along the tube, temperatures may be taken as uniform everywhere in the vapor phase.

If the vapor entering the tube is superheated, then the entire condensation process becomes much more complicated. Some of the most important effects arising from this condition have been observed and discussed by several investigators (5, 24, 45). The first and most obvious difference is that the vapor has to be cooled before it can condense. Consequently, a temperature gradient exists in the core of the tube which depends not only on the amount of superheat, but also on the magnitude of the subcooling of the condensate. The peculiarities of this dependence have been observed and discussed by Jakob (5), who found that, as the subcooling increased, the temperature of the core of the vapor became higher at the outlet end instead of lower. He explained this observation by pointing out that at higher subcooling, the vapor-liquid interface is at a lower temperature; and, consequently, any vapor molecule hitting the surface will have a much greater tendency to condense instead of returning to the core. At lower subcooling greater number of molecules can approach the interface, then return to the vapor core at a lower temperature level and cause an overall reduction of the vapor temperature. Another important effect of superheat occurs at and near the interface. Thermodynamic equilibrium does not exist anymore, and the condensate surface temperature is different from that of saturation. As it was mentioned above, the condensate is subcooled, and the surface temperature is also lowered. To the author's knowledge the correlation of Balekjian and Katz (5), based on some of Schrage's work (45), is the best available on this phenomenon.

Data in this investigation were all taken with saturated vapor, therefore, the effect of superheat did not appear.

CHAPTER III

CONDENSATION ON THE TUBE WALLS

The Momentum-Energy Equation

A solution to the problem of condensation on an inclined surface may be obtained by writing the momentum and energy equations for the condensate flow. By using the concept of similarity, these equations may be reduced to a single ordinary differential equation with only one dependent and one independent variable*.

Consider the flow of condensate along the surface in the positive x direction as shown in Figure 3.1. At some position x_o the condensate film thickness is y_s. The momentum equation in the x direction can be written as follows.

$$\frac{d}{dx}\int_0^{y_s}\rho_l u^2 dy + \frac{d}{dx}\int_{y_s}^{y_\infty}\rho_v u^2 dy + \mu_l \frac{\partial u}{\partial y}\bigg|_w = y_s g(\rho_l - \rho_v)\sin\phi \qquad (3.1)$$

where x distance along plate, ft.

y distance perpendicular to plate into the fluid, ft.

ρ_l liquid mass density, slugs/ft^3

ρ_v vapor mass density, slugs/ft^3

u velocity in x direction, ft/sec

μ_l liquid viscosity, lbf-sec/ft^2

g gravitational acceleration, ft/sec^2

ϕ surface inclination to horizontal

---

* This approach is due to Mr. Michael M. Chen.

The energy equation becomes,

$$-k_\ell \frac{\partial t}{\partial y}\bigg|_w = -\frac{d}{dx}\int_0^{y_s} \lambda \rho_\ell u \, dy - \frac{d}{dx}\int_0^{y_s} c_{p\ell} (t_s - t) \, \rho_\ell u \, dy \tag{3.2}$$

where k_ℓ thermal conductivity of liquid, Btu/sec-ft-°F

t temperature, °F

t_s temperature at the liquid-vapor interface, y_s, °F

λ latent heat of vaporization, Btu/slug

$c_{p\ell}$ specific heat of liquid, Btu/slug-°F

To non-dimensionalize the above equations, define the following quantities as special properties of the velocity and temperature profiles.

$$u_a \equiv \frac{1}{y_s}\int_0^{y_s} u \, dy$$

$$\Delta t \equiv t_s - t_w$$

where t_w is wall temperature

$$y^+ \equiv \frac{y}{y_s}$$

$$u^+ \equiv \frac{u}{u_a}$$

$$t^+ \equiv \frac{t - t_w}{\Delta t}$$

$$A \equiv \frac{\partial u^+}{\partial y^+}\bigg|_w$$

$$B \equiv \int_0^1 u^{+2} \, dy^+$$

$$C \equiv \int_0^1 u^+(1-t^+)\,dy^+ = 1 - \int_0^1 u^+ t^+\,dy^+$$

$$D \equiv \left.\frac{\partial t^+}{\partial y^+}\right|_w$$

Substituting these relations into the momentum equation (3.1) and ignoring the contribution of the vapor phase, since $\rho_v << \rho_l$ for ordinary applications, yields*,

$$\frac{d}{dx}\rho_\ell u_a^2 y_s B + \mu_\ell \frac{u_a}{y_s} A = y_s g(\rho_\ell - \rho_v)\sin\phi \tag{3.3}$$

Similarly the energy equation (3.2) becomes,

$$k_\ell \frac{\Delta t}{y_s} D = \frac{d}{dx}\lambda \rho_\ell u_a y_s + \frac{d}{dx} c_{p\ell}\Delta t \rho_\ell u_a y_s C \tag{3.4}$$

Define, $f \equiv u_a y_s$, the volumetric liquid flow rate per unit length of tube, and $\zeta \equiv \dfrac{c_{p\ell}\Delta t}{\lambda}$.

Thus equation (3.4) becomes,

$$\begin{aligned} k_\ell \frac{\Delta t}{y_s} D &= \frac{d}{dx}\lambda \rho_\ell f + \frac{d}{dx}\lambda \zeta \rho_\ell f C \\ &= \frac{d}{dx}\lambda \rho_\ell f(1 + C\zeta) \end{aligned} \tag{3.5}$$

---

* It is shown in the appendix that this can be done provided

$$\frac{\rho_v \mu_v}{\rho_\ell \mu_\ell} << 1$$

If there is a similarity solution to these equations, then the functions of the velocity and temperature profiles, A, B, C, D, are independent of x. If, in addition, the temperature remains constant along the wall, the equations may be reduced to a single ordinary differential equation in the following manner.

From equation (3.5),

$$\frac{1}{y_s} = \frac{\rho_l \lambda (1 + C\zeta)}{k_l \Delta t\, D} \cdot \frac{df}{dx}$$

$$y_s = \frac{k_l \Delta t\, D}{\rho_l \lambda \, (1 + C\zeta) \frac{df}{dx}} \tag{3.6}$$

$$\frac{dy_s}{dx} = - \frac{k_l \Delta t\, D}{\rho_l \lambda \, (1 + C\zeta)} \cdot \frac{\frac{d^2 f}{dx^2}}{\left(\frac{df}{dx}\right)^2} \tag{3.7}$$

Multiplying equation (3.3) by $y_s / \mu_l u_a A$ and using equations (3.6) and (3.7) together with the definition of f yields,

$$\frac{B \rho_l y_s}{A \mu_l u_a} \left[2 u_a y_s \frac{du_a}{dx} + u_a^2 \frac{dy_s}{dx} \right] + 1 = \frac{g (\rho_l - \rho_v) \, y_s^2 \sin \phi}{A \mu_l u_a}$$

$$\frac{B \rho_l}{A \mu_l} \left[2 y_s \frac{df}{dx} - f \frac{dy_s}{dx} \right] + 1 = \frac{g (\rho_l - \rho_v) \, y_s^3 \sin \phi}{A \mu_l u_a y_s}$$

$$\frac{B D k_\ell \Delta t}{A \mu_\ell \lambda (1 + C\zeta)} \left[2 + \frac{f \frac{d^2 f}{dx^2}}{\left(\frac{df}{dx}\right)^2} \right] + 1 =$$

$$\left[\frac{k_\ell \Delta t\, D}{\rho_\ell \lambda (1 + C\zeta)} \right]^3 \cdot \frac{g(\rho_\ell - \rho_v) \sin\phi}{A \mu_\ell f \left(\frac{df}{dx}\right)^3} \tag{3.8}$$

Define a dimensionless flow rate and distance as follows,

$$F \equiv f \left[\frac{D^3 g (\rho_\ell - \rho_v) k_\ell^3 \Delta t^3 \ell^3}{A \mu_\ell \rho_\ell^3 \lambda^3 (1 + C\zeta)^3} \right]^{-\frac{1}{4}} \tag{3.9}$$

where ℓ is a characteristic length.

$$X \equiv \frac{x}{\ell}, \qquad F' \equiv \frac{dF}{dX}$$

Thus equation (3.8) becomes,

$$1 - \frac{\sin\phi}{F (F')^3} = - \frac{B D k_\ell \Delta t}{A \mu_\ell \lambda (1 + C\zeta)} \left[2 + \frac{F F''}{(F')^2} \right] \quad \text{or} \tag{3.10}$$

$$1 - \frac{\sin\phi}{F (F')^3} = - \epsilon \left[2 + \frac{F F''}{(F')^2} \right] \tag{3.10a}$$

The right hand side of the equation represents the effect of momentum. The results of Nusselt's analysis indicate that this effect is small.

Thus the right hand side of the equation may be considered as a small perturbation term, and the complete equation may be solved by successive approximations.

The heat transfer coefficient may be computed by considering the heat transferred at the wall.

$$h_m \Delta t = k_\ell \left.\frac{\partial t}{\partial y}\right|_w = D k_\ell \frac{\Delta t}{y_s}$$

where h_m - heat transfer coefficient

$$h_m = \frac{D k_\ell}{y_s}$$

$$= \frac{\rho_\ell \lambda (1 + C\zeta)}{\Delta t} \cdot \frac{df}{dx}$$

$$= \left[\frac{D^3 g \rho_\ell (\rho_\ell - \rho_v) k_\ell^3 \lambda (1 + C\zeta)}{A \mu_\ell \ell \Delta t}\right]^{\frac{1}{4}} F' \qquad (3.11)$$

The local Nusselt number is

$$Nu = \frac{h_m \ell}{k_\ell} = \left[\frac{D^3 g \rho_\ell (\rho_\ell - \rho_v) \lambda (1 + C\zeta) \ell^3}{A \mu_\ell k_\ell \Delta t}\right]^{\frac{1}{4}} F'$$

$$= \left[\frac{D^3 (1 + C\zeta)}{A}\right]^{\frac{1}{4}} \left[\frac{g \rho_\ell (\rho_\ell - \rho_v) \ell^3 \lambda}{\mu_\ell k_\ell \Delta t}\right]^{\frac{1}{4}} F' \qquad (3.12)$$

The mean Nusselt number becomes,

$$\overline{Nu} = \left[\frac{D^3 (1 + C\zeta)}{A}\right]^{\frac{1}{4}} \left[\frac{g \rho_\ell (\rho_\ell - \rho_v) \ell^3 \lambda}{\mu_\ell k_\ell \Delta t}\right]^{\frac{1}{4}} \cdot \frac{F}{X} \qquad (3.13)$$

Application of the Momentum-Energy Equation to a Round Horizontal Tube

First Approximation

For condensation on a horizontal tube define $l \equiv r_o$, the radius of the condensing surface, in the equations. If the condensate film thickness is very much smaller than r, the previously derived equations may be applied. From equation (3.10a)

$$F(F')^3 - \sin\phi = -\epsilon\left[2F(F')^3 + F^2F'F''\right] \qquad (3.14)$$

The boundary condition is, F = 0 at $\phi = 0$ at the top of the tube. Express F in polynomial form.

$$F = F_o + F_1\epsilon + F_2\epsilon^2 + \ldots \qquad (3.15)$$

where ϵ was defined in equation (3.10a).

F_o may be found by letting ϵ approach zero.

$$F_o(F_o')^3 - \sin\phi = 0 \qquad (3.16)$$

Therefore,

$$F_o = \left(\frac{4}{3}\right)^{\frac{3}{4}}\left[\int_0^{\phi}\sin^{1/3}\phi\, d\phi\right]^{\frac{3}{4}} \qquad (3.17)$$

The function $\left[\int_0^{\phi}\sin^{1/3}\phi\, d\phi\right]^{\frac{3}{4}}$ is tabulated in Appendix VI.

Substituting into equation (3.13) yields the first approximation of the Nusselt number for a round tube as a function of the distance or angle from the topmost point.

$$\overline{Nu}_o = \left(\frac{4}{3}\right)^{\frac{3}{4}} \left[\frac{D^3(1+C\xi)}{A}\right]^{\frac{1}{4}} \left[\frac{g\rho_\ell(\rho_\ell-\rho_v)\lambda r_o^3}{\mu_\ell k_\ell \Delta t}\right]^{\frac{1}{4}} \times$$

$$\times \frac{\left[\int_0^\phi \sin^{1/3}\phi \, d\phi\right]^{\frac{3}{4}}}{\phi} \qquad (3.18)$$

If the Nusselt number is to be based on the total area of the tube and not only on the part where condensation actually occurs, the above equation has to be multiplied by ϕ/π .

$$\overline{\overline{Nu}}_o = \left(\frac{4}{3}\right)^{\frac{3}{4}} \left[\frac{D^3(1+C\xi)}{A}\right]^{\frac{1}{4}} \left[\frac{g\rho_\ell(\rho_\ell-\rho_v)\lambda r_o^3}{\mu_\ell k_\ell \Delta t}\right]^{\frac{1}{4}} \times$$

$$\times \frac{\left[\int_0^\phi \sin^{1/3}\phi \, d\phi\right]^{\frac{3}{4}}}{\pi} \qquad (3.19)$$

As a first approximation, Nusselt's parabolic velocity and linear temperature distributions may be used. That is,

$$u^+ = 3y^+ - \frac{3}{2}{y^+}^2 \qquad (3.20)$$

$$t^+ = y^+ \qquad (3.21)$$

Then A = 3, B = 6/5, C = 3/8, and D = 1. The mean Nusselt number then becomes,

$$\overline{\overline{Nu}}_o = \frac{(4)^{\frac{3}{4}}}{3\pi}(1+\tfrac{3}{8}\zeta)^{\frac{1}{4}}\left[\frac{g\rho_\ell(\rho_\ell-\rho_v)\lambda r_o^3}{\mu_\ell k_\ell \Delta t}\right]^{\frac{1}{4}} \times$$

$$\times\left[\int_0^\phi \sin^{1/3}\phi \, d\phi\right] \qquad (3.22)$$

Since ζ is usually very small, the equation may be expressed in a more convenient form as follows.

$$\overline{\overline{Nu}}_o = 0.300\left[\frac{g\rho_\ell(\rho_\ell-\rho_v)\lambda(1+\frac{3}{8}\zeta)r_o^3}{\mu_\ell k_\ell \Delta t}\right]^{\frac{1}{4}}\left[\int_0^\phi \sin^{1/3}\phi \, d\phi\right]^{\frac{3}{4}} \qquad (3.23)$$

For small values of ζ, the numerical results of the above equation are identical to those obtained by the Nusselt analysis. The effect of ζ and the Prandtl number may be found by successively evaluating the higher order terms in equation (3.15) and by refining the velocity and temperature profiles.

<u>Second Approximation</u>

To find F_1, substitute the first two terms of equation (3.15) into the left hand side of equation (3.14).

$$(F_o+\epsilon F_1)(F_o'+\epsilon F_1')^3 - \sin\phi = -\epsilon\left[2F_o(F_o')^3 + F_o^2 F_o' F_o''\right] \qquad (3.24)$$

If the terms containing ϵ^2 and ϵ^3 are neglected, the equation reduces to,

$$3F_0(F_0')^2F_1' + (F_0')^3F_1 = -\left[2F_0(F_0')^3 + F_0^2F_0'F_0''\right] \tag{3.25}$$

Equation (3.25) can be solved explicitly for F_1 as follows,

$$\left[F_0(F_0')^3\right]^{\frac{2}{3}}\left[3F_0^{\frac{1}{3}}F_1' + F_0^{-\frac{2}{3}}F_0'F_1\right] = -\left[2F_0(F_0')^3 + F_0^2F_0'F_0''\right]$$

$$\sin^{2/3}\phi \; \frac{d}{d\phi}\left[3F_0^{\frac{1}{3}}F_1\right] = -\sin\phi\left[2 + \frac{F_0F_0''}{(F_0')^2}\right]$$

$$F_0^{\frac{1}{3}}F_1 = -\frac{2}{3}\int_0^{\phi}\sin^{1/3}\phi \, d\phi - \frac{1}{3}\int_0^{\phi}\frac{F_0F_0''}{(F_0')^2}\sin^{1/3}\phi \, d\phi$$

Substituting the values of F_0, F_0', and F_0'' from equation (3.17) and simplifying yields,

$$F_0^{\frac{1}{3}}F_1 = -\frac{F_0^{\frac{4}{3}}}{2} + \frac{1}{9}\int_0^{\phi}\left[\sin^{1/3}\phi - \frac{4}{3}\cot\phi\int_0^{\phi}\sin^{1/3}\phi \, d\phi\right]d\phi$$

Defining,

$$I_1 = \frac{\frac{4}{3}\int_0^{\phi}\sin^{1/3}\phi \, d\phi}{\sin^{4/3}\phi} \tag{3.26}$$

and substituting gives,

$$F_1 = -\frac{5}{12}F_0 - \frac{F_0^{-\frac{1}{3}}}{9}\int_0^{\phi} I_1 \sin^{1/3}\phi \cos\phi \, d\phi \tag{3.27}$$

Define,

$$I_2 \equiv \int_0^{\phi} I_1 \sin^{1/3}\phi \cos\phi \, d\phi \tag{3.28}$$

Values for this function were obtained graphically.

Equation (3.27) becomes

$$F_1 = -\frac{5}{12}F_0 - \frac{F_0^{-\frac{1}{3}}}{9} I_2 \tag{3.29}$$

With this solution the second approximation of the Nusselt number is

$$\overline{Nu}_1 = \left(\frac{4}{3}\right)^{\frac{3}{4}} \left[\frac{D^3(1 + C\zeta)}{A}\right]^{\frac{1}{4}} \left[\frac{g\rho_l(\rho_l - \rho_v)\lambda r_0^3}{\mu_l k_l \Delta t}\right]^{\frac{1}{4}} \times$$

$$\times \frac{\left[\int_0^{\phi} \sin^{1/3}\phi \, d\phi\right]^{\frac{3}{4}}}{\phi} \left[1 - \epsilon\left(\frac{5}{12} + \frac{I_2}{12\int_0^{\phi} \sin^{1/3}\phi \, d\phi}\right)\right] \tag{3.30}$$

or

$$\overline{\overline{Nu}}_1 = \frac{1}{\pi}\left(\frac{4}{3}\right)^{\frac{3}{4}} \left[\frac{D^3(1 + C\zeta)}{A}\right]^{\frac{1}{4}} \left[\frac{g\rho_l(\rho_l - \rho_v)\lambda r_0^3}{\mu_l k_l \Delta t}\right]^{\frac{1}{4}} \times$$

$$\times \left[\int_0^{\phi} \sin^{1/3}\phi \, d\phi\right]^{\frac{3}{4}} \left[1 - \epsilon\left(\frac{5}{12} + \frac{I_2}{12\int_0^{\phi} \sin^{1/3}\phi \, d\phi}\right)\right] \tag{3.31}$$

To find improved velocity and temperature profiles, the momentum and energy equations may be solved for a fluid element between y and y_s. The momentum equation is,

$$\frac{d}{dx}\int_{y}^{y_s}\rho_\ell u^2 dy + u\frac{d}{dx}\int_{0}^{y}\rho_\ell u\, dy + \mu_\ell \frac{\partial u}{\partial y} - \mu_\ell \frac{\partial u}{\partial y}\bigg|_s -$$

$$-u_s \frac{d}{dx}\int_{0}^{y_s}\rho_\ell u\, dy = (y_s - y)\, g(\rho_\ell - \rho_v)\sin\phi \qquad (3.32)$$

By an order of magnitude estimate of the vapor momentum equation, which is developed in Appendix I, it can be concluded that

$$\mu_\ell \frac{\partial u}{\partial y}\bigg|_s + u_s \frac{d}{dx}\int_{0}^{y_s}\rho_\ell u\, dy \approx \frac{\mu_v \rho_v}{\mu_\ell \rho_\ell} << 1$$

Consequently, these two terms effectively cancel each other, although individually they are not negligible. Using this relation the momentum equation becomes in non dimensional form,

$$\frac{d}{dx}\rho_\ell u_a^2 y_s \int_{y^+}^{1} u^{+2} dy^+ + u_a u^+ \frac{d}{dx}\rho_\ell u_a y_s \int_{0}^{y^+} u^+ dy^+ +$$

$$+\mu_\ell \frac{u_a}{y_s}\frac{\partial u^+}{\partial y^+} = y_s(1-y^+)\, g(\rho_\ell - \rho_v)\sin\phi$$

Multiplying by $y_s/\mu_\ell u_a$, and assuming again that the velocity and temperature profiles are independent of x leads to the following derivation (similarly to equation 3.8),

$$\frac{Dk_\ell \Delta t}{\mu_\ell \lambda (1 + C\zeta)} \left\{ \left[2 + \frac{ff''}{(f')^2} \right] \int_{y^+}^{1} u^{+2} dy^+ + \right.$$

$$\left. + u^+ \int_0^{y^+} u^+ dy^+ \right\} + \frac{du^+}{dy^+} =$$

$$= \frac{g(\rho_\ell - \rho_v)}{\mu_\ell} \left[\frac{Dk_\ell \Delta t}{\mu_\ell \lambda (1 + C\zeta)} \right]^3 \cdot \frac{\sin\phi}{f(f')^3} (1 - y^+)$$

or

$$\frac{du^+}{dy^+} = A \frac{\sin\phi}{F(F')^3} (1 - y^+) - \frac{Dk_\ell \Delta t}{\mu_\ell \lambda (1 + C\zeta)} \left\{ \left[2 + \right. \right.$$

$$\left. \left. + \frac{FF''}{(F')^2} \right] \int_{y^+}^{1} u^{+2} dy^+ + u^+ \int_0^{y^+} u^+ dy^+ \right\}$$

$$= A(1 - y^+) - \frac{A}{B} \epsilon \left\{ \left[2 + \frac{FF''}{(F')^2} \right] \left[-B(1 - y^+) + \right. \right.$$

$$\left. \left. + \int_{y^+}^{1} u^{+2} dy^+ \right] + u^+ \int_0^{y^+} u^+ dy^+ \right\}$$

Substituting the definition of B on the right hand side yields

$$\frac{du^+}{dy^+} = A(1-y^+) - \frac{A}{B}\epsilon\left\{\left[2 + \frac{FF''}{(F')^2}\right]\left[By^+ + \int_0^{y^+} u^{+2}\,dy^+\right] + u^+\int_0^{y^+} u^+\,dy^+\right\} \tag{3.33}$$

As before, if ϵ is small, the equation may be solved by successive evaluation of the terms in the series expansion for u* and A.

$$u^+ = u_o^+ + \epsilon u_1^+ + \ldots$$

$$A = A_o + \epsilon A_1 + \ldots$$

Let

$$\frac{\partial u_o^+}{\partial y^+} = A_o(1-y^+)$$

with the boundary condition

$$\int_0^1 u^+ dy^+ = 1$$

therefore,

$$u_o = 3\left(y^+ - \frac{1}{2}y^{+2}\right) \tag{3.6}$$

with $A_o = 3$, $B_o = 6/5$, $D_o = 1$

$$\int_0^{y^+} u_o^{+2}\,dy^+ = 3y^{+3} - \frac{9}{4}y^{+4} + \frac{9}{20}y^{+5} \tag{3.34}$$

$$u_o^+\int_0^{y^+} u_o^+\,dy^+ = \frac{9}{2}y^{+3} - \frac{15}{4}y^{+4} + \frac{3}{4}y^{+5} \tag{3.35}$$

Substituting into (3.33) gives the second approximation of the velocity profile.

$$\frac{du_1^+}{dy^+} = A_1(1-y^+) - \frac{5}{2}\left\{\left[2 + \frac{2I_1\cos\phi}{5}\right]y^+ + \right.$$

$$+\left[\frac{19}{2} + I_1\cos\phi\right]y^{+3} - \left[\frac{15}{2} + \frac{3I_1\cos\phi}{4}\right]y^{+4} +$$

$$\left. + \left[\frac{3}{2} + \frac{3I_1\cos\phi}{20}\right]y^{+5}\right\}$$

Integrating,

$$u_1^+ = A_1\left(y^+ - \frac{1}{2}y^{+2}\right) - \frac{5}{2}\left\{\left[1 + \frac{I_1\cos\phi}{5}\right]y^{+2} + \right.$$

$$+\left[\frac{19}{8} + \frac{I_1\cos\phi}{4}\right]y^{+4} - \left[\frac{3}{2} + \frac{3I_1\cos\phi}{20}\right]y^{+5} +$$

$$\left. + \left[\frac{1}{4} + \frac{I_1\cos\phi}{40}\right]y^{+6}\right\} \qquad (3.36)$$

Apply the boundary conditions.

$$\int_0^1 u^+ dy^+ = \int_0^1 (u_o^+ + \epsilon u_1^+ + \dots)\, dy^+ = 1$$

$$\int_0^1 u_o^+ dy^+ + \epsilon \int_0^1 u_1^+ dy^+ = 1$$

Since the first term is equal to unity,

$$\int_0^1 u_1^+ dy^+ = 0$$

$$\frac{1}{3} A_1 - \frac{5}{2}\left\{\left[\frac{1}{3} + \frac{I_1 \cos\phi}{15}\right] + \left[\frac{19}{40} + \frac{I_1\cos\phi}{20}\right] - \right.$$

$$\left. - \left[\frac{1}{4} + \frac{I_1\cos\phi}{40}\right] + \left[\frac{1}{28} + \frac{I_1\cos\phi}{280}\right]\right\} = 0$$

$\therefore$

$$A_1 = \frac{499}{112} + \frac{5 I_1 \cos\phi}{7} \tag{3.37}$$

$$u_1^+ = \left[\frac{499}{112} + \frac{5I_1\cos\phi}{7}\right] y^+ - \left[\frac{1059}{224} + \frac{6I_1\cos\phi}{7}\right] y^{+2} -$$

$$- \left[\frac{95}{16} + \frac{5I_1\cos\phi}{8}\right] y^{+4} + \left[\frac{15}{4} + \frac{3I_1\cos\phi}{8}\right] y^{+5} -$$

$$- \left[\frac{5}{8} + \frac{I_1\cos\phi}{16}\right] y^{+6}$$

$$= Y_1 y^+ - Y_2 y^{+2} - Y_4 y^{+4} + Y_5 y^{+5} - Y_6 y^{+6} \tag{3.38}$$

The energy equation becomes,

$$-k_\ell \frac{\partial t}{\partial y} = -\frac{d}{dx}\int_0^{y_s} \lambda \rho_\ell u \, dy - \frac{d}{dx}\int_0^{y_s} c_{p\ell} t_s \rho_\ell u \, dy +$$

$$+ \frac{d}{dx} c_{p\ell} t \int_0^{y} \rho_\ell u \, dy + \frac{d}{dx}\int_y^{y_s} c_{p\ell} t \rho_\ell u \, dy \qquad (3.39)$$

or in non-dimensional form

$$k_\ell \frac{\Delta t}{y_s} \frac{\partial t^+}{\partial y^+} = \frac{d}{dx} \lambda \rho_\ell u_a y_s \int_0^1 u^+ dy^+ + \frac{d}{dx} c_{p\ell} t_s \rho_\ell u_a y_s \int_0^1 u^+ dy^+ -$$

$$- \frac{d}{dx} c_{p\ell} (\Delta t \, t^+ + t_w) \rho_\ell u_a y_s \int_0^{y^+} u^+ dy^+ -$$

$$- \frac{d}{dx} \rho_\ell u_a y_s \int_{y^+}^1 c_{p\ell} (\Delta t \, t^+ + t_w) \, u^+ dy^+$$

$$= \rho_\ell (\lambda + c_{p\ell} \Delta t) f' - \rho_\ell c_{p\ell} \Delta t \, f' t^+ \int_0^{y^+} u^+ dy^+ - \rho_\ell c_{p\ell} \Delta t \, f' \int_{y^+}^1 t^+ u^+ dy^+$$

$\therefore$

$$\frac{\partial t^+}{\partial y^+} = \frac{y_s \rho_\ell (\lambda + c_{p\ell} \Delta t) f'}{k_\ell \Delta t} - \frac{y_s \rho_\ell c_{p\ell} f'}{k_\ell} t^+ \int_0^{y^+} u^+ dy^+ -$$

$$- \frac{y_s \rho_\ell c_{p\ell} f'}{k_\ell} \int_{y^+}^1 t^+ u^+ dy^+ \qquad (3.40)$$

Substituting the value of y_s from equation (3.6),

$$\frac{\partial t^+}{\partial y^+} = D\frac{1+\varsigma}{1+C\varsigma} - \frac{D\varsigma}{1+C\varsigma}\left[t^+\int_0^{y^+} u^+ dy^+ + \int_{y^+}^{1} t^+ u^+ dy^+\right]$$

$$= \frac{D\varsigma}{1+C\varsigma}\left[\frac{1}{\varsigma} + 1 + t^+\int_0^{y^+} u^+ dy^+ + \int_{y^+}^{1} t^+ u^+ dy^+\right] \qquad (3.41)$$

or,

$$\frac{\partial t^+}{\partial y^+} = D\frac{1+\varsigma}{1+C\varsigma} - \varsigma\frac{D}{1+C\varsigma}\left[t^+\int_0^{y^+} u^+ dy^+ + \int_{y^+}^{1} t^+ u^+ dy^+\right] \qquad (3.42)$$

Let

$$t^+ = t_0^+ + \varsigma t_1^+ + \ldots$$
$$C = C_0 + \varsigma C_1 + \ldots$$
$$D = D_0 + \varsigma D_1 + \ldots$$
$$\left.\frac{\partial t_0^+}{\partial y^+}\right|_w = D_0$$

with boundary condition $t_0^+ = 0$ at $y^+ = 0$ and $t_0^+ = 1$ at $y^+ = 1$

$$t_0^+ = y^+, \quad D_0 = 1, \quad C_0 = \frac{3}{8}$$

Substituting into (3.42) results,

$$\frac{\partial t_0^+}{\partial y^+} + \varsigma\frac{\partial t_1^+}{\partial y^+} = \frac{1+\varsigma D_1}{1+\frac{3}{8}\varsigma}\left\{1 + \varsigma\left[1 - y^+\int_0^{y^+} 3(y^+ - \tfrac{1}{2}y^{+2})\,dy^+ - \int_{y^+}^{1} 3(y^{+2} - \tfrac{1}{2}y^{+3})\,dy^+\right]\right\}$$

$$= \frac{1+\varsigma D_1}{1+\frac{3}{8}\varsigma}\left\{1 + \varsigma\left[\frac{3}{8} - \frac{1}{2}y^{+3} + \frac{1}{8}y^{+4}\right]\right\}$$

After integrating and collecting terms

$$t^+ = \frac{1+\xi D_1}{1+\frac{3}{8}\xi}\left[\left(1+\frac{3}{8}\xi\right)y^+ - \xi\left(\frac{1}{8}y^{+4} - \frac{1}{40}y^{+5}\right)\right] \tag{3.43}$$

To satisfy the boundary condition at the interface, $t_s^+ = 1$,

$$1 = \frac{1+\xi D_1}{1+\frac{3}{8}\xi}\left[1+\frac{3}{8}\xi - \xi\left(\frac{1}{8}-\frac{1}{40}\right)\right]$$

$$D_1 = \frac{1}{10\left(1+\frac{3}{8}\xi\right) - \xi} \tag{3.44}$$

$$t^+ = \frac{1}{1-\dfrac{\xi}{10\left(1+\frac{3}{8}\xi\right)}}\left[y^+ - \frac{\xi}{1+\frac{3}{8}\xi}\left(\frac{1}{8}y^{+4} - \frac{1}{40}y^{+5}\right)\right] \tag{3.45}$$

This result is identical to the one obtained by Rohsenow (40).

Next find

$$C = 1 - \int_0^1 u^+ t^+ \, dy^+$$

Substituting from equations (3.6), (3.38), (3.45), and neglecting higher order terms containing $\epsilon \cdot \xi$ gives,

$$C = 1 - \int_0^1 \left[3\left(y^+ - \tfrac{1}{2}y^{+2}\right) + \epsilon\left(Y_1 y^+ - Y_2 y^{+2} - Y_4 y^{+4} + \right.\right.$$

$$\left.\left. + Y_5 y^{+5} - Y_6 y^{+6}\right)\right]\left[\frac{1}{1 - \frac{\zeta}{10\left(1+\frac{3}{8}\zeta\right)}}\right]\left[y^+ - \right.$$

$$\left. - \frac{\zeta}{1+\frac{3}{8}\zeta}\left(\frac{1}{8}y^{+4} - \frac{1}{40}y^{+5}\right)\right]dy^+$$

or

$$C = 1 - \frac{3}{1 - \frac{\zeta}{10\left(1+\frac{3}{8}\zeta\right)}}\left[\frac{5}{24} - \frac{19}{1920}\cdot\frac{\zeta}{1+\frac{3}{8}\zeta} + \right.$$

$$\left. + \epsilon\left(\frac{Y_1}{3} - \frac{Y_2}{4} - \frac{Y_4}{6} + \frac{Y_5}{7} - \frac{Y_6}{8}\right)\right] \qquad (3.46)$$

$$C = 1 - \frac{5}{8\left[1 - \frac{\xi}{10(1+\frac{3}{8}\xi)}\right]} + \frac{3}{1 - \frac{\xi}{10(1+\frac{3}{8}\xi)}}\left[\frac{\xi \times 10^{-2}}{1+\frac{3}{8}\xi} + \right.$$

$$\left. + \epsilon(0.227 + 0.0346\, I_1 \cos\phi)\right] \qquad (3.47)$$

Using the series expansion form of the constants and substituting equations (3.37) and (3.44) gives the additional quantities to be used in equations (3.30) and (3.31).

$$A = 3 + \epsilon\left(4.45 + \frac{5 I_1 \cos\phi}{7}\right) \qquad (3.48)$$

$$D = 1 + \frac{\xi}{10 + \frac{11}{4}\xi} \qquad (3.49)$$

$$\epsilon = \frac{2 k_l \Delta t}{5 \mu_l \lambda (1 + C\xi)} = \frac{2\xi}{5(\bar{Pr})(1 + C\xi)} \qquad (3.50)$$

In the derivation of the basic equation it was assumed that A, B, C, and D are independent of ϕ. From the above equations it is obvious then, that the second approximation is valid only where the terms containing $\epsilon I_1 \cos\phi$ are small compared to the others.

The results indicate that a small Prandtl number decreases the Nusselt number; while a large Prandtl number tends to increase it slightly. The effect of the Prandtl number as given by this analysis is shown in Figure 3.3. Here the ratio of the Nusselt number obtained from these equations to the number calculated from the original Nusselt analysis (which is essentially the first approximation described above) is plotted as a function of the temperature difference and the Prandtl number. The angle term containing I_2 was ignored in these calculations since its value is negligible up to an angle of about 150°. For ordinary fluids ϵ is usually very small and further approximations are unnecessary. The last approximation already shows that similarity does not exist for a circular tube except at $\phi = 0$. The change of the velocity profile is very small up to an angle of about 150°. Based on these observations, Chen (11) concluded that reasonably good approximation may be obtained by assuming that the velocity profile remains similar to the one occurring at $\phi = 0$. This means that $FF''/(F')^2 = 0$, and equation 3.10a becomes,

$$(1+\epsilon)F(F')^3 = \sin\phi \tag{3.51}$$

with $F(0) = 0$, the solution becomes

$$F = \left(\frac{4}{3}\right)^{\frac{3}{4}}(1+\epsilon)^{-\frac{1}{4}}\left[\int_0^{\phi}\sin^{1/3}\phi\, d\phi\right]^{\frac{3}{4}} \tag{3.52}$$

The velocity profiles now are similar and can be solved by either the perturbation method or by successive substitutions in equation 3.33. The results of this solution are also shown in Figure 3.3 together with the results of Sparrow and Gregg (47) which will be discussed in the next section.

The Boundary Layer Equations

The problem of film condensation on a surface curved in two dimensions may be approached from the exact Navier-Stokes equations. If it is assumed that the thickness of the condensate layer is much smaller than the radius of curvature at any point, then the equations describing the condensate flow at that point will be the same as that for a flat plate inclined at the same angle to the horizontal. Thus the Navier-Stokes equations may be written in the following form:

$$\frac{\partial u}{\partial \xi} + u\frac{\partial u}{\partial x} + v\frac{\partial u}{\partial y} = \frac{g(\rho_l - \rho_v)\sin\phi}{\rho_l} - \frac{1}{\rho_l}\frac{\partial p}{\partial x} + \nu\left(\frac{\partial^2 u}{\partial x^2} + \frac{\partial^2 u}{\partial y^2}\right) \qquad (3.51)$$

$$\frac{\partial v}{\partial \xi} + u\frac{\partial v}{\partial x} + v\frac{\partial v}{\partial y} = \frac{g(\rho_l - \rho_v)\cos\phi}{\rho_l} - \frac{1}{\rho_l}\frac{\partial p}{\partial y} + \nu\left(\frac{\partial^2 v}{\partial x^2} + \frac{\partial^2 v}{\partial y^2}\right) \qquad (3.52)$$

$$\frac{\partial u}{\partial x} + \frac{\partial v}{\partial y} = 0 \qquad (3.53)$$

The x direction is along the plate in the downward direction; the y direction is perpendicularly into the fluid; and ϕ is the downward inclination of the plate to the horizontal as shown in Figure 3.1. This notation is identical with the one used in the momentum-energy method.

The boundary conditions have to be established. At the wall no slipping occurs, consequently:

at $\quad y = 0 \qquad u = v = 0 \qquad (3.54)$

At the vapor interface the conditions are not simple as it was pointed out before. In order to obtain a similarity transformation, it may be assumed as an approximation that

$$\text{at } y = y_s\,, \qquad \frac{\partial u}{\partial y} = 0 \tag{3.55}$$

This assumption leads to higher heat transfer rates than those predicted by the energy-momentum method.

The order of magnitude considerations applied in the derivation of the ordinary boundary layer equations can also be used in this case. As a result, the Navier-Stokes equations reduce to the following form,

$$\frac{\partial u}{\partial \xi} + u\frac{\partial u}{\partial x} + v\frac{\partial u}{\partial y} = \frac{g(\rho_l - \rho_v)\sin\phi}{\rho_l} + \nu\frac{\partial^2 u}{\partial y^2} \tag{3.56}$$

$$\frac{\partial u}{\partial x} + \frac{\partial v}{\partial y} = 0 \tag{3.53}$$

These equations describe the flow without any heat transfer effects. To include these, the energy equation is needed in addition. The derivation of all these equations may be found in the references (43). For steady state conditions, the complete set of equations describing the flow and the heat transfer become,

$$u\frac{\partial u}{\partial x} + v\frac{\partial u}{\partial y} = \frac{g(\rho_l - \rho_v)\sin\phi}{\rho_l} + \nu\frac{\partial^2 u}{\partial y^2} \tag{3.57}$$

$$\frac{\partial u}{\partial x} + \frac{\partial u}{\partial y} = 0 \tag{3.53}$$

$$\rho_l c_{pl}\left(u\frac{\partial t}{\partial x}+v\frac{\partial t}{\partial y}\right)=k_l\frac{\partial^2 t}{\partial y^2} \qquad (3.58)$$

The boundary conditions are:

at $y = 0$ $\quad u = v = 0$ and $t = t_w$ (3.59)

at $y = y_s$ $\quad \frac{\partial u}{\partial y} = 0$ and $t = t_s$ (3.60)

These are actually the standard boundary layer equations with the additional assumptions that the buoyancy forces within the liquid and the viscous dissipation energy are negligible.

The problem now arises, how to solve these equations in particular cases. One obvious way is the numerical method applied directly to the above partial differential equations. An alternative approach is to reduce the partial differential equations to ordinary differential equations by the use of properly selected stream functions. This latter method is described in the following text. Denoting differentiation by a letter subscript, the stream function, Ψ, is defined in the usual manner that will automatically satisfy the continuity equation.

$$u = \Psi_y \qquad (3.61)$$

$$v = -\Psi_x \qquad (3.62)$$

The remaining two equations become:

$$\Psi_y \Psi_{xy} - \Psi_x \Psi_{yy} = \frac{g(\rho_l-\rho_v)\sin\phi}{\rho_l} + \nu \Psi_{yyy} \qquad (3.63)$$

$$\Psi_y t_x - \Psi_x t_y = \alpha_l t_{yy} \qquad (3.64)$$

where $\alpha_t = \dfrac{k_\ell}{c_{p\ell}\rho_\ell}$

The corresponding boundary conditions are:

at $y = 0$ $\quad \Psi_y = 0, \quad \Psi_x = 0, \; t = t_w$ (3.65)

at $y = y_s$ $\quad \Psi_{yy} = 0, \; t = t_s$ (3.66)

Let

$$G(x) \equiv \frac{g(\rho_\ell - \rho_v)\sin\phi}{\rho_\ell} \tag{3.67}$$

Then the question is, for what types of functions of G(x) will the above relations reduce to ordinary differential equations. If this reduction can be accomplished, there is a transformation of the form:

$$\Psi = a\, J(\eta)\cdot j(x)\cdot \bar{g}(y) \quad \text{, where} \quad \eta = \eta(x, y) \tag{3.68}$$

which will indeed yield this result. Substituting relations (3.67) and (3.68) into (3.63) gives,

$$a^2\Big\{ J^2\left[jj'(\bar{g}')^2 - jj'\bar{g}\bar{g}''\right] + JJ'\left[j^2\bar{g}\bar{g}'\eta_{xy} + j^2(\bar{g}')^2\eta_x - \right.$$
$$\left. - j^2\bar{g}\bar{g}''\eta_x - jj'\bar{g}^2\eta_{yy}\right] + JJ''\left[j^2\bar{g}\bar{g}'\eta_x\eta_y - jj'\bar{g}^2\eta_y^2\right] +$$
$$+ (J')^2\left[jj'\bar{g}^2\eta_y^2 + j^2\bar{g}^2\eta_y\eta_{xy} - j^2\bar{g}\bar{g}'\eta_x\eta_y - j^2\bar{g}^2\eta_x\eta_{yy}\right]\Big\} =$$
$$= G + \nu a\left[Jj\bar{g}''' + J'\left(3j\bar{g}''\eta_y + 3j\bar{g}'\eta_{yy} + j\bar{g}\eta_{yyy}\right) + \right.$$
$$\left. + 3J''\left(j\bar{g}'\eta_y^2 + j\bar{g}\eta_y\eta_{yy}\right) + J'''\left(j\bar{g}\eta_y^3\right)\right] \tag{3.69}$$

Obviously all coefficients of the function J and its derivatives must be of the form: G • (constant), in order to render the expression reducible to an ordinary differential equation. If these coefficients are examined and it is noted that G must be a function of x only, then the following relations are found to exist,

$$\bar{g}(y) = E, \text{ a constant} \tag{3.70}$$

$$\eta_y = N(x) \tag{3.71}$$

Substituting into (3.69) produces,

$$a^2\left[-JJ''(jj'E^2N^2) + (J')^2(jj'E^2N^2 + j^2E^2NN')\right] =$$

$$= G + \nu a J'''(jEN^3) \tag{3.72}$$

Divide both sides by $a^2(jj'E^2N^2)$.

$$-JJ'' - (J')^2\left(1 + \frac{jN'}{Nj'}\right) = \frac{G}{a^2jj'E^2N^2} + \frac{\nu}{a}J'''\left(\frac{N}{j'E}\right) \tag{3.73}$$

The coefficients of J'^2 and J''', in parentheses, are constant. Therefore:

$$\frac{jN'}{Nj'} = B_0, \text{ a constant} \tag{3.74}$$

$$\frac{N}{j'E} = B_1, \text{ a constant} \tag{3.75}$$

Substituting N from (3.75) into (3.74) gives,

$$jj'' = B_0(j')^2 \tag{3.76}$$

All functions of j satisfying relation (3.76) will, therefore, reduce the equation to an ordinary differential equation, provided that the term containing G is also dimensionless. Dividing (3.76) by jj' results in an exact differential with the following solutions:

$$j = \begin{bmatrix} |E_0 + E_1 x|^n & \text{when } B_0 \neq 1 \\ E_2 e^{E_3 x} & \text{when } B_0 = 1 \end{bmatrix} \tag{3.77}$$

with the relation between B_0 and n:

$$n = \frac{1}{1 - B_0} \tag{3.78}$$

Substituting these results into (3.73) shows the types of functions for G that will allow a transformation of this kind to be performed.

When $B_0 \neq 1$:

$$G = E_4 |E_0 + E_1 x|^{4n-3} \tag{3.79}$$

When $B_0 = 1$

$$G = E_5 e^{4E_3 x} \tag{3.80}$$

It is convenient to express all functions in terms of the variation of gravity along the plate, G.

For the first class of allowable functions,

$$G = E_4 |E_0 + E_1 x|^m \tag{3.79}$$

$$j \sim |E_0 + E_1 x|^{\frac{m+3}{4}} \tag{3.79a}$$

$$N \sim |E_0 + E_1 x|^{\frac{m-1}{4}} \tag{3.79b}$$

$$\eta \sim |E_0 + E_1 x|^{\frac{m-1}{4}} \cdot y \tag{3.79c}$$

$$\Psi \sim J|E_0 + E_1 x|^{\frac{m+3}{4}} \tag{3.79d}$$

For the second class,

$$G = E_5 \, e^{E_5 x} \tag{3.80}$$

$$j \sim e^{\frac{E_6 x}{4}} \tag{3.80a}$$

$$N \sim e^{\frac{E_6 x}{4}} \tag{3.80b}$$

$$\eta \sim e^{\frac{E_6 x}{4}} \cdot y \tag{3.80c}$$

$$\Psi \sim J e^{\frac{E_6 x}{4}} \tag{3.80d}$$

Equation (3.73), defining J, now can be written in the following form:

$$J''' + \frac{a}{\nu B_1} JJ'' - \frac{a}{\nu B_1}\left(1 + \frac{jj''}{(j')^2}\right)(J')^2 + \frac{G}{\nu a B_1^3 E^4 j (j')^3} = 0 \tag{3.81}$$

This is a variation of the well-known Falkner-Skan equation appearing in boundary layer theory.

The energy equation can now be investigated separately. From (3.68), (3.71), and (3.75), the following relation can be found,

$$\eta = B_1 E j' y \quad \text{such that } \eta = 0 \text{ when } y = 0 \tag{3.82}$$

$$\Psi = aEJj \tag{3.83}$$

Substituting into equation (3.64) yields:

$$aB_1E^2J'jj't_x - (aB_1E^2J'jj''y + aEJj')t_y = \alpha_t t_{yy} \tag{3.84}$$

In order to render this equation dimensionless, define,

$$T(\eta) = \frac{t_s - t}{t_s - t_w} = \frac{t_s - t}{\Delta t} \tag{3.85}$$

where Δt may be a function of x only. Then, if t_s remains constant, equation (3.84) becomes

$$(aB_1E^2J'jj')(-B_1Ej''yT'\Delta t - T\Delta t_x) - (aB_1E^2J'jj''y +$$

$$+ aEJj')(-B_1Ej'T'\Delta t) = -\alpha_t B_1^2E^2(j')^2T''\Delta t \tag{3.86}$$

Performing the operations and making the equation dimensionless yields,

$$T'' + \frac{a}{\alpha_t B_1}\left[JT' - \left(\frac{j\Delta t'}{j'\Delta t}\right)J'T\right] = 0 \tag{3.87}$$

Accordingly, if $\frac{j}{j'} \cdot \frac{\Delta t'}{\Delta t}$ is a constant, the energy equation will also be reduced to an ordinary differential equation by the previous transformations.

Thus equations (3.63) and (3.64) may be transformed into the following ordinary differential equations,

$$J''' + \frac{a}{\nu B_1}\left[JJ'' - (1+E_7)(J')^2\right] + \frac{E_8}{\nu a B_1^3 E^4} = 0 \tag{3.88}$$

$$T'' + \frac{a}{\alpha_\ell B_1}\left[JT' - E_9 J'T\right] = 0 \tag{3.89}$$

where $E_7 \equiv \frac{jj''}{(j')^2}$, $E_8 \equiv \frac{G}{j(j')^3}$, and $E_9 \equiv \frac{j}{j'} \cdot \frac{\Delta t'}{\Delta t}$ (3.90a, b, c)

The boundary conditions are:

at $\eta = 0$ $J = 0,\ J' = 0,\ T = 1$ (3.91)

at $\eta = \eta_s$ $J'' = 0,\ T = 0$ (3.92)

These equations can be solved for any known value of η_s. In order to find η_s along the surface, an energy balance equation may be written between two cross sections of the condensate layer, $x = x_o$ and $x = x$.

$$\int_{x_o}^{x} k_\ell\left(\frac{\partial t}{\partial y}\right)_{y=0} dx = \int_0^{y_s} \lambda \rho_\ell u\, dy + \int_0^{y_s} \rho_\ell u c_{p\ell}(t_s - t)\, dy \tag{3.93}$$

This equation is the same as (3.2) the energy equation of the momentum-energy method. Substituting the previous dimensionless relations leads to the following derivation,

$$-k_\ell T'(0) B_1 \int_{x_o}^{x} \Delta t\, j'\, dx = \lambda \rho_\ell a j \int_0^{\eta_s} J'(1 + ST)\, d\eta$$

$$-\frac{B_1 k_\ell T'(0)}{1 + E_9}\left[\Delta t j - \Delta t(x_o) j(x_o)\right] =$$

$$= \lambda \rho_\ell a j \left[J(\eta_s) - J(0) + S\int_0^{\eta_s} J'T\, d\eta\right] \tag{3.94}$$

The integral can be eliminated by using equation (3.89) together with its boundary conditions (3.91) and (3.92).

$$-\frac{B_1 k_\ell T'(0)}{1+E_q}\left[\Delta t j - \Delta t(x_0) j(x_0)\right] =$$

$$= \lambda \rho_\ell a j \left\{ J(\eta_s) + \right.$$

$$\left. + \frac{\xi}{1+E_q}\int_0^{\eta_s}\left[(JT)' + \frac{\alpha_t B_1}{a} T''\right] d\eta \right\}$$

$$\frac{B_1 k_\ell T'(0)\, \Delta t(x_0)\, j(x_0)}{1+E_q} =$$

$$= \lambda \rho_\ell a j\, J(\eta_s) + \frac{B_1 k_\ell \Delta t\, j\, T'(\eta_s)}{1+E_q} \tag{3.95}$$

This equation then determines η_s. If $\Delta t(x_o)$ or $f(x_o)$ is equal to zero, however, further simplification is possible which results in the following expression:

$$\frac{J(\eta_s)}{T'(\eta_s)} = \frac{B_1 k_\ell \Delta t}{(1+E_q)\lambda \rho_\ell a} \tag{3.96}$$

It is clear now that, if Δt is constant, η_s is independent of x. In the above equation "a" may be set equal to α_t, and E may be selected such that the constant in equation 3.88 is unity. B_1 is essentially arbitrary. The equations then become,

$$J''' + \frac{1}{B_1 \, Pr}\left[JJ'' - (1+E_7)(J')^2\right] + 1 = 0 \qquad (3.88a)$$

$$T'' + \frac{1}{B_1}\left[JT' - E_9 J'T\right] = 0 \qquad (3.89a)$$

$$\frac{J(\eta_s)}{T'(\eta_s)} = -\frac{B_1}{1+E_9}\cdot\frac{c_{p\ell}\Delta t}{\lambda} = -\frac{B_1}{1+E_9}\,\xi \qquad (3.96a)$$

Examining the set of permissible functions reveals that the flat plate problem with constant G can indeed by solved by this method, but the circular tube with G varying as sin x cannot be solved directly. Sparrow presented the flat plate solution, and later used Hermann's (21) approximate function to obtain a solution to the circular tube problem (46, 47).

In finding an approximate solution, Hermann matched the constants of a set of four equations such that these equations were satisfied exactly at $\phi = \pi/2$. Since no similarity exist at this point, while at $\phi = 0$ it does, this approximation is certainly no better than Chen's described before.

Comparing the energy-momentum method to Sparrow's results, as shown in Figure 3.3, indicates that the previous one yields consistantly lower values for the heat transfer rate. The discrepancy is due obviously to the difference in the interface boundary conditions.

The ones assumed in the momentum-energy method conform closer to the usual physical situation existing, such as an essentially stagnant vapor condensing on a surface.

Since for ordinary fluids the corrections are insignificant, the results of all these methods will have to be compared to those obtained from data on liquid metals. It was mentioned before that Misra and Bonilla's results qualitatively show the marked reduction in heat transfer rates for liquid metals.

CHAPTER IV

THE AXIALLY FLOWING CONDENSATE ON THE BOTTOM OF THE TUBE

It is evident that all the condensate formed inside the tube has to leave through the outlet end. If there is a considerable amount of vapor passing through the tube, such as in the first pass of a multi-pass condenser, then the shear exerted on the surface of the liquid by the relatively fast-moving vapor controls the flow pattern and the effect of gravity becomes negligible. Experimental proof may be found in the fact that the data obtained in horizontal and in vertical tubes can be correlated by the same curve above a certain Reynolds number (2).

If, however, the tube is part of a single-pass condenser, then the vapor shear is zero at the outlet and negligible for a certain distance upstream. Now gravity is the controlling factor at least in the downstream portion of the tube. This is the problem to be investigated in the following section.

Free-Surface Flow . . . An Old Problem with a New Twist

If vapor shear is relatively low, the condensate forming on the sides of the tube collects on the bottom; then it has to flow out axially and is discharged at the outlet. The depth of this axial flow has a marked influence on the heat transfer. This depth is considerably larger than the thickness of the condensate film on the sides. Therefore, the axial condensate flow reduces the effective heat transfer area in the tube. It will be shown later, quantitatively, that the amount of heat passing through the bottom condensate layer is negligible compared to the heat transferred on the side walls.

Consequently, as far as the overall problem is concerned, the most important factor is the depth of the flow. If the depth could be established, the effective heat transfer area could also be found.

The problem of liquid discharge from a partially filled tube, or the more general problem of liquid discharge from any open channel has been an old one, in particular, with the civil engineers. They have been confronted with such problems ever since they undertook the task of controlling rivers, harbors, and building hydraulic structures such as channels or dams. On examining their work in this field, one can find a problem which is very closely related to the one at hand. This is the discharge from a so-called lateral spillway. Here the liquid is fed into the open channel all along its length and is discharged through one end. The similarity to the condensate flow problem is obvious. Upon closer examination, however, some rather important differences occur. First of these is the size. Compared to even the largest condenser tube used in practice, the smallest lateral spillway or any similar structure is enormous. As a result, the lateral spillway contains usually turbulent flow, while the condensate flow can be laminar, transient, or turbulent, with the laminar type usually dominating a great part of the tube. In the case of turbulent flow the velocity distribution is much more uniform than in the laminar or even transient case. Thus, the lateral spillway problem is much more amenable to a one-dimensional analysis, although the methods used can be applied in either case. Another important difference arises from the axial vapor shear acting on the surface of the condensate layer in the upstream portion of the tube. This affects the flow pattern in several ways, two of which are the tendency to reduce the depth and to induce rather strong traveling waves on the surface. The first of these increases, the second decreases the effective heat transfer area. A third difference between the two types of phenomena is that the amount of condensate feeding into the bottom layer at any point along the tube depends on the depth, while in a lateral spillway such an interdependence usually does not exist.

What are exactly the characteristics of the phenomena occurring on the bottom of the tube? In order to answer this question as thoroughly as possible it is not enough to investigate the axial flow all by itself. The interactions at the boundaries, such as vapor shear at the free surface, and their possible effects on the flow should also be considered, at least qualitatively.

The axial flow of condensate is non-uniform in two respects. First the quantity flowing increases downstream; second the cross-section changes along the length. Of primary interest here is the latter variation: the establishment of the surface profile. There are actually two parts to this problem: one is to find a control point or cross-section at which the depth may be predicted; the other is to determine the change of depth, starting from the control section, all along the tube. On both of these problems there was a great amount of work done, in particular, by the civil engineers who needed methods for predicting open channel flows (23)(32).

The Critical Depth of Free-Surface Flows

The problem of establishing a control point has been approached through the use of the so-called critical depth theory. This states that in a free surface flow at some point the specific energy of the stream will go through a minimum. The specific energy of the stream may be defined as follows:

$$H = \frac{1}{\rho_m V_m A} \int_A \left(\frac{p}{\rho g} + \frac{V^2}{2g} + s \right) \rho V dA \qquad (4.1)$$

where H specific head, ft

ρ density, slugs/ft^3

V velocity, ft/sec

A cross-sectional area of flow, perpendicular to the stream lines, ft^2

p pressure, lbf/ft^2

g gravitational acceleration, ft/sec^2

s elevation above a given datum level, ft

subscript m - mean value

To illustrate this theory and its implications, first the flow in a rectangular channel will be investigated with the assumptions that the velocity and density distributions are uniform and that the pressure distribution is hydrostatic, that is, the streamlines are essentially straight. Defining the depth of the liquid by h, the above equation becomes,

$$H = \frac{V^2}{2g} + h + s_o \tag{4.2}$$

where s_o elevation of the channel bottom above a datum, ft

h depth of flow, ft

For a given flow rate, Q ft^3/sec, and flow rate per unit width of the channel, $q = \frac{Q}{b}$ ft^3/sec-ft, the velocity may be expressed as

$$V = \frac{Q}{bh} = \frac{q}{h} \tag{4.3}$$

Substituting into (4.2) yields:

$$H = \frac{q^2}{2gh^2} + h + s_o \tag{4.4}$$

For the given cross-section taking $s_o = 0$, specific heat versus depth plots in a family of curves with the flow rate as an independent parameter. A typical graph is shown in Figure 4.1.

The minimums of the specific head curves may be found by differentiating equation (4.4) with respect to h and setting the result equal to zero.

$$\frac{\partial H}{\partial h} = -\frac{q^2}{g h_c^3} = 0$$

$$h_c = \sqrt[3]{\frac{q^2}{g}} \tag{4.5}$$

Some physical significance may be found in this expression if the corresponding critical velocity is calculated.

$$V_c = \sqrt{g h_c} \tag{4.6}$$

This expression is identical with the velocity of wave propagation on the surface of a liquid h_c deep. Thus the critical depth and the corresponding critical flow is analogous to the sonic flow occurring at the throat of a nozzle or at the outlet of a duct.

Equation (4.4) and the corresponding curves in Figure 4.1 show that for any specific heat greater than the minimum two alternate depths may exist, one greater and one smaller than the critical depth. Correspondingly the velocities are either sub- or supercritical. Which one of these flows exists in a given channel depends on how the fluid enters at the upstream end, the losses occurring in the channel, and the slope of the channel. In a long horizontal tube, the flow will always become subcritical provided no shear stress exists at the free surface to impart energy to the fluid. If at the outlet end there is a change to a steeper slope or a so-called free discharge exists, the control point in the form of critical depth must occur near this end. The exact location depends on how the transition from subcritical to supercritical flow occurs. This transition in turn is influenced primarily by the geometry of the channel near the outlet. It has been established experimentally in hydraulics that the critical depth actually occurs a very short distance (about 3 or 4 times the depth) upstream of a so-called free overfall. If the transition geometry is gradual, such as in the case of an elbow at the outlet, the critical depth would occur somewhere in the elbow. This is one of the possible reasons for lower surface profiles found (15) in horizontal pipes with elbows at the outlet. At very low flow rates surface tension effects become more important and tend to raise the top of the liquid layer.
In the case of the free overfall, at low flow rates the liquid will

not separate from the tube but will adhere to the lip and flow downward. By increasing the pressures in the flow at the outlet, this effect also tends to raise the surface level.

The effect of non-uniform velocity distribution on the critical depth should be investigated next. If the bottom of the channel is taken as datum, equation (4.1) may be written (23) as:

$$H = \alpha \frac{Q^2}{2gA^2} + \beta h \tag{4.7}$$

where

$$\alpha \equiv \frac{1}{AV_m^3} \int_A V^3 dA \tag{4.8}$$

$$\beta \equiv \frac{1}{Qh} \int_A \left(\frac{p}{\rho g} + s \right) V dA \tag{4.9}$$

Thus α is a function of the velocity distribution; while β is a function of the velocity distribution, and it also depends on the curvature of the streamlines, that is, the deviation of the pressure from hydrostatic. In particular, if the pressure is exactly hydrostatic, $\beta = 1$. If the streamlines curve downward $\beta < 1$, if they curve upward $\beta > 1$. For fully developed, laminar flow in a pipe $\alpha = 2$.

Now the minimum energy principle may be stated as:

$$\frac{\partial H}{\partial h} = \frac{Q^2}{2gA^2} \cdot \frac{\partial \alpha}{\partial h} + \alpha \frac{\partial}{\partial h}\left(\frac{Q^2}{2gA^2} \right) + \beta + h \frac{\partial \beta}{\partial h} = 0 \tag{4.10}$$

If it is assumed that the variation of α and β are small near the critical depth, the above equation simplifies to:

$$\frac{\alpha}{\beta}\frac{\partial}{\partial h}\left(\frac{Q^2}{2gA^2}\right)+1=0 \tag{4.11}$$

Again investigate the two-dimensional flow.

$$\frac{\alpha}{\beta}\frac{\partial}{\partial h}\left(\frac{q^2}{2gh^2}\right)+1=0$$

$$-\frac{\alpha}{\beta}\cdot\frac{q^2}{gh_c^3}+1=0$$

$$h_c=\sqrt[3]{\frac{\alpha}{\beta}\cdot\frac{q^2}{g}} \tag{4.12}$$

Thus non-uniform velocity distributions tend to increase the depth.

From the foregoing discussion the following general conclusions may be drawn:

a. In order to be able to use the critical depth theory successfully, a horizontal channel or tube with a sharp cut-off should be used. Then the critical depth will always occur in the horizontal part near the outlet end. If the length-diameter ratio of the tube is large, the exact location of this control point becomes unimportant.

b. The critical depth theory is expected to predict depths that are too low when the flows are small, particularly if the velocity distribution is neglected in the calculations.

Now consider the circular cross-section of Figure 3.2.

$$A = r_o^2(\theta_c - \sin\theta_c \cos\theta_c) \tag{4.13}$$

$$h = r_o(1 - \cos\theta_c) \tag{4.14}$$

$$\frac{\partial}{\partial h} = r_o \sin\theta_c \frac{\partial}{\partial \theta_c} \tag{4.15}$$

Substituting into equation (4.11), and simplifying yields,

$$\frac{16\alpha}{\beta} \cdot \frac{Q^2}{g r_o^5} = \frac{(2\theta_c - \sin 2\theta_c)^3}{\sin\theta_c} = \frac{(\phi_c - \sin\phi_c)^3}{\sin\frac{\phi_c}{2}} \tag{4.16}$$

This function is plotted together with some of the experimental results in Figure 7.1. If α/β is assumed to be equal to unity, the correlation with experimental data is rather good at high flow rates, above $Q/\sqrt{g r_o^5} = 0.15$, and becomes progressively worse at lower flow rates. If, for laminar flows, Re $<$ 3,000, it is assumed that $\alpha/\beta = 2$, the correlation becomes more satisfactory; although the deviation still remains considerable at the lowest flow rates.

Equation (4.16) can be expressed in another form which allows a very accurate approximation in terms of the depth-diameter ratio, h/D. Define the section factor as:

$$Z = A\sqrt{\frac{A}{b}} \tag{4.17}$$

where Z section factor, $ft^{2.5}$

A cross-sectional area of flow, ft^2

b top width of flow, ft

For the circular cross-section at the critical point

$$Z_c = \frac{r_o^{2.5}(\phi_c - \sin\phi_c)^{\frac{3}{2}}}{4\left(\sin\frac{\phi_c}{2}\right)^{\frac{1}{2}}} = Q\sqrt{\frac{\alpha}{\beta g}}$$

$$\frac{Z_c}{r_o^{2.5}} = \sqrt{\frac{\alpha}{\beta}}\cdot\frac{Q}{\sqrt{g r_o^5}} = \frac{(\phi_c - \sin\phi_c)^{\frac{3}{2}}}{4\left(\sin\frac{\phi_c}{2}\right)^{\frac{1}{2}}} \tag{4.18}$$

If $Z_c/r_o^{2.5}$ is expressed in terms of h_c/d_o, the resulting relation can be approximated for the range $0.02 < h_c/d_o < 0.9$ by the following relation:

$$\frac{Z_c}{r_o^{2.5}} = 5.426\left(\frac{h_c}{d_o}\right)^{1.956} \tag{4.19}$$

This expression is practically exact for the range $0.04 < h_c/d_o < 0.85$, and it is 12% too high at $h_c/d_o = 0.02$, 7% too low at $h_c/d_o = 0.9$. Since Z goes to infinity as h_c/d_o approaches one, the approximate relation should not be used beyond the limits specified.

Substituting (4.19) into (4.18) yields:

$$\sqrt{\frac{\alpha}{\beta}}\cdot\frac{Q}{\sqrt{g r_o^5}} = 5.426\left(\frac{h_c}{d_o}\right)^{1.956} \tag{4.20a}$$

or

$$\frac{h_c}{d_o} = 0.4212\left(\sqrt{\frac{\alpha}{\beta}}\cdot\frac{Q}{\sqrt{g r_o^5}}\right)^{0.5112} \tag{4.20b}$$

These equations then relate theoretically the flow rate and the critical depth for a circular tube. For the range investigated in the experiments, $\sqrt{\alpha/\beta}$ may be assumed to be 1.4 for Re $<$ 3000 (based on the hydraulic diameter of the flow) and 1.1 for Re $>$ 3000.

The experimental work showed excellent agreement with these relations for high flow rates. For low flow rates of $Q_{1_0}/\sqrt{gr_o^5} < 0.08$, however, the correlation became progressively worse, primarily because surface tension prevented the formation of a free nappe, and the liquid adhered to the lip of the tube. The experimental results indicate that for these lower flow rates the central angle subtended by the condensate near the outlet remains constant at $\phi_1 = 90°$ (see Figure 7.1).

The Profile of the Free Surface

In hydraulics the problem of predicting free-surface profiles, the so-called backwater curves, has been studied for a long time. As a result, there is an extensive literature available as reference; and all text books in hydraulics treat this problem more or less in detail (23)(43). Their analyses, however, do not consider any shear acting on the surface of the flow; and they are usually one-dimensional. Also, most of the investigators are dealing with uniform flow rates along the channels, with relatively few examining the effect of such a variation. Li (33) derived equations for surface profiles in rectangular and triangular horizontal channels, with the assumptions that the velocity distribution is uniform, friction may be neglected, and the flow rate varies linearly along the length. His estimates of the friction effect indicated that the calculated upstream depth would have increased by not more than 10% in the most extreme cases.

Let us examine the problem of condensate flow inside a circular tube by developing the generalized one-dimensional continuous flow equations for a two-phase mixture with condensation.

Equations of State:

For the liquid density

$$\rho_\ell = \text{constant} \tag{4.21a}$$

For the vapor of an ordinary refrigerant under the usual operating conditions the pressure drop along a condenser tube is small compared to the absolute pressure. Consequently, the density,

$$\rho_v = \text{constant} \tag{4.21b}$$

Velocity of Surface Waves on the Bottom Condensate Layer:

$$c^2 = \frac{gA_\ell}{b} \tag{4.22a}$$

where c Velocity of surface wave, ft/sec

g Gravitational acceleration, ft/sec^2

A_ℓ Liquid cross-sectional area, ft^2

b Width of the liquid free surface, ft

In differential form

$$\frac{dc}{c} = \frac{1}{2}\left(\frac{dA_\ell}{A_\ell} - \frac{db}{b}\right) \tag{4.22b}$$

Definition of the Froude Number:

$$\overline{Fr}^2 \equiv \frac{Q_\ell^2}{A_\ell^2 c^2} = \frac{Q_\ell^2 b}{gA_\ell^3} \tag{4.23a}$$

$$\frac{d\overline{Fr}^2}{\overline{Fr}^2} = \frac{dQ_\ell^2}{Q_\ell^2} + \frac{db}{b} - \frac{dA_\ell^3}{A_\ell^3} \tag{4.23b}$$

where F_r Froude Number

Q_ℓ Liquid volumetric flow rate, ft^3/sec

With the above definition a Froude Number of unity corresponds to the critical depth in any cross-section.

Continuity:

$$\Gamma_\ell = Q_\ell \rho_\ell \tag{4.24a}$$

$$\Gamma_v = Q_v \rho_v \tag{4.24b}$$

$$\Gamma_\ell + \Gamma_v = \Gamma_{in} \, , \tag{4.25a}$$

$$d\Gamma_\ell = - d\Gamma_v \tag{4.25b}$$

$$dQ_v = -\frac{\rho_\ell}{\rho_v} dQ_\ell \tag{4.26}$$

where Γ_v and Γ_ℓ Vapor and liquid mass flow rates, slugs/sec

Q_v Vapor volumetric flow rate, ft^3/sec

Energy Equation for Overall Heat Transfer:

$$h_m A_h \Delta t_m = \Gamma_{in} \left(h_{in} - h_{out} \right) \tag{4.27}$$

where h_m Heat transfer coefficient, Btu/sec ft^2 °F

A_h Heat transfer area, ft^2

Δt_m Mean temperature differential between vapor and surface, to be considered as a constant, °F

Γ_{in} Total mass flow rate at any cross section, slugs/sec

h_{in} and h_{out} Enthalpies at inlet and exit, Btu/slug

Energy Equation for Liquid Flow:

Equation 4.2 has to be modified to include the effect of a variable pressure in the vapor phase. Thus,

$$H = \frac{p}{\rho_l g} + h + s_o + \frac{Q_l^2}{2gA_l^2} \tag{4.28a}$$

$$dH = \frac{dp}{\rho_l g} + dh + ds_o + \frac{Q_l^2}{2gA_l^2}\left(\frac{dQ_l^2}{Q_l^2} - \frac{dA_l^2}{A_l^2}\right) \tag{4.28b}$$

Momentum Equations:

For the vapor phase,

$$-A_v\, dp - \tau_s P_v\, dz = C_v\, d\left(\frac{\rho_v Q_v^2}{A_v}\right) \tag{4.29}$$

where A_v Vapor cross-sectional area, ft²

P_v Wetted perimeter of vapor, ft

z Axial direction, ft

τ_s Vapor wall shear stress, lbf/ft²

C_v Correction factor for velocity distribution

For the liquid phase

$$-A_l\, dp - d(\rho_l g A_l s_c) + \tau_s b\, dz -$$

$$-\tau_w P_w\, dz + \rho_l g A_l \frac{ds_o}{dz} dz =$$

$$= C_v\, d\left(\frac{\rho_l Q_l^2}{A_l}\right) - 2\underbrace{\int_z^{z+dz}\int_0^{y_s} \rho_l\, u w\, dy\, dz}_{\text{wall condensate}} \tag{4.30}$$

where s_c Depth of centroid of A_ℓ below free surface, ft

τ_w Liquid shear stress on walls, lbf/ft^2

P_w Wetted perimeter of liquid on walls, ft

u, w Velocity components of condensate layer on walls where it reaches the bottom condensate

The shear stresses may be expressed as follows

$$\tau_s = f_v \rho_v \frac{Q_v^2}{2A_v^2} \tag{4.31a}$$

$$\tau_w = f_\ell \rho_\ell \frac{Q_\ell^2}{2A_\ell^2} \tag{4.31b}$$

where f_v and f_ℓ are friction factors for the vapor and the liquid, and can be approximated by the usual expressions in terms of the Reynolds number.

$$f_v = a_i\left(\overline{Re_v}\right)^{b_i} = a_i\left(\frac{4\rho_v Q_v}{\mu_v P_v}\right)^{b_i} \tag{4.32a}$$

$$f_\ell = a_i\left(\overline{Re_\ell}\right)^{b_i} = a_i\left(\frac{4\rho_\ell Q_\ell}{\mu_\ell P_w}\right)^{b_i} \tag{4.32b}$$

Based on Gazley's data (16), the constants may be taken as follows

for $Re < 3000$ $\quad a_i = 18,\ b_i = -1,\ C_v = 1.33$ (4.33a)

for $Re > 3000$ $\quad a_i = 0.0085,\ b_i = 0,\ C_v = 1$ (4.33b)

Geometry of Flow:

All geometrical functions may be expressed in terms of θ_c, half of the central angle subtended by the bottom condensate layer.

$$\phi_c = 2\theta_c \tag{4.34a}$$

$$\phi = \pi - \theta_c \tag{4.34b}$$

$$b = 2r_o \sin\theta_c \tag{4.34c}$$

$$A_\ell = r_o^2\left(\theta_c - \frac{\sin 2\theta_c}{2}\right) \tag{4.34d}$$

$$A_v = r_o^2\left(\pi - \theta_c + \frac{\sin 2\theta_c}{2}\right) \tag{4.34e}$$

$$h = r_o(1 - \cos\theta_c) \tag{4.34f}$$

$$P_v = 2r_o(\pi - \theta_c + \sin\theta_c) \tag{4.34g}$$

$$P_w' = 2r_o\theta_c \tag{4.34h}$$

$$A_\ell s_c = r_o^3\left[\frac{2}{3}\sin^3\theta_c - \cos\theta_c\left(\theta_c - \frac{\sin 2\theta_c}{2}\right)\right] \tag{4.34i}$$

Some of these functions are tabulated in Appendix VI.

Additional Relations:

Based on equations (3.9) and (3.17), using the constants A_o, B_o, and D_o of the first approximation (see page 23) and Rohsenow's (40) value of 0.68 for C, and noting that the change of volumetric flow rate $dQ_\ell/dz = 2f$, the following relation may be established.

$$dQ_\ell = 2\left[\frac{g(\rho_\ell - \rho_v)k_\ell^3 r_o^3 \Delta t^3}{3\mu_\ell \rho_\ell^3 \lambda^3(1+0.68\xi)^3}\right]^{\frac{1}{4}}\left[\frac{4}{3}\int_0^{\phi} \sin^{1/3}\phi \, d\phi\right]^{\frac{3}{4}} dz = \Omega \, dz \tag{4.36}$$

The last term of equation (4.30) may be estimated by integrating the velocity profiles of equations (5.2) and (5.5) together with relations (3.6), (3.9), and (3.17).

$$\underset{\text{wall condensate}}{2\int_z^{z+dz}\int_0^{Y_s} \rho_\ell u w \, dy \, dz} = \left[\frac{5 k_\ell r_o \tau_s \Delta t}{3\mu_\ell \lambda(1+0.68\xi)}\right]\left[\frac{\int_0^{\phi}\sin^{1/3}\phi \, d\phi}{\sin^{1/3}\phi}\right] \cdot dz \tag{4.37}$$

The last expression, the momentum influx of the wall condensate, is based on the assumption that the condensate on the bottom and on the walls meet at an angle. Physically this situation is impossible; surface tension will create a smooth transition which will considerably increase the thickness of the wall condensate and, consequently, reduce the magnitude of the term. Since this effect is small to begin with, it is reasonable to omit it entirely.

For the determination of the liquid surface profile equation (4.30) has to be solved. Dividing this expression by $\rho_\ell g r_o^3$, and defining $\sigma \equiv ds_o/dz$ results:

$$d\left(\frac{A_\ell s_c}{r_o^3}\right) = \left[\frac{A_\ell \sigma}{r_o^3} + \frac{\tau_s b}{\rho_\ell g r_o^3} - \right.$$

$$\left. - \frac{\tau_w P_w}{\rho_\ell g r_o^3} - \frac{A_\ell}{r_o^2}\frac{d}{dz}\left(\frac{p}{\rho_\ell g r_o}\right) - 2C_v \frac{d}{dz}\left(\frac{Q_\ell^2}{A_\ell g r_o^3}\right)\right] dz \tag{4.38}$$

The numerical solution of this equation may be simplified by the following assumptions. First the vapor friction factor, f_v, may be considered a constant, 0.0085, even in the laminar region. Since the vapor shear is very small for $Re_v < 3000$, this simplification will not introduce a serious error. Second, the liquid feed rate $\Omega = dQ/dz$ may be taken as constant along the tube. Experimental evidence, as shown in the data in Appendix III, Table A-6, indicates that for the range of flow rates examined, the liquid level was very uniform for most part of the tube. For the inclined tube the liquid depth was observed to be essentially constant after the initial liquid ramp reported in Appendix III, Table A-5. Examining the angle function in equation (4.36), tabulated in Appendix VI, reveals that Ω is not too sensitive to variations of ϕ in the range of 120° to 160°. Consequently, the error caused by this assumption can be easily minimized by selecting a good mean value for the condensate depth when determining Ω. The resulting relations become,

$$-\frac{dp}{dz} = \frac{0.00425\rho_v Q_v^2 P_v}{A_v^3} + \frac{2\rho_v Q_v}{A_v^2} \cdot \frac{dQ_v}{dz} \tag{4.39}$$

where the factor C_v was taken as unity.

$$Q_\ell = \Omega z \tag{4.40}$$

$$Q_v = \Omega \frac{\rho_\ell}{\rho_v}(L - z) \tag{4.41}$$

Substituting into (4.38) yields:

$$d\left(\frac{A_\ell s_c}{r_o^3}\right) =$$

$$= \left\{ \frac{A_\ell \sigma}{r_o^3} + \frac{0.00425\Omega^2 \rho_\ell (L-z)^2 b}{A_v^2 \rho_v g r_o^3} - \frac{9\mu_\ell \Omega z P_w^2}{4A_\ell^2 \rho_\ell g r_o^3} + \right.$$

$$\left. + \frac{A_\ell \rho_\ell \Omega^2}{A_v^2 \rho_v g r_o^3}\left[\frac{0.00425 P_v (L-z)^2}{A_v} - 2(L-z)\right] - \frac{d}{dz}\left[\frac{1.33\Omega^2 z^2}{A_\ell g r_o^3}\right]\right\} dz \tag{4.42}$$

The liquid flow was assumed to be laminar everywhere. This was actually the case for all condensation experiments.

This equation may be integrated numerically, provided that the geometry is known at one point. For a horizontal tube or for a very slightly downward tilted tube, where the downstream liquid flow is definitely subcritical, a critical depth will exist at the outlet. As it was pointed out previously, at low flow rates the outlet end still controls the flow, but the depths are considerably increased due primarily to surface tension effects. The depth of flow becomes less as the inclination is increased; the exposed wall area, and consequently the effective heat transfer increases. This improvement, however, is eventually counteracted by the effect the inclination produces on the wall condensate. Hassan and Jakob (19) showed that, theoretically, the heat transfer rate varies as $\cos^{1/4}(\sin^{-1}\sigma)$ during condensation on an infinite circular tube. As long as $2\, r_o \tan(\sin^{-1}\sigma) \ll L$, this relation is the best available estimate of the influence of inclination on the heat transfer through the wall condensate. The experimental data Appendix III, Table A-5, show a considerable decrease in condensate depth as the tube is tilted a small amount of the order of $\sigma = 0.010$, but tilting the tube further did not affect the depth very much.

For inclined tubes the establishment of a control section becomes very difficult, if not well nigh impossible. One may argue that under such conditions the flow depth starts at zero at the inlet. This assumption leads to a numerical step-by-step solution of equation (4.42). On the other hand, careful consideration of the flow patterns observed in the experiments suggest another type of boundary condition, which not only gives very good results, but also renders the mathematical solution extremely simple.

Again the experimental observations revealed that the flow depths were very uniform along most of the tube. The only departure from near uniform depth occurred near the entrance region and, in the horizontal tube, very close to the outlet end. This observation suggests for a boundary condition that the depth should remain very nearly constant in the downstream portion of the tube. Such an assumption will lead to the elimination of the terms containing area variations after equation (4.42) is integrated, and the resulting relation becomes:

$$\frac{L}{r_o}\cdot\frac{A_\ell}{r_o^2}\,\sigma\left[z^+\right]_1^2 -$$

$$-0.001417\frac{\rho_\ell}{\rho_v}\cdot\frac{\Omega^2L^2}{g r_o^5}\cdot\frac{L}{r_o}\left(\frac{r_o^2}{A_v}\right)^2\sin\theta_c\left[(1-z^+)^3\right]_1^2 -$$

$$-1.125\frac{\Omega^2L^2}{g r_o^5}\cdot\frac{\mu_\ell}{\rho_\ell\Omega}\left(\frac{r_o}{r_{h\ell}}\right)^2\left[z^{+2}\right]_1^2 +$$

$$+\frac{\rho_\ell}{\rho_v}\cdot\frac{\Omega^2L^2}{g r_o^5}\cdot\frac{A_\ell}{r_o^2}\left(\frac{r_o^2}{A_v}\right)^2\left[(1-z^+)^2-0.001417\frac{L}{r_o}\cdot\frac{r_o}{r_{hv}}(1-z^+)^3\right]_1^2 -$$

$$-2.67\frac{r_o^2}{A_\ell}\cdot\frac{\Omega^2L^2}{g r_o^5}\left[z^{+2}\right]_1^2 = 0 \qquad (4.43)$$

where $z^+ = \dfrac{z}{L}$

$r_h = \dfrac{A}{P}$

$\left[\;\right]_1^2$ indicates limits of integration.

The results were actually not very sensitive to the limits. As Table 4.1 shows, integrating between three sets of limits did not change the value of the calculated condensate angle, θ_c, by more than 2°; and all results were reasonably close to the observed one, with the limits $z^+ = 0.5$ to $z^+ = 1$ giving the best value.

The method developed here also lends itself to a simple optimizing procedure to find the slope with the highest heat transfer rate. It has been shown that the heat transfer coefficient varies as $\left[\int_0^{\phi} \sin^{1/3}\phi \, d\phi\right]^{3/4}$ and as $\cos^{1/4}(\sin^{-1}\sigma)$. Therefore, when σ is plotted against ϕ (or θ_c), the scale for ϕ can be also marked for the values of the first function, and the scale for σ for the values of the second. The optimizing procedure becomes simply a matter of plotting σ, then finding the point along the curve for which the product

$$\cos^{1/4}(\sin^{-1}\sigma)\left[\int_0^{\phi} \sin^{1/3}\phi \, d\phi\right]^{\frac{3}{4}} \tag{4.44}$$

is maximum. Such a chart is shown in Figure 4.2 with the σ curve plotted for Run No. 119.

For the horizontal position Table 4.2 shows a comparison of the values of ϕ for test runs with various flow rates. These values were computed by integrating step-by-step starting from a known depth at the outlet end. The agreement between measured and calculated angles is only fair, but the obtained mean values for ϕ over the length of the tube are still satisfactory for use in the heat transfer calculations, due to the insensitiveness of relation (4.44) to variations of ϕ in the range considered. The step-by-step integration of equation (4.42) involves small differences of the angle function on the left hand side. Consequently, errors in estimating the friction factors influence these calculations rather strongly, and the discrepancies found are not surprising.

TABLE 4.1

COMPARATIVE RESULTS IN INCLINED CONDENSER TUBES

Run No.	92	106	110	112	119	121	124	124	124	126
Slope, σ	0.010	0.020	0.040	0.040	0.1736	0.1736	0.1736	0.1736	0.1736	0.1736
Measured Flow Rate, $Q_{\ell o}/\sqrt{gr_o^{5}}$	0.1256	0.1274	0.1858	0.1350	0.0995	0.1401	0.1739	0.1739	0.1739	0.1590
Limits of Integration in Equation (4.43), z^+	0.5-1	0.5-1	0.5-1	0.5-1	0.5-1	0.5-1	0.0-1	0.3-1	0.5-1	0.5-1
Calculated Condensate Angle, ϕ	133°	138.2°	139.3°	141.5°	153.3°	150.7°	147.5°	147.5°	147.5°	149.5°
Observed Condensate Angle, ϕ	140°	140°	140°	142.5°	151°	149°	150.8°	149.5°	148.8°	149°
Calculated Heat Transfer Coefficient, h_m, Btu/hr ft²°F	252	255	227	253	313	270	234	233	232	260
Measured Heat Transfer Coefficient, h_m, Btu/hr ft² °F	250	241	222	229	318	263	241	241	241	252

TABEL 4.2

COMPARATIVE RESULTS IN HORIZONTAL CONDENSER TUBES

Run No.	36	36	36	36	37	37	37	37	79	82
Measured Flow Rate, $Q_{lo} / \sqrt{g r_o^5}$	0.1637	0.1637	0.1637	0.1637	0.0333	0.0333	0.0333	0.0333	0.1181	0.1507
Location along Tube, z^+	1	0.7	0.3	mean	1	0.7	0.3	mean	mean	mean
Condensate Angle Calculated from Critical Depth at Outlet, ϕ	125°	114°	104°	113°	145°	131°	128°	134.5°	122°	113°
Condensate Angle Calculated from Observed Depth at Outlet, ϕ	125°	114°	104°	113°	133°	129.5°	127°	129.8°	122°	113°
Observed Condensate Angle, ϕ	125°	119.5°	119°	121°	133°	131.5°	121°	128.5°	121°	122.5°
Calculated Heat Transfer Coefficient, h_m, Btu/hr ft² °F	-	-	-	-	-	-	-	-	231	209
Measured Heat Transfer Coefficient, h_m, Btu/hr ft²°F	-	-	-	-	-	-	-	-	238	202

Heat Conduction Through the Axially Flowing Condensate on the Bottom of the Horizontal Tube

So far only heat transfer through the thin condensate layer on the walls of the tube has been considered. To complete the investigation, heat transfer through the axially flowing condensate on the bottom must also be evaluated. It was shown previously that at least the upstream portion of this condensate flow must be laminar since the liquid velocities increase from zero at the entrance end. If the flow is laminar and secondary flows are neglected, then heat will be transferred across this condensate by conduction only. The geometry of the cross section is shown in Figure 3.2, with an enlarged view of the corner A shown. For the sake of obtaining a well-defined boundary, it is assumed that the bottom condensate and the film meet at an angle as shown. The thermal boundary conditions may be assumed to be uniform saturation temperature, t_s, at the interface, and uniform wall temperature, t_w. In order to further simplify the solution, it may be assumed that the variations of condensate depth along the tube are gradual enough to be neglected at any particular cross-section. Thus, the governing equation can be simplified into Laplace's equation for heat conduction in two dimensions.

$\nabla^2 t = 0$ or in cylindrical coordinates

$$\frac{\partial^2 t}{\partial r^2} + \frac{1}{r}\frac{\partial t}{\partial r} + \frac{1}{r^2}\frac{\partial^2 t}{\partial \theta^2} = 0 \qquad (4.45)$$

The boundary conditions are:

$$\text{at } r = r_o \qquad t = t_w \qquad (4.46)$$

$$\text{at } r\cos\theta = r_o\cos\theta_c \qquad t = t_s \quad \text{to the edge of the film} \qquad (4.47)$$

In this form the problem becomes one of pure conduction. The particular configuration involved suggests a solution by conformal mapping. The equation of the tube circle in the x-y coordinate system shown is

$$x^2+(y+r_o\cos\theta_c)^2 = r_o^2$$
$$x^2+y^2+2yr_o\cos\theta_c = r_o^2\sin^2\theta_c \qquad (4.48)$$

Dividing by $r_o^2 \sin^2\theta_c$, and defining $X \equiv x/r_o\sin\theta_c$ and $Y \equiv y/r_o\sin\theta_c$ yields:

$$X^2+Y^2+2Y\cot\theta_c = 1$$

The moon-shaped cross-section ABCDEF of the bottom condensate may be mapped into the infinite slab A'B'C'D'E'F' shown in Figure 3.2b by using the complex transformation equation:

$$w = \ln\frac{z-1}{z+1}$$

where $w = u + iv$ and $z = X + iY$. Consequently,

$$w = \ln\frac{X-1+iY}{X+1+iY}$$

Multiplying both the numerator and denominator by $X + 1 - iY$ and simplifying yields:

$$w = \ln\left[\frac{X^2+Y^2-1}{(X+1)^2+Y^2} + i\,\frac{2Y}{(X+1)^2+Y^2}\right]$$

Since $w = u + iv$,

$$e^{u+iv} = e^u(\cos v + i\sin v) = \frac{X^2+Y^2-1}{(X+1)^2+Y^2} + i\frac{2Y}{(X+1)^2+Y^2}$$

Consequently,

$$e^u\cos v = \frac{X^2+Y^2-1}{(X+1)^2+Y^2} \quad \text{and} \quad e^u\sin v = \frac{2Y}{(X+1)^2+Y^2}$$

$$\tan v = \frac{2Y}{X^2 + Y^2 - 1} \tag{4.49}$$

The temperature distribution in the complex u-v plane is linear between t_w along A'B'C' and t_s along B'E'F'. Mathematically:

$$\frac{t - t_w}{\Delta t} = \frac{v - \phi}{\pi - \phi} \quad \text{or} \quad t^+ = \frac{v - \phi}{\pi - \phi} \tag{4.50}$$

Substituting the value of v from equation (4.49) gives the temperature distribution in the X-Y plane:

$$t^+ = \frac{\tan^{-1}\dfrac{2Y}{X^2 + Y^2 - 1} - \phi}{\pi - \phi} \tag{4.51}$$

The heat transfer through the condensate may be computed from:

$$\frac{q'}{L} = \int_{-\left(r_o \sin\phi - \frac{y_{so}}{\sin\phi}\right)}^{\left(r_o \sin\phi - \frac{y_{so}}{\sin\phi}\right)} k_\ell \left[-\frac{\partial t}{\partial y}\right]_{y=0} dx$$

where q' - heat transferred through bottom condensate, Btu/sec.

Substituting the dimensionless relations and using equation (4.51) yields:

$$\frac{q'}{L} = \int_{-\left(1-\frac{y_{so}}{r_o \sin^2\phi}\right)}^{\left(1-\frac{y_{so}}{r_o \sin^2\phi}\right)} k_\ell \Delta t \left[\frac{1}{\pi-\phi}\left(\frac{2}{1-X^2}\right)\right] dX$$

$$= \frac{2k_\ell \Delta t}{\pi-\phi}\cdot\frac{1}{2}\ln\left|\frac{1+X}{1-X}\right|_{-\left(1-\frac{y_{so}}{r_o \sin^2\phi}\right)}^{\left(1-\frac{y_{so}}{r_o \sin^2\phi}\right)}$$

$$= \frac{2k_\ell \Delta t}{\pi-\phi}\ln\left[\frac{2r_o \sin^2\phi}{y_{so}} - 1\right]$$

$$= \frac{2k_\ell \Delta t}{\pi-\phi}\ln\left[\frac{d_o \sin^2\phi}{y_{so}} - 1\right] \qquad (4.52)$$

Comparison of Heat Fluxes through the Bottom Condensate and through the Film on the Tube Walls

The heat flux per unit length through the condensing film may be computed from equation (3.18) with the constants taken as $A = 3$, $B = 6/5$, $C = 0.68$, and $D = 1$.

$$\frac{q}{L} = \left(\overline{Nu}_o \frac{k_\ell}{r_o}\right)(2\phi r_o)\Delta t$$

$$= \frac{2(4)^{\frac{3}{4}}}{3}\left[\frac{g\rho_\ell(\rho_\ell-\rho_v)\lambda(1+0.68\delta)k_\ell^3}{\mu_\ell}\right]^{\frac{1}{4}}\left[\int_0^\phi \sin^{1/3}\phi\, d\phi\right]^{\frac{3}{4}}\left[r_o\Delta t\right]^{\frac{3}{4}} \qquad (4.53)$$

Dividing equation (4.52) by (4.53) yields:

$$\frac{q'}{q} = 1.060\left[\frac{\mu_\ell k_\ell \Delta t}{g\rho_\ell(\rho_\ell-\rho_v)\lambda(1+0.68\delta)r_o^3}\right]^{\frac{1}{4}} \frac{\ln\left[\frac{d_o \sin^2\phi}{y_{so}} - 1\right]}{(\pi-\phi)\left[\int_0^\phi \sin^{1/3}\phi\, d\phi\right]^{\frac{3}{4}}} \qquad (4.54)$$

From equations (3.6), (3.9), and (3.17), with the same constants as given before equation (4.53), and setting $X = \phi$

$$\frac{d_o}{y_{so}} = \frac{2r_o\rho_\ell\lambda(1+0.68\delta)}{k_\ell\Delta t}\cdot\frac{df}{dx}$$

$$= \frac{\sqrt{2}\,\sin^{1/3}\phi}{\left[\int_0^\phi \sin^{1/3}\phi\, d\phi\right]^{\frac{1}{4}}}\left[\frac{g\rho_\ell(\rho_\ell-\rho_v)\lambda(1+0.68\delta)r_o^3}{\mu_\ell k_\ell\Delta t}\right]^{\frac{1}{4}} \qquad (4.55)$$

The ratio of heat fluxes, then, depends on the fluid properties, the quantity $\left[\Delta t/r_o^3(1 + 0.68\,\xi)\right]^{1/4}$, and the depth of the bottom condensate expressed in terms of the central half-angle ϕ. Figure 4.4 shows that this ratio is always very small for such vapor velocities where the bottom condensate still exists as a distinctly separate flow regime. For the highest flow rates encountered in the experiments with Refrigerant-113, the heat loss through the bottom condensate in a horizontal tube was about 2.5% of the heat transmitted through the condensate film on the wall according to these estimates. Turbulence of any sort in the liquid will increase this ratio, but these calculations show that the bottom condensate effectively insulates part of the condenser tube. The ratio expressed by equation (4.54) goes through a maximum near $\phi = 170°$ because the theoretical film thickness goes to infinity as ϕ approaches 180°, and the assumed geometry cannot be satisfied near this point.

One more comment is in order here. For the above calculations a sharp angle was assumed to exist where the condensate film on the wall meets the liquid flowing on the bottom of the tube. Physically this situation is impossible. A smooth surface profile connecting the two flow regimes increases the liquid thickness in this vicinity where most of the heat transfer through the bottom condensate occurs. Consequently, the actual heat transfer becomes even less than predicted by the above relations.

CHAPTER V

INTERACTIONS BETWEEN PHASES

General Considerations

Due to shear at the interfaces and the geometrical restrictions imposed by the tube, the flow patterns of the two phases are strongly interrelated. The liquid collecting in the tube restricts the vapor flow area. Waves generated at the surface increase the effective shear stress and cause an additional pressure drop in the vapor phase. On the other hand, the high velocity vapor flow draws the liquid along and causes surface instabilities. If the vapor enters the tube at a downward angle instead of axially, the bottom condensate layer will be lowered by the momentum of the incoming stream. Vapor shear was taken into account in the previous Chapter to determine the depth of the bottom condensate. Surface waves have insignificant effect on the heat transfer since the liquid acts as an effective insulator and the vapor pressure drop is negligible. However, the thin layer of wall condensate might be seriously affected by the vapor drag, especially near the entrance region. To investigate the magnitude of this phenomenon, a simple analysis was developed. Instabilities of the interface were not considered at all. The liquid film was treated as laminar everywhere, and the vapor was assumed to flow axially.

Another effect arising from the presence of two phases is surface tension. It influenced the flow pattern of the liquid primarily in two ways. First and foremost it prevented the axially flowing condensate from breaking away at the outlet into a so-called free nappe; and, consequently, raised the surface above that predicted by the critical depth theory. A rough order of magnitude estimate was developed for the maximum flow rate above which this effect becomes negligible. A second, rather insignificant, effect of surface tension was the smooth transition of the free surfaces where the wall condensate met the liquid flowing axially on the bottom. As it was found before, most of the heat transfer through the bottom condensate occurred near this region; and, consequently, this effect reduced this heat transfer rate considerably, while the wall condensate heat transfer was not influenced very much.

The Effect of Shear on the Condensate Film in a Horizontal Tube

Consider the flow of condensate on the walls of the horizontal tube. Due to gravity, the condensate will tend to flow downward and collect on the bottom of the tube. The axially flowing vapor, however, will tend to drag the liquid along due to the shear stress at the interface. Since the liquid layer is very thin compared to the tube radius, the curvature of the wall may be neglected. As a good first approximation momentum changes may also be ignored. Then the force balance for a small control volume, $(y_s - y)r_o d\phi dz$, can be written as follows.

In the ϕ direction:

$$g(\rho_l - \rho_v)\sin\phi\,(y_s - y)r_o\,d\phi\,dz - \mu\frac{\partial u}{\partial y}r_o\,d\phi\,dz = 0 \qquad (5.1)$$

which can be integrated to find the velocity distribution and the mean velocity, u_a

$$u = \frac{g(\rho_l - \rho_v)\sin\phi}{\mu_l}\left(y_s y - \frac{y^2}{2}\right) \tag{5.2}$$

$$u_a = \frac{g(\rho_l - \rho_v)\sin\phi}{3\mu_l} y_s^2 \tag{5.3}$$

In the axial, z direction:

$$\tau_v r_o \, d\phi \, dz - \mu_l \frac{\partial w}{\partial y} r_o \, d\phi \, dz = 0 \tag{5.4}$$

which can be integrated to obtain,

$$w = \frac{\tau_v}{\mu_l} y \tag{5.5}$$

$$w_a = \frac{\tau_v}{2\mu_l} y_s \tag{5.6}$$

where w is the velocity in z direction.

For laminar flow of the condensate, heat transfer is by conduction only and the temperature distribution may be assumed to be linear. Then the energy balance for an element $y_s r_o d\phi dz$ becomes:

$$\lambda(1 + 0.683) \, d\Gamma_l = k_l \frac{\Delta t}{y_s} r_o \, d\phi \, dz \tag{5.7}$$

where $\Gamma_l = Q_l \rho_l$, mass flow rate of condensate.

The mass flow rate may be expressed in terms of velocities.

$$d\Gamma_l = \frac{\partial(\rho_l u_a y_s \, dz)}{\partial \phi} d\phi + \frac{\partial(\rho_l w_a y_s r_o \, d\phi)}{\partial z} dz \tag{5.8}$$

Substituting equations (5.3), (5.6), and (5.8) into (5.7) yields:

$$\frac{g\rho_\ell(\rho_\ell-\rho_v)}{3\mu_\ell r_o} y_s \frac{\partial(y_s^3 \sin\phi)}{\partial\phi} + \frac{\rho_\ell}{2\mu_\ell} y_s \frac{\partial(y_s^2 \tau_v)}{\partial z} = \frac{k_\ell \Delta t}{\lambda'} \tag{5.9}$$

where $\lambda' = (1 + 0.68\frac{c_p \Delta t}{\lambda})$

The boundary conditions may be selected by careful examination of the flow. At the entrance of the tube an initial condensate layer thickness may be prescribed. For example, if the vapor flow can be assumed to be axial at the entrance, then a zero initial thickness may be considered. The flow must be symmetrical with respect to the vertical through the center of the tube. From the physical standpoint the thickness is finite at the top of the tube and the liquid surface continuous. It must be realized, however, that certain mathematical solutions might not be able to conform with these last two requirements. The vapor shear stress, τ_v, depends on the mass flow rate and, consequently, on z; but it may be assumed to be independent of ϕ, the angular position. The temperature difference, Δt, may be taken as constant.

Numerical Solution

Expanding equation (5.9) results:

$$\frac{g\rho_\ell(\rho_\ell-\rho_v)}{3\mu_\ell r_o}\left(\sin\phi\, y_s \frac{\partial y_s^3}{\partial\phi} + y_s^4 \cos\phi\right) +$$

$$+ \frac{\rho_\ell}{3\mu_\ell}\tau_v \frac{\partial y_s^3}{\partial z} + \frac{\rho_\ell}{2\mu_\ell} y_s^3 \frac{d\tau_v}{dz} = \frac{k_\ell \Delta t}{\lambda'} \tag{5.10}$$

Substituting $\bar{p} = y_s^{\,3}$ and rearranging yields,

$$\frac{\partial \bar{p}}{\partial z} = \frac{1}{\tau_v}\left[\frac{3\mu_l k_l \Delta t}{\rho_l \lambda'} - \frac{g(\rho_l - \rho_v)}{r_o}\left(\sin\phi\, \bar{p}^{\frac{1}{3}} \frac{\partial \bar{p}}{\partial \phi} + \right.\right.$$

$$\left.\left. + \bar{p}^{\frac{4}{3}} \cos\phi\right) - \frac{3}{2}\bar{p}\frac{\partial \tau_v}{\partial z}\right] \tag{5.11}$$

The shear stress may be expressed as a function of the Reynolds number or the mass flow rate in the following form (Equations 4.31, 4.32, 4.33)

$$\tau_v = \frac{d_{hv}^{\,b_i}}{2\rho_v \mu_v^{\,b_i} A_v^{\,2+b_i}}\, a_i \Gamma_v^{\,2+b_i} \tag{5.12}$$

$$\frac{\partial \tau_v}{\partial z} = \frac{d_{hv}^{\,b_i}}{2\rho_v \mu_v^{\,b_i} A_v^{\,2+b_i}}\, a_i (2+b_i) \Gamma_v^{\,1+b_i} \frac{d\Gamma_v}{dz} \tag{5.13}$$

where the subscript $(\ )_v$ refers to the vapor phase of the flow

d_h hydraulic diameter, ft

a_i, b_i constants depending on the range of the Reynolds number

Since at any cross section

$$\Gamma_l + \Gamma_v = \Gamma_{\text{inlet}} \text{ a constant}$$

$$d\Gamma_l = - d\Gamma_v \tag{5.14}$$

From equations (5.14) and (5.7)

$$\frac{\partial \Gamma_v}{\partial z} = - \frac{2 k_l \Delta t}{\lambda'} \int_0^{\phi} \frac{r_o}{y_s}\, d\phi \tag{5.15}$$

For a numerical solution equations (5.11), (5.12), (5.13), and (5.15) can be written in finite difference form. Since $\bar{p}_o$ at $z = 0$ is known, $\bar{p}_1$ at a small distance Δz away can be calculated. The procedure can be repeated until the end of the tube is reached or Γ_v becomes zero. Care has to be taken in the selection of points, since the thickness tends to infinity at the top of the tube at the outlet end.

In finite difference form the governing equations can be written as follows:

$$\Delta\bar{p}_n = \frac{\Delta z}{\tau_v}\left[\frac{3\mu_\ell k_\ell \Delta t}{\rho_\ell \lambda'} - \frac{g(\rho_\ell-\rho_v)}{r_o}\left\{\sin\phi\,\bar{p}_n^{\frac{1}{3}}\left(\frac{\partial\bar{p}}{\partial\phi}\right)_n + \right.\right.$$

$$\left.\left. + \bar{p}_n^{\frac{4}{3}}\cos\phi\right\} - \frac{3}{2}\bar{p}_n\frac{\partial\tau_v}{\partial z}\right] \tag{5.11a}$$

$$\left(\frac{\partial\bar{p}}{\partial\phi}\right)_n = \frac{1}{2\Delta\phi}\left(3\bar{p}_n - 4\bar{p}_{n-1} + \bar{p}_{n-2}\right), \quad n \geq 3$$

$$= \frac{-1}{2\Delta\phi}\left(3\bar{p}_n - 4\bar{p}_{n+1} + \bar{p}_{n+2}\right), \quad n = 1,2 \tag{5.14 a \& b}$$

$$\frac{d\Gamma_v}{dz} = -\frac{2k_\ell\Delta t}{\lambda'}\sum_{n=1}^{m}\frac{r_o\Delta\phi}{\bar{p}_n^{\frac{1}{3}}} \tag{5.15a}$$

Equations (5.12) and (5.13) remain the same.

Since the computer could not start with $\bar{p}_o = 0$, several small thicknesses were assumed for the first value of $\bar{p}$. The magnitude of these were determined as arbitrary fractions of the thickness at the top of the round tube without shear; that is,

$$y_{s1} = K\sqrt[4]{\frac{3\mu_\ell k_\ell r_o \Delta t}{g\rho_\ell(\rho_\ell-\rho_v)\lambda'}} \tag{5.16}$$

where K is an arbitrary constant.

The bottom condensate depth was assumed to be constant at $\phi_c = 120°$. The fluid properties used were those of Refrigerant-113, and the tube radius taken was that of the experimental condenser. In order to avoid time consuming trial and error procedures, the tube length was not specified. Instead the entering vapor flow rate was given and the corresponding tube length could be determined from the calculations.

Flow rates were varied from 0.2×10^{-4} to 4.8×10^{-4} lbf sec/ft or slugs/sec; temperature differences were from 2 to 25 °F; and the increments were taken as $r_o/10$ and 3°, $r_o/20$ and 2°.

The results showed that even for flow rates and temperature differences considerably higher than the ones encountered in the experiments, the film thickness reached essentially the same value as predicted by the no-shear theory in less than three radius lengths along the tube. Consequently shear has negligible effects as far as the thinning out of the condensate film is concerned. The experimental observations, however, indicated that the film had a wavy surface at the entrance of the tube at the highest flow rates. Such an instability problem was, of course, not included in the above analysis.

The numerical solutions became unstable after the thickness reached the no-shear values; and, consequently, the calculations could not be continued to the end of the tube. The purpose of this analysis, namely the estimate of the effect of shear near the entrance, was, however, fulfilled. A typical set of surface profiles are shown in Figure 5.1.

<u>Estimate of Transition Flow Rate for Surface Tension Effects</u>

An order of magnitude estimate may be made of the minimum flow rate below which the nappe cannot break away by considering the minimum momentum required to balance the surface tension of the solid liquid boundary formed as the nappe springs free. If uniform velocity distribution is assumed, the momentum of the flow in the horizontal direction is,

$$\rho_\ell V_m^2 A_\ell = \rho_\ell \frac{Q_\ell^2}{A_\ell} \tag{5.16}$$

The horizontal component of the surface tension at the lip of the tube outlet is:

$$P_w \sigma_{\ell v} \sin\gamma \tag{5.17}$$

where P_w wetted tube perimeter, ft

$\sigma_{\ell v}$ surface tension of liquid film, lbf/ft

γ contact angle

Equating the two expressions yields:

$$Q_\ell^2 = \frac{P_w A_\ell \sigma_{\ell v} \sin\gamma}{\rho_\ell}$$

or in dimensionless form for a round tube:

$$\frac{Q_\ell}{\sqrt{g r_o^5}} = \sqrt{\frac{2\theta_c(\theta_c - \sin\theta_c\cos\theta_c)\sigma_{\ell v}\sin\gamma}{g\rho_\ell r_o^2}} \tag{5.18}$$

For the water-plastic combination a contact angle of approximately 45° was measured. The resultant flow rate is, assuming $\theta_c = 45°$, and taking $\sigma_{l\upsilon} = 4.93 \times 10^{-3}$ lbf/ft corresponding to the approximate water temperature used of 80 °F,

$$\frac{Q_l}{\sqrt{g r_o^5}} = 0.1113$$

For the Refrigerant-113 and copper combination a contact angle of 50°,* taking $\theta_c = 45°$ and $\sigma_{l\upsilon} = 1.302 \times 10^{-3}$ lbf/ft, yields,

$$\frac{Q_l}{\sqrt{g r_o^5}} = 0.0914$$

These flow rates are both in the regime where the observed outlet depths begin to deviate from the critical depths predicted by the theory, and where the above effect became noticeable in the experiments with water.

* Personal communication from Professor P. Griffith of MIT.

CHAPTER VI

THE EXPERIMENTAL WORK

Fluid Mechanics Analogy Experiments

It was recognized at the beginning of this work that one of the weak points of previous analyses was the determination of the depth of the axially flowing condensate. The first part of the experiments was set up in order to gain more insight into the problem of a liquid flowing along a horizontal tube with the flow rate varying along the length of the tube. The importance of the outlet end conditions has been pointed out before. In these experiments special attention was given to the flow conditions existing in this region.

Description of the Apparatus

The apparatus is shown in Figures 6-1 and 6-2, and schematically in Figure 6-3. The test section consisted of a transparent plastic tube 54 inches long with an internal diameter of 1.10 inches. At twelve points along the tube, equally spaced at 4.5 inches, means were provided for admitting liquid on both sides and for letting vapor or air out at the top. This arrangement is shown in Figure 6-4. Liquid was supplied to these points from a distributor which also served as a flow-rate measuring device for each supply point. The flow rates were determined on the Venturi principle by measuring the liquid static pressure differential between the top of the distributor block and in the small stainless steel tubes through which the fluid had to flow to reach the test section. These pressure differences were read on manometers. The flow rates could be adjusted by small needle valves. The distributor chamber on top of the distributor block housed a metal and a cloth filter, and it had a valve on top which served both as a flow regulator and air bleed. This valve was connected to a line which returned the excess liquid to the collecting tank at the outlet of the test section. From this tank a small Monel Metal pump circulated the fluid through a standard commercial filter back into the distributor. Although means were provided for supplying air at the entrance of the test section, and for bleeding it off at twelve points along the tube, this part of the setup was not utilized. During the first trials it was discovered that the ripples caused by the fluid streams entering at the supply points were large enough to be "caught" by very low flows of air. The ensuing wave pattern could not be expected to be similar to the one occurring during a condensation process. Since in the second phase of the experiments the actual condensation flow patterns were to be observed, the analogy studies with a high vapor shear stress were abandoned. Thus the first phase of the experimental work endeavored primarily to establish flow depths near the end of the horizontal tube and to find the critical Reynolds numbers at which transition from laminar to turbulent flow occurs. These experiments were performed using distilled water as the fluid. This setup could not be used effectively for inclined tube experiments because in supercritical flows the liquid streams entering at the twelve supply points generated strong, oblique standing waves that made any depth measurement meaningless.

Experimental Procedure.

After the pump was started, the flow rates were adjusted at the supply points to the desired quantities. The overall flow rate was controlled by either varying the pump speed, or by regulating the valves at the pump outlet or at the distributor bleed. It was found that for the required flow rates the pump worked steadiest at a relatively low speed. Thus, most of the controlling was achieved by the valves with the pump running at the optimum. The flow rates to the individual supply points were regulated by the small needle valves mentioned before. After equilibrium was reached, the total volume flow rate was measured at the tube outlet with a graduate and a stop watch. The depth of the flow at any point was established by wrapping a strip of paper around the tube, and marking both the circumference and the points where the surface of the liquid met the walls, viewed diagonally across the tube. The temperature of the liquid was measured by a mercury-in-glass thermometer graduated in increments of 0.2 °F. Turbulence was determined by injecting ink axially into the stream through a small stainless steel syringe.

Condensation Experiments

Since very little experimental data was available in the literature that could be used directly to check the validity of the analysis, it became clear that an experimental setup was needed to furnish heat transfer data. In addition, it was deemed important that the apparatus should also furnish some information on the flow conditions existing in the tube. Refrigerant 113 ($C_2Cl_3F_3$) was chosen as the fluid because of its favorable pressure-temperature relationships.

Description of the Apparatus

The equipment is shown in Figures 6-5, 6-6, 6-7, and schematically in Figure 6-8. The vapor was generated in a 12 1/8" high boiler, made of 5 1/2" standard brass pipe, set on top of a 2000 watt flat plate heater. Inside the top of the boiler was a circular splash plate. A 7/8" o.d. copper tube served as riser from the boiler. A heater wire wrapped around an insulated portion of the tube served as superheater. The vapor passed from the riser into the 1/2" o.d. entrance tube through a heat-resistant flexible hose. The entrance tube contained a stainless steel thermocouple well and the connection to the first mercury manometer. The entrance tube joined the top of the test section at an angle of approximately 45° to allow the installation of a glass reticle at the front end of the test section. This window served both for observation and for illumination of the interior of the equipment. The condenser section consisted of a 28.25 inch long 5/8" o.d. standard finned copper tube.

The condensed liquid was discharged into a 100 cc burette. This burette was sealed into the bottom leg of the copper tee into which the outlet end of the test section was soldered. The other two legs of the tee, one directly opposite to the outlet of the test section and one on top contained observation windows. The burette was sealed with two O-rings and several layers of Glyptal compound. The observation windows were glued to a brass bushing which was sealed in the tee by two O-rings. The tee also contained the mercury manometer connection, which also served as the purge line, the condensate outlet thermocouple, and a liquid overflow connection. At the bottom of the measuring burette a needle valve was installed to serve both as a flow regulator and a shut-off device for the measurements. The overflow line had a liquid seal at the top, to prevent the escape of any vapor, and a shut-off valve.

The liquid returned to a one liter capacity glass receiver through a 3/8" o.d. copper line. The receiver supplied the boiler through a short copper tubing which was connected to the charging valve too. All parts, except the test section, the observation windows, and manometers, were insulated with glass wool insulation covered with aluminum foil. The burette insulation was divided into several sections which could be moved up and down to allow for readings to be taken at several intervals along the tube.

The electrical input to the heaters was regulated by two Variacs. The power was measured by a wattmeter connected to a switch box, which made it possible to measure the power going into both heaters with the same wattmeter.

Temperatures were measured at the entrance of the test section, at six points along the tube, at the outlet, and at any two other points as required. All thermocouples were made of No. 30 gauge copper-constantan thermocouple wires with the reference junctions kept in an iced thermos bottle. The inlet junction was housed in a stainless steel well located along the axis of the short inlet tube. The outlet junction was located right behind the lower edge of the test section. This junction was silver soldered protruding outside the stainless steel tubing through which the connections led to the outside. The location of this thermocouple forced at least part of the condensate to flow along the steel tube until it reached a splash guard which directed it into the measuring burette. The six thermocouples along the test section were soldered into grooves cut into the tube parallel to the fins. Three of these were located on the top, three at diametrically opposite points on the bottom. Four were one-sixth of the tube length from each end and two in the middle. The thermocouple wires were connected to a Leeds and Northrup semi-precision potentiometer through a ten-point selector switch.

The air velocities around the test section were controlled by two fans which were adjusted to provide a reasonably uniform flow distribution along the tube. The air velocities were measured with an Anemotherm Air Meter.

Photographs of the flow conditions inside the test tube were taken through the outlet observation window, while illumination was provided with a photographic flood light through the reticle at the entrance. Because of condensation on the reticle, pictures could not be taken through it, although visual observations were possible. A single-lens reflex camera was used with special lens attachments that provided closeup pictures at relatively restricted depth of focus. Thus the approximate location of the flow pattern picture could be determined. Visual measurements of the central angle subtended by the bottom condensate were also made with the aid of a glass reticle marked with diagonals 30° apart. To reduce the blow-out hazard, a power cut-off switch was installed at the top of the outlet manometer on the atmospheric side.

Experimental Procedure

The apparatus was placed in a constant temperature room. The system was evacuated, then it was charged with distilled Refrigerant 113. The test section was leveled by adjusting the four bolts on which the framework rested. An optical level was used to establish the horizontal position of the tube. To obtain any desired slope, up to about 10°, accurately machined steel blocks were placed under the two supporting bolts near the entrance of the test section. The following procedure was used for the test runs.

First the room temperature was established. In order to reduce the possibility of air leaking into the system, this temperature was set at such level that during the runs the system pressure always stayed above atmospheric pressure. This meant that for low flow rates of vapor higher room temperatures had to be used than for high flow rates. The air velocities around the condenser were checked next. The purge line vacuum pump was started; the main heater and, when necessary, the superheater were turned on and set at the required power level. For most runs the liquid overflow valve was kept closed, and the burette outlet needle valve was adjusted such that during equilibrium the burette was nearly full of liquid. This arrangement minimized the amount of condensation occurring outside the test section. After an initial warm-up period, the purge line was opened very slightly. The bleed flow rate was kept at a minimum by adjusting both a needle valve and a pinchcock on the vacuum line. After equilibrium was reached, data were taken in the following order, unless some special circumstances arose:

1. Barometric pressure
2. Mercury and refrigerant levels in the manometers
3. Thermocouple millivolt readings
4. Flow rates in the burette
5. Visual observations and measurements of the flow pattern
6. Photographs of the interior flow pattern at various points along the test section
7. Heater wattages and variac settings.

CHAPTER VII

DISCUSSION, CONCLUSIONS, AND RECOMMENDATIONS FOR FUTURE WORK

Discussion

The fluid mechanics analogy setup was built for the purpose of providing direct access for measurements on the liquid used. It could not fulfill all the requirements of a really close analogy to the condensation process, but it provided very useful quantitative and qualitative results that could not be obtained from a condensation experiment.

The data for these water analogy experiments are tabulated in Appendix III, Tables A-2 and A-3, for a range of flow rates of $0.02 < Q_{lo}/\sqrt{gr_o^5} < 0.6$. The results of flow depth measurements at the outlet of a horizontal tube are plotted in Figure 7.1 for both the fluid mechanics analogy and condensation experiments. The curves in the figure indicate the variation of critical depth as calculated from equation (4.16). The solid line, with $\sqrt{\alpha/\beta} = 1$ may be used for the turbulent range, $\overline{Re} > 3{,}000$; the dashed line, with $\sqrt{\alpha/\beta} = 1.414$ is applicable to laminar flows, $\overline{Re} < 3{,}000$. The experimental points for both fluids agree well with the curves, down to a flow rate of about $Q_{lo}/\sqrt{gr_o^5} = 0.08$. Below this point, the measured flow depth remained essentially constant at $\phi_c = 90°$, deviating from the theoretical curve. One, minor reason for this discrepancy is the fact that at lower flow rates the actual position of the critical depth moves closer to the outlet end of the tube where the surface profile varies rather rapidly. Thus the measurements, taken at an essentially fixed distance upstream from the end, would tend to yield greater depths. Another, much more important reason is the increasing importance of the surface tension at the lower flow rates. It was observed during the experiments with water that while at high flow rates the liquid broke away horizontally from the end of the tube to form a free nappe, at low flow rates the liquid clung to the lower lip of the outlet and flowed downward and sometimes even slightly backward from the end of the tube. This flow pattern resulted in a sharp downward curvature of the surface profile. The forces due to surface tension became large enough to effectively dam up the flow and, together with the change in pressure distribution at the overflow, caused an increase in depth. Under such circumstances the relatively simple critical depth theory was unsatisfactory since it accounted only for gravity. An order of magnitude estimate of surface tension effects was discussed in Chapter V.

The estimated accuracy of the measurements was 3% for the flow rates and 3° for the subtended angles at the point of measurement approximately 1 1/2 diameter distance from the outlet end.

The fluid mechanics analogy experiments also allowed the determination of the critical Reynolds number where transition from laminar to turbulent flow occurs. These data are shown in Table A-3 of Appendix III. The critical Reynolds number was found to be 3,580 with a minimum of disturbances and 2,830 with strong disturbances near the measuring point at the outlet.

What the fluid mechanics analogy setup could not simulate was the effect of vapor shear and the proper flow pattern in the inclined position. Both of these shortcomings arose from the local disturbances caused by the relatively concentrated liquid feeds. Even the smallest of air flows in the tube caught these local ripples and made the entire surface wavy. Consequently, it was considered meaningless to try to compare these flow patterns to the ones actually found in a condenser tube. When the tube was inclined and the flow became rather fast, these feed points generated comparatively large, standing oblique waves which made any depth measurements meaningless.

The condensation experiments provided a great deal of quantitative and qualitative information. The most important numerical results were the ones for condensate flow depths and heat transfer rates.

All these data are also tabulated in Appendix III, Tables A-5 and A-6. Flow rates varied in the range $0.007 < Q_{\ell} / \sqrt{g r_o^5} < 0.2$; the slopes ranged from $\sigma = 0$ to $\sigma = 0.1736$.

The outlet depth data for the horizontal position was discussed above, together with the water analogy data. The measured surface profiles in the horizontal position were compared to the calculated profiles in Chapter IV (p. 65), and representative values were shown in Table 4.2. The agreement was fairly good, provided that the actual outlet depth was used as the starting point for the step-by-step integration procedure. The data also indicate that the mean depth along the horizontal tube remained essentially constant for the entire range of flows at a value of $\phi_{cm} = 120°$.

For the inclined positions, a marked decrease of depth was observed up to a slope of about 0.01; a further increase in slope decreased the depth rather slowly. The ranges of mean condensate angles observed for each inclination are summarized, together with the heat transfer data, in Figures 7.2a and 7.2b. These mean angles were compared to the results calculated from equation (4.43) in Chapter IV, and comparative values were tabulated in Table 4.1. The agreement was considered good.

The measurements of the subtended angles are estimated to be within 5° of true values in the downstream portion and progressively worse upstream becoming probably about twice as much near the inlet. The flow rates are accurate to 3%.

The heat transfer data are presented in Figures 7.2a and 7.2b. The theoretical lines and experimental data correlate rather well. The increased heat transfer coefficients for the inclined tubes are clearly distinguishable. A few of the low points are mainly due to small quantities of air in the apparatus particularly at the flow rates where the inside pressure was nearly the same as the atmospheric. The greatest source of error in these measurements lies in the determination of the mean wall temperature and, consequently, the magnitude of the temperature difference. There was a strong variation of temperatures from the top to the bottom of the tube, although axial variations were small. The temperature deviated from 9 to 21% from the mean with the inclined tubes, particularly the one with the greatest slope, yielding the smaller values. The temperatures for the inlet vapor and the discharged condensate could be taken within 0.2 °F, but the wall temperature fluctuations varied from practically zero at the low flow rates to 1° at the highest. Room temperature fluctuated within 1.5° of the mean. The accuracy of volumetric flow rates was about 2%. The heat transfer results are estimated to be within about 15% of true values.

The manometer readings indicated that the maximum pressure drop in the condenser tube was of the order of 5 mm Mercury. The two, independently mounted manometers did not allow accurate readings of such small magnitudes.

Some qualitative observations do not show up in the results and will be discussed here. The biggest problem in performing the experiments with the condensation setup was to eliminate the effect of air in the system. In spite of the precautions taken small amounts of air always remained in the system, in part because the refrigerant contained some of it itself. Finally the purge line had to be installed at the outlet of the test section. The bleed was regulated at such a rate that the visual observations showed no reduction in the wall condensate film thickness. This change in thickness could be detected as a hardly noticeable ring at some cross section of the tube. By increasing the bleed rate such a ring could be made to travel to the downstream end of the tube and disappear. In order to eliminate the air from the liquid, it was allowed to boil for at least two hours before the first test of a day was started. In addition, the room temperature was kept at such a level that the system pressure was always above atmospheric. At the lower flow rates and pressure levels it was sometimes quite difficult to keep the aforementioned condensate ring at the outlet end of the tube, and a few of the data points are low quite probably because of this phenomenon.

The variation of wave patterns and ripples was very interesting to observe. In the horizontal position waves caused by the vapor shear on the bottom condensate appeared at relatively low flow rates. First they were only near the entrance region; then, with increased flow rates, they spread over the entire surface. These large shear waves, however, disappeared for the most part along the surface profiles as the tube was inclined. Instead, very tiny, oblique standing ripples occurred near the walls; and at higher flow rates occasional large traveling gravity waves were generated near the point where the liquid ramp existing in the entrance region joined the rather uniform surface along the tube. While the shear waves were rather uniform and periodic with a size up to about one-quarter of the depth; the gravity waves appeared rather randomly, traveling all by themselves, and their size was comparable to the depth. These observations indicate, among other things, that the vapor pressure drop should be less in an inclined tube not only because the vapor cross-sectional area increases, but also because of the disappearance of shear waves.

At the very highest flow rates very strong disturbances were observed at the entrance. In the horizontal tube no distinguishable bottom condensate existed here. In the inclined tube ripples appeared on the wall. Once vapor shear becomes dominant, the analytical results based on the existence of a primarily gravity controlled free-surface flow cannot be used. It is recommended, therefore, that these results should not be applied above a vapor Reynolds number of about 35,000, which was approximately the highest value encountered in these experiments.

The surface profiles, when not considering the waves, were fairly uniform along the tube for most runs. In the horizontal tubes the greatest variations occurred near the outlet, and also at the entrance due to the momentum of the vapor stream. In the inclined position, except for the smallest inclinations, the flow formed a ramp at the entrance then continued rather uniformly to the end.

Conclusions

Heat transfer rates for laminar condensation of a pure vapor in horizontal and inclined tubes can be predicted by the use of the methods presented. For fluids of Prandtl numbers greater than one, the first approximation of the momentum energy solution, equation (3.23), which is equivalent to Nusselt's results, can be employed for estimating film coefficients as a function of the condensate angle, with Rohsenow's (40) value of 0.68 used for C. For liquid metals, a correction factor from Figure 3.3 is needed, although there is no good experimental data available to check these curves. The depth of the bottom condensate can be established for horizontal or essentially subcritical flows by a step-by-step integration of equation (4.42) starting at the outlet. For horizontal tubes with a straight-cut discharge, the critical depth can be assumed to exist at the outlet if $Q_{lo} / \sqrt{g r_o^5} > 0.08$. For lower flow rates a constant outlet angle of $\phi_c = 90°$ can be used as shown in Figure 7.1. As a matter of fact, for fluids similar to Refrigerant-113, a constant mean depth of $\phi_{cm} \simeq 120°$ may be assumed over the entire range up to $Q_{lo} / \sqrt{g r_o^5} = 0.2$. These methods will yield conservative figures if applied to a condenser tube with an elbow at the outlet.

For inclined tubes equation (4.43) together with equations (4.34) can be used (integrating from $z^+ = 0.5$ to $z^+ = 1$) for calculating $\theta_{cm} = \phi_{cm}/2$.

Chaddock (10) showed that a horizontal tube is better for heat transfer than a vertical one. The results of these investigations indicate that when condensation occurs inside a single-pass condenser tube, a slight downward slope will enhance heat transfer. The optimum slope for a given flow rate can be estimated from equation (4.43) together with Figure 4.3, as described in Chapter IV. This relation is expected to yield good results even if there is an elbow at the outlet.

At high vapor flow rates above an entering vapor Reynolds number of about 35,000, these relations are no longer valid because gravity effects are negligible and the orientation of the tube becomes unimportant. In such a case, heat transfer data can be correlated in terms of a Reynolds number, irrespective of slope (2). Consequently, for condensation inside tubes, the horizontal and inclined positions are at no time worse than the vertical, and in most cases they are better. The only exception is the case of extremely short tube with a length-diameter ratio of less than about 6.

The following are brief descriptions of the calculating procedures to be used for predicting the performance of horizontal and inclined single pass condenser tubes. In each case the following quantities are specified: the entering vapor condition, the temperature differential between vapor and wall, the dimensions and slope of the tube.

For the horizontal tube two procedures may be used. The quicker and more approximate one is to assume a constant mean condensate angle of $\phi_{cm} = 120°$. Consequently, with $\phi = 180° - (\phi_{cm}/2) = 120°$, the flow rate can be calculated by integrating equation (4.36); and the Nusselt number can be evaluated from equation (3.23) with C = 0.68. The more accurate method is to assume a ϕ_{cm} and a corresponding ϕ, calculate the flow rate as before, then from Figure 7.1 find an outlet depth corresponding to the flow rate there. Starting from this end calculate the surface profile by integrating equation (4.42) stepwise along the tube. Find the mean value of ϕ over the length of the tube and compare it to the assumed value. If the two are within 10% the agreement may be considered satisfactory; otherwise a new mean angle should be assumed and the procedure repeated. With the final value of ϕ, the Nusselt number can be estimated from equation (3.23) as above.

For the inclined tube first assume a constant mean condensate angle ϕ_{cm} and its corresponding ϕ. Using ϕ, calculate the constant change of flow rate, Ω, from equation (4.36). Substitute this value into equation (4.43) and set the limits between $z^+ = 0.5$ and $z^+ = 1$. Using the angle functions (based on equations (4.34)) tabulated in Appendix VI, find several values of σ corresponding to different assumed angles. Plot the $\sigma - \phi$ curve, as shown in Figure 4.3, and find the angle ϕ corresponding to the given slope. The agreement between this value of ϕ and the originally assumed one should be within about 3° in this case. If it is not, assume a new value for ϕ and repeat the procedure. With the final value of ϕ and Ω, the flow rate and the Nusselt number can be evaluated as before from equations (4.36) and (3.23), with the latter expression multiplied by $\cos^{1/4}(\sin^{-1}\sigma)$. Actually both this function, and the angle integral function appearing in (3.23) can be read off directly from the chart in Figure 4.3. To estimate the optimum slope for the given Ω, find the point on the $\sigma - \phi$ curve for which the product of the other two coordinates, relation (4.44), is maximum.

For both horizontal and inclined tubes, the entering vapor Reynolds number should be ascertained to be less than 35,000.

Recommendations for Future Work

The many complex processes occurring during condensation inside a tube suggest a number of investigations, some of which would be highly practical while others might have only academic interest. Here a few of what seem to be the most important leads will be mentioned.

1. Experimental data is needed on liquid metals for checking the existing analyses.

2. The effect of superheat should be investigated in view of the newer theories predicting a lowering of heat transfer rates with high superheats.

3. Condensation experiments could be done with different outlet end conditions, particularly with elbows of different diameter to radius of curvature ratios, and with tubes of various length-diameter ratios.

4. The vapor flow inside a tube with a liquid occupying the bottom section could be investigated theoretically. Assuming laminar flow and neglecting liquid velocities, the flow pattern of the vapor may be calculated for different vapor-liquid cross-sectional area ratios. Then the boundary conditions found at the interface can be used to solve for the liquid velocity distribution.

5. The problem of condensation in a tube or channel with no gravity acting should be examined. Here the problem of how to move the condensate becomes important. One possibility to be explored is condensation on a porous wall through which the condensate is sucked at various rates.

6. Further experiments will be necessary with high vapor vapor velocities to study the transition regime where gravity becomes unimportant.

In all of the experimental investigations visual observations should be considered extremely important to establish the exact flow conditions occurring.

NOMENCLATURE

a	constant in boundary layer equations
a_i	constant in friction factor equations
$\mathcal{A}$	$\left.\frac{\partial u^+}{\partial y^+}\right\rvert_w$
$\mathcal{A}_{0,1,\ldots}$	perturbation terms of A
A	cross sectional area of flow, ft^2
A_h	heat transfer area, ft^2
A_ℓ	liquid cross sectional area, ft^2
A_v	vapor cross sectional area, ft^2
b	width of liquid surface, ft
b_i	exponent in friction factor equations
B	$\int_0^1 u^{+2} dy^+$
$B_{0,1,\ldots}$	constants in boundary layer equations
c	velocity of surface waves, ft/sec
$c_{p\ell}$	liquid specific heat, $Btu\text{-}ft^4/lbf\text{-}sec^2\text{-}{}^\circ F$ or $Btu/slug\text{-}{}^\circ F$
C	$1 - \int_0^1 u^+ t^+ dy^+$
$C_{0,1,\ldots}$	perturbation terms of C
C_v	correction factor for velocity distribution
$d_{h\ell}$	liquid hydraulic diameter, ft
d_{hv}	vapor hydraulic diameter, ft
d_o	diameter of tube, ft
D	$\left.\frac{\partial t^+}{\partial y^+}\right\rvert_w$
$D_{0,1,\ldots}$	perturbation terms of D

e	base of natural logarithms
$E_{0,1,\ldots}$	quantities defined in boundary layer equations
f	$u_a y_s$, volumetric wall condensate flow rate per unit length, $ft^3/sec\text{-}ft$
f_ℓ	liquid friction factor
f_v	vapor friction factor
F	$u_a y_s \left[\dfrac{D^3 g(\rho_\ell - \rho_v) k_\ell^3 \Delta t^3 \ell^3}{A \mu_\ell \rho_\ell^3 \lambda^3 (1 + C\zeta)^3}\right]^{-1/4}$, dimensionless flow rate
$\overline{Fr}$	$\dfrac{Q_\ell}{A_\ell}\sqrt{\dfrac{b}{gA_\ell}} = \dfrac{Q_\ell}{Z\sqrt{g}}$, Froude number
g	gravitational acceleration, ft/sec^2
$\bar{g}(y)$	function in boundary layer equations
$G(x)$	$\dfrac{g(\rho_\ell - \rho_v)\sin\phi}{\rho_\ell}$, variation of gravity in x direction, ft/sec^2
h	depth of flow, ft
h_c	critical depth, ft
h_m	heat transfer coefficient, $Btu/sec\text{-}ft^2\text{-}{}^\circ F$
h_{in}	enthalpy of mass entering tube, Btu/slug
h_{out}	enthalpy of mass leaving tube, Btu/slug
H	specific energy of liquid flow, ft
i	$\sqrt{-1}$
I_1	$\frac{4}{3}\sin^{-4/3}\phi \int_0^\phi \sin^{1/3}\phi \, d\phi$
I_2	$\int_0^\phi I_2 \sin^{1/3}\phi \cos\phi \, d\phi$
$j(x)$	function in boundary layer equations
$J(\eta)$	function in boundary layer equations

k_ℓ	thermal conductivity of liquid, Btu/sec-ft-°F
K	constant
$\mathcal{K}$	$\dfrac{k_\ell \Delta t\, D}{\mu_\ell \lambda (1 + C\xi)}$
ℓ	characteristic length, ft
L	length of tube, ft
m	exponent
n	exponent
N(x)	function in boundary layer equations
Nu	$\dfrac{h_m \ell}{k}$, $\dfrac{h_m r_o}{k}$, Nusselt number
$\overline{Nu}$	mean Nusselt number based on arc ϕ
$\overline{\overline{Nu}}$	mean Nusselt number based on total circumference, $\phi = \pi$
p	pressure, lbf/ft^2
$\bar{p}$	y_s^3
P_v	$r_o(\phi + \sin \phi)$, vapor wetted perimeter, ft
P_w	$r_o \phi_c$, liquid wetted perimeter, ft
$\overline{Pr}$	$\dfrac{c_p \mu_\ell}{k}$, Prandtl number
q	heat flow through wall condensate, Btu/sec
q'	heat flow through bottom condensate, Btu/sec
$\bar{q}$	volumetric liquid flow rate per unit width of channel, ft^3/sec-ft
Q	volumetric flow rate, ft^3/sec
Q_ℓ	liquid volumetric flow rate, ft^3/sec
$Q_{\ell o}$	liquid volumetric flow rate at outlet of tube, ft^3/sec
Q_v	vapor volumetric flow rate, ft^3/sec

r	radial distance, ft
r_o	radius of tube, ft
$r_{h\ell}$	$\frac{A_\ell}{P_w}$, hydraulic radius of liquid, ft
r_{hv}	$\frac{A_v}{P_v}$, hydraulic radius of vapor, ft
$\overline{Re}$	$\frac{4\rho Q}{\mu P}$, Reynolds number
$\overline{Re}_\ell$	$\frac{4\rho_\ell Q_\ell}{\mu_\ell P_w}$, liquid Reynolds number
$\overline{Re}_v$	$\frac{4\rho_v Q_v}{\mu_v P_v}$, vapor Reynolds number
s	elevation, ft
s_o	elevation of channel bottom, ft
s_c	depth of centroid of A_ℓ below surface, ft
t	temperature, °F
t_s	saturated vapor and condensate surface temperature, °F
t_w	wall temperature, °F
Δt	$t_s - t_w$
t^+	$\frac{t - t_w}{\Delta t}$
$T(\eta)$	$\frac{t_s - t}{\Delta t}$
u	velocity in x direction, ft/sec; except in complex transformation of bottom condensate cross section where
u	coordinate in complex u-v plane
u_a	$\frac{1}{y_s}\int_0^{y_s} u\,dy$, mean velocity, ft/sec
u^+	u/u_a

υ	velocity in y direction, ft/sec
v	coordinate in complex plane
V	velocity, ft/sec
V_c	critical velocity, ft/sec
V_m	mean velocity, ft/sec
ω	velocity in z direction, ft/sec
w	$u + iv$, complex variable
x	distance, ft
X	dimensionless distance in direction
y	distance, ft
y_s	wall condensate film thickness, ft
y_{so}	wall condensate film thickness at surface of bottom flow, ft
y_∞	y at ∞
y^+	y/y_s
Y	dimensionless distance in y direction
$Y_{1,2,\ldots}$	quantities defined in equation (3.38)
z	distance in axial direction, ft
z^+	z/L, dimensionless distance in z direction
Z	$A_\ell \sqrt{\frac{A_\ell}{b}} = r_o^{2.5}(\phi_c - \sin\phi_c)^{\frac{3}{2}}/4\sqrt{\sin\phi_c/2}$, section factor, $ft^{2.5}$

Greek Letters

α	$\frac{1}{AV_m^3}\int_A V^3 dA$, velocity correction
α_t	$\frac{k_\ell}{c_{p\ell}\rho_\ell}$, thermal diffusivity, ft^2/sec
β	$\frac{1}{Qh}\int_A \left(\frac{p}{\rho g} + s\right) VdA$, pressure correction
γ	contact angle
Γ	mass flow rate, slugs/sec
Γ_{in}	total mass flow rate in tube, slugs/sec
Γ_ℓ	liquid mass flow rate, slugs/sec
Γ_v	vapor mass flow rate, slugs/sec
ϵ	$\frac{BDk_\ell \Delta t}{A\mu_\ell \lambda (1 + C\zeta)}$
ζ	$\frac{c_{p\ell}\Delta t}{\lambda}$, dimensionless temperature difference
$\eta(x,y)$	transform variable for boundary layer equations
η_s	η at y_s
θ	angle in condensate
θ_c	$\phi_c/2$, condensate subtended half angle
λ	latent heat of vaporization, Btu-ft^4/lbf-sec^2 or Btu/slug
λ'	$\lambda(1 + C\zeta)$, generally $C = 0.68$
μ	viscosity, lbf-sec/ft^2
μ_ℓ	liquid viscosity, lbf-sec/ft^2
μ_v	vapor viscosity, lbf-sec/ft^2
ν	kinematic viscosity, ft^2/sec
ξ	time, sec

ρ_l	liquid mass density, lbf-sec^2/ft^4 or slugs/ft^3
ρ_v	vapor mass density, lbf-sec^2/ft^4 pr s;igs/ft^3
σ	$\frac{ds_o}{dz}$, slope
σ_{lv}	surface tension, lbf/ft
τ_s	vapor shear stress at interface, lbf/ft^2
τ_w	liquid shear stress on walls, lbf/ft^2
ϕ	surface inclination to horizontal. For round tube it is the angle from top of tube to a point on wall
ϕ_c	$2\theta_c$, central angle subtended by bottom condensate
	stream function
Ω	dQ_l /dz, axial rate of change of condensate flow, ft^3/sec-ft

<u>Subscripts and Superscripts not Defined in Nomenclature</u>

$(\ )_{x,y,..}$	differentiation with respect to variable in subscript
$(\ )_s$	at the liquid surface
$(\ )_w$	at the wall
$(\ )'$, $(\ )''$, $(\ )'''$	derivatives

BIBLIOGRAPHY

1. Abramowitz, M., "Tables of Functions," J. of Research, National Bureau of Standards, 47, 288, 1951.

2. Akers, W. W., H. A. Deans, and O. K. Grosser, "Condensing Heat Transfer within Horizontal Tubes," Second Nat'l Heat Transfer Conference, AIChE-ASME Preprint 1, 1958.

3. Akers, W. W. and H. R. Rosson, "Condensation Inside a Horizontal Tube," Third Nat'l Heat Transfer Conference, ASME-AIChE Preprint 114, 1959.

4. Altman, M., F. W. Staub, and R. H. Norris, "Local Heat Transfer and Pressure Drops for Refrigerant-22 Condensing in Horizontal Tubes," Third Nat'l Heat Transfer Conference, ASME-AIChE Preprint 115, 1959.

5. Balekjian, G. and D. L. Katz, "Heat Transfer from Superheated Vapors to a Horizontal Tube," Paper No. 57-Ht-27, ASME-AIChE Joint Heat Transfer Conference, August 11, 1957.

6. Benning, A. F. and R. C. McHarness, "The Thermodynamic Properties of 'Freon-113' (CCl_2F-$CClF_2$)," E. E. du Pont de Nemours & Co., Inc., Bulletin No. T-113A.

7. Bromley, L. A., "Effect of Heat Capacity on Condensation," Ind. Eng. Chem., 44, No. 12, 2966, 1952.

8. Bromley, L. A., R. S. Brodkey, and N. Fishman, "Effect of Temperature Variation around a Horizontal Tube, Ind. Eng. Chem., 44, No. 12, 2962, 1952.

9. Carpenter, F. G. and A. P. Colburn, "Effect of Vapor Velocity on Condensation Inside Tubes," General Discussion on Heat Transfer, London, England, 1951, U.S. Section I.

10. Chaddock, J. B., "Film Condensation of Vapor in Horizontal Tubes," Sc.D. Thesis, MIT, 1955; and Refrigerating Engineering, 65, No. 4, 37, April, 1957.

11. Chen, M. M., "An Analytical Study of Laminar Film Condensation; Part I, Flat Plates, and Part II, Single and Multiple Horizontal Tubes," To be presented at the semi-annual meeting of the ASME, 1960, at Buffalo, N. Y., ASME Paper Nos. 60-H-44A and B.

12. Chow, V. T., "Integrating the Equation of Gradually Varied Flow," Proc. ASCE, 81, No. 838, Nov. 1955. Discussion by A. S. Harrison, Proc. ASCE, 82, No. 1010, June, 1956.

13. Chu, J. C., et al, "Heat Transfer Coefficient of Condensing Vapors," J. of Appl. Chem., 73, Feb. 1951.

14. Colburn, A. P., "Problems in Design and Research on Condensers of Vapors and Vapor Mixtures," Proc., Inst. of Mech. Eng., 164, 448, 1951.

15. Dixon, J. R.,"Condensate Flow in Horizontal Tubes," S.M. Thesis, MIT, 1953.

16. Gazley, C., Jr., et al, "Co-Current Gas-Liquid Flow," Parts I, II and III, Heat Transfer and Fluid Mechanics Institute, 1949.

17. Grigull, U., "Heat Transfer in Film Condensation," Forsch. Ing. Wes., 18, No. 1, 10, 1952.

18. Hakimi, N., "Refrigerant-12 Condensation Inside a Horizontal Tube," S.M. Thesis, MIT, 1959.

19. Hassan, K. and M. Jakob, "Laminar Film Condensation of Pure Saturated Vapors on Inclined Circular Cylinders," ASME Paper No. 57-A35, 1957.

20. Hassan, K., "Laminar-Film Condensation of Pure Saturated Vapors at Rest on Non-Isothermal Surfaces," ASME Paper No. 58-A-232, 1958.

21. Hermann, R., "Heat Transfer by Free Convection from Horizontal Cylinders in Diatomic Gases," NACA TM 1366, 1954.

22. Hinds, J., "Side Channel Spillways," Trans. Am. Soc. Civ. Eng., 89, 881, 1926.

23. Jaeger, C., Engineering Fluid Mechanics, Blackie & Sons, Ltd., London, 1956.

24. Jakob, M., Heat Transfer, John Wiley & Sons, Inc., New York, 1949.

25. Jakob, M., Mech Eng., 58, 729, 1936.

26. Jakob, M., S. Erk, and H. Eck, Zeitschr. d. Ver. deutsch. Ing., 73, 1517, 1929.

27. Katz, D. L., et al, "Condensation of Freon-12 with Finned Tubes," Refr. Eng., 33, 211 and 315, 1947.

28. Katz, D. L. and J. M. Geist, "Condensation on Six Finnes Tubes in a Vertical Row," Trans. ASME, 70, 907, 1948.

29. Kenney, G. R., A. E. Abramson and J. L. Sloop, Internal Liquid-Film Cooling Experiments with Air-Stream Temperatures to 2000 °F in 2 and 4 inch Diameter Horizontal Tubes, NACA Rep. No. 1067, 1952.

30. Knuth, E. H., "The Mechanics of Film Cooling - Part I, Jet Propulsion, 24, 359, 1954; Part II, 25, No. 1, 16, 1955.

31. Lamb, Sir H., Hydrodynamics, Dover Publications New York, 1945.

32. Lehtinen, J. A., "Film Condensation in a Vertical Tube Subject to Varying Vapor Velocity," Sc.D. Thesis, MIT, June 1957.

33. Li, W., "Open Channels with Non-Uniform Discharge," Proc. ASCE, 80, No. 381, January 1954.

34. McAdams, W. H., Heat Transmission, McGraw-Hill Book Co., Inc. New York, 3rd. Edition, 1954.

35. Markwood, W. H. and A. F. Benning, "Thermal Conductances and Heat Transmission Coefficients of 'Freon' Refrigerant," E. I. du Pont de Nemours & Co. Bulletin No. B-9, 1942.

36. Misra, B. and C. F. Bonilla, "Heat Transfer in the Condensation of Metal Vapors," Chem. Eng., Progress Symposium Series No. 18, Vol. 52, 7.

37. Nusselt, W., "The Surface Condensation of Steam," Zeitsch. d. Ver. deutsch. Ing., 60, 541 and 569, 1916.

38. Peck, R. E. and W. A. Reddie, "Heat Transfer Coefficients for Vapor Condensing on Horizontal Tubes, " Ind. and Eng. Chem., 43, No. 12, 2926, 1951.

39. Potter, R. C. and S. P. Patel, "Condensation of 'Freon-12' Inside a Horizontal Tube," Refr. Eng., 64, No. 5, 45, 1956.

40. Rohsenow, W. M., "Heat Transfer and Temperature Distribution in Laminar Film Condensation," ASME Paper No. 54-A-144, 1954.

41. Rohsenow, W. M., J. H. Webber, and A. T. Ling, "Effect of Vapor Velocity on Laminar and Turbulent Film Condensation," ASME Paper No. 54-A-145, 1954.

42. Rouse, H., Engineering Hydraulics, Proc. of the Fourth Hydraulics Conference, Iowa Inst. of Hydraulic Research, 1949, John Wiley & Sons, Inc.

43. Schlichting, H., Boundary Layer Theory, McGraw-Hill Book Co., Inc., New York, 1955.

44. Schmidt, T. E., "Heat Transfer during Condensation in Containers and Tubes," Kaltetechnik, 282, Nov. 1951.

45. Schrage, R. W., A Theoretical Study of Interphase Mass Transfer, Columbia University Press, New York, 1953.

46. Sparrow, E. M. and J. L. Gregg, "A Boundary-Layer Treatment of Laminar-Film Condensation," Trans. ASME, Series C, J. of Heat Transfer, 81, 13, 1959.

47. Sparrow, E. M. and J. L. Gregg, "Laminar Condensation Heat Transfer on a Horizontal Cylinder," Trans. ASME, Series C. J. of Heat Transfer, 81, 291, 1959.

48. Staub, L. B., et al, "Open-Channel Flow at Small Reynolds Numbers," Trans. ASCE, 123, No. 2935, 1958.

49. Tepe, J. B. and A. C. Mueller, "Condensation and Subcooling Inside an Inclined Tube," Chem. Eng. Prog., 43, 267, 1947.

50. Trapp, A., "Heat Transfer for the Condensation of Ammonia," Warme und Kaltetechnik, 42, 161, 1940.

51. Trapp, A., "Condensation of Alcohol Vapors," Zeitschrift de. Ver. deutsch Ing., 85, 959, 1941.

52. Young, F. L. and W. J. Wohlenberg, "Condensation of Saturated Freon-12 Vapor on a Bank of Horizontal Tubes, " Trans. ASME, 64, 787, 1942.

LIST OF FIGURES

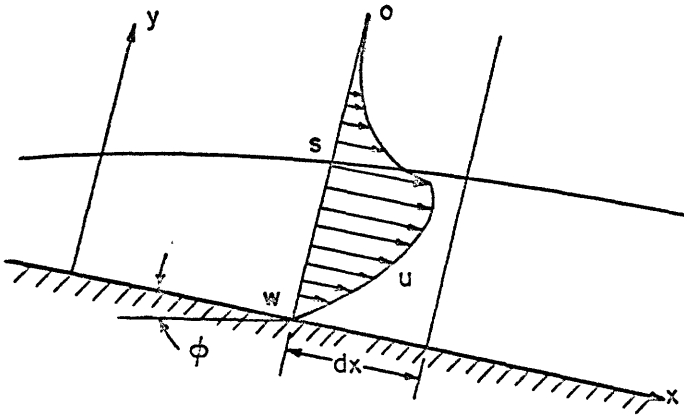

CONDENSATE FLOW ON AN INCLINED SURFACE
FIG. 3.1

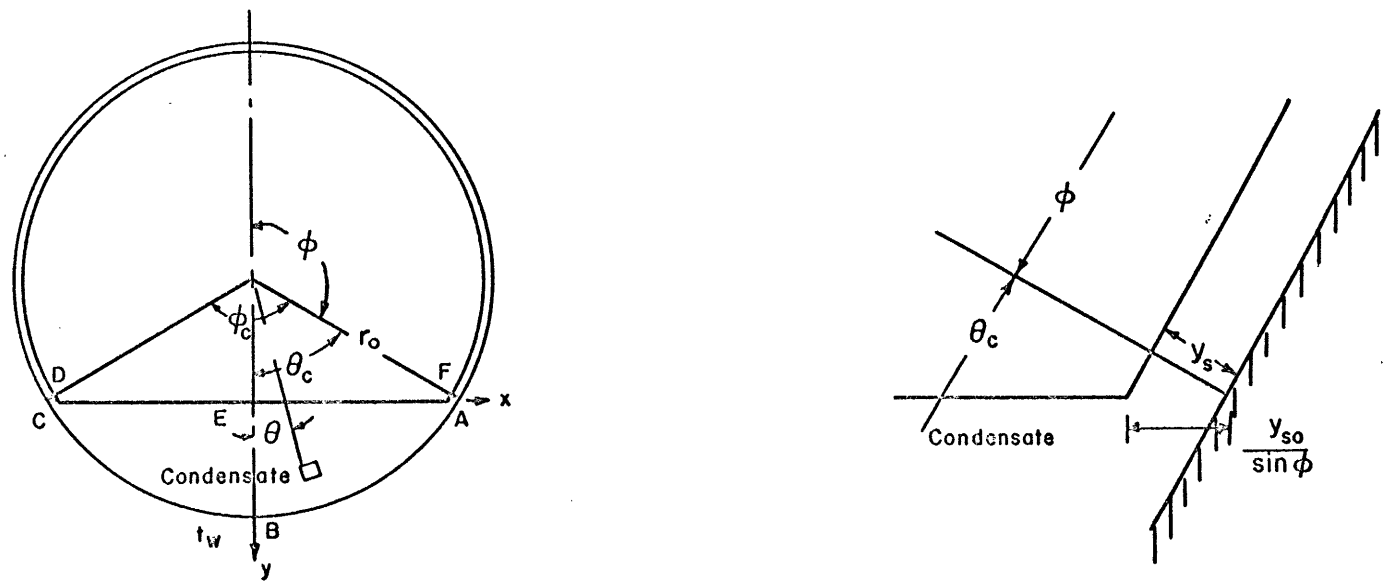

GEOMETRY OF CONDENSATE FLOW INSIDE THE TUBE
FIG. 3.2a

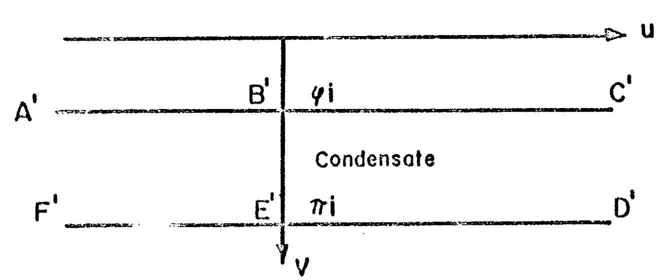

GEOMETRY OF CONDENSATE FLOW ON COMPLEX u-v PLANE
FIG. 3.2b

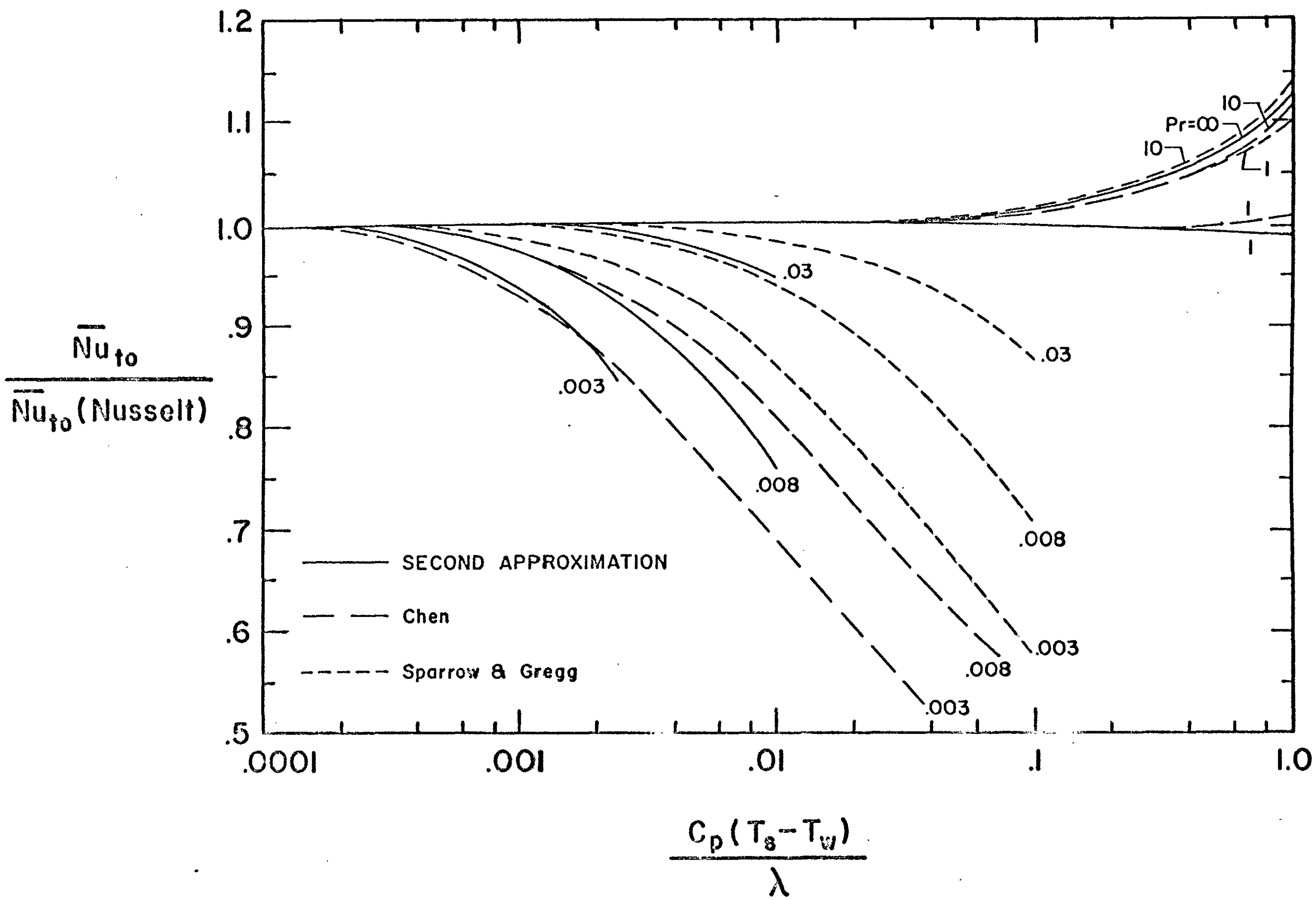

THEORETICAL HEAT TRANSFER RESULTS
FIG. 3.3

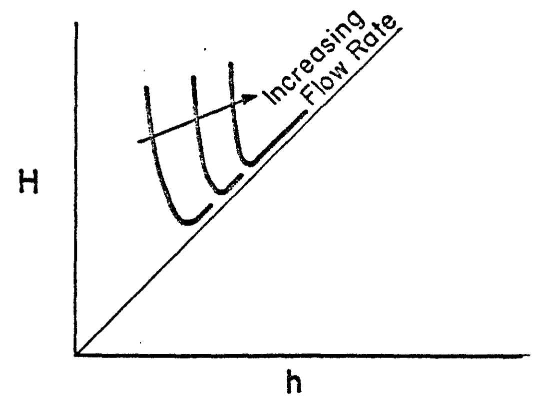

SPECIFIC HEAD VS. DEPTH FOR FREE SURFACE FLOWS
FIG. 4.1

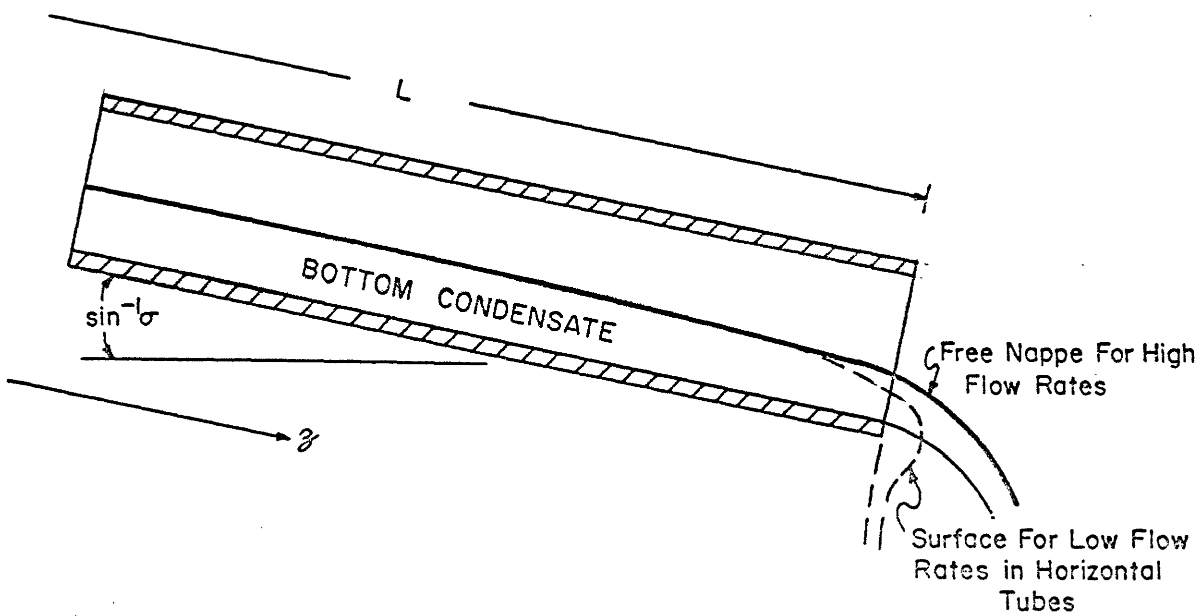

GEOMETRY OF BOTTOM FLOW ALONG THE TUBE
FIG. 4.2

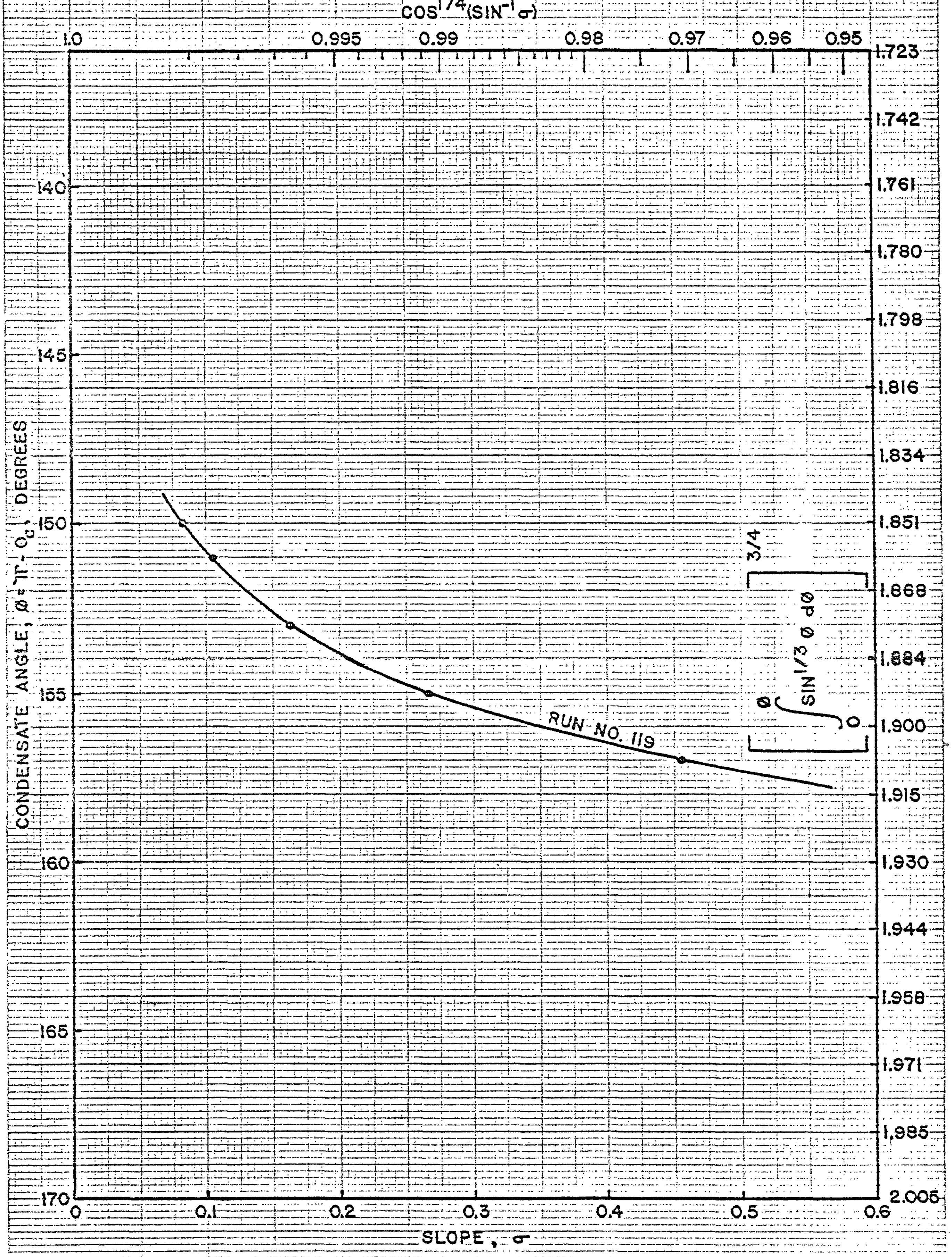

SLOPE OPTIMIZING CHART FOR CONDENSER TUBES

FIG. 4.3

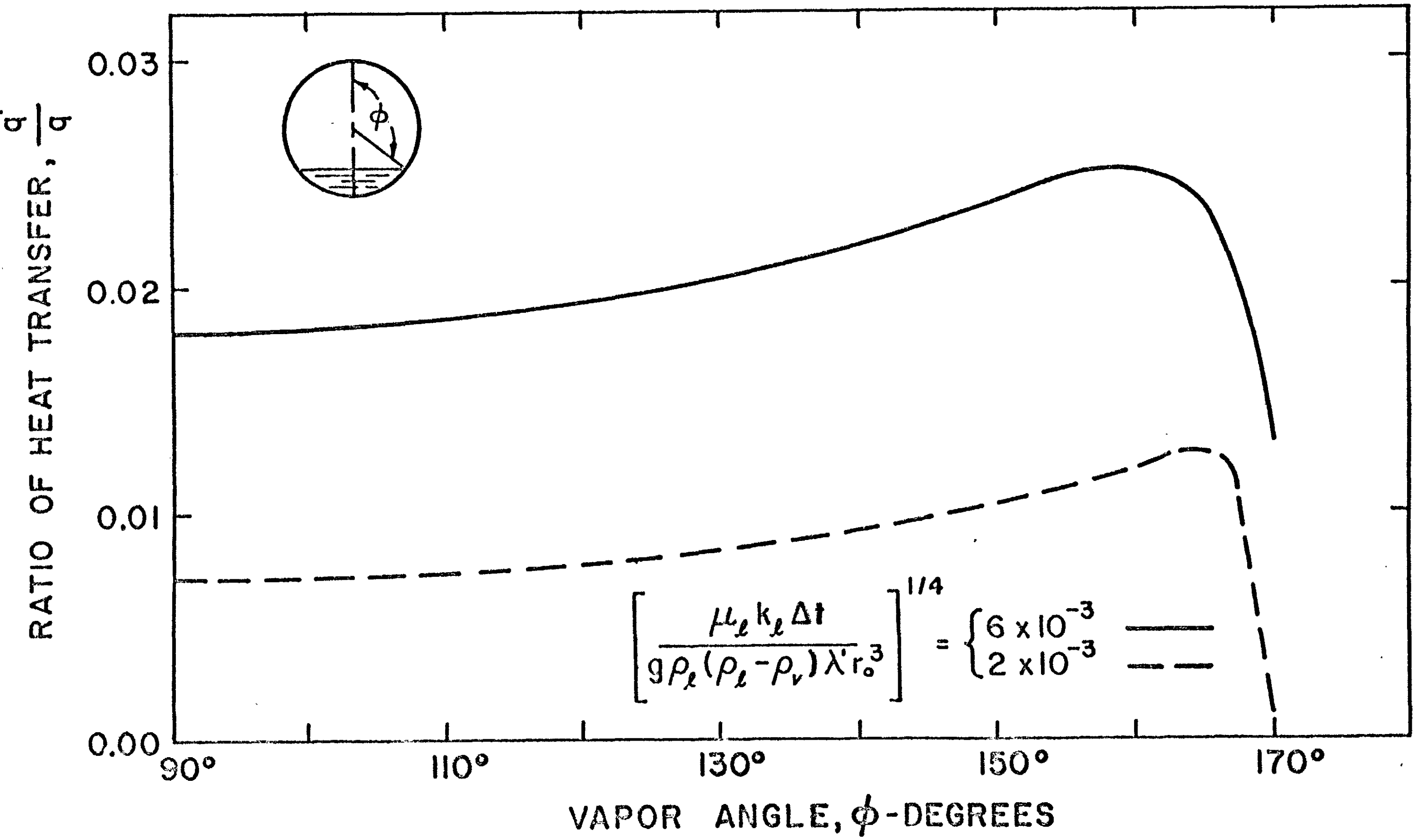

RATIO OF HEAT QUANTITIES TRANSFERRED THROUGH THE BOTTOM CONDENSATE AND THE WALLS

FIG. 4.4

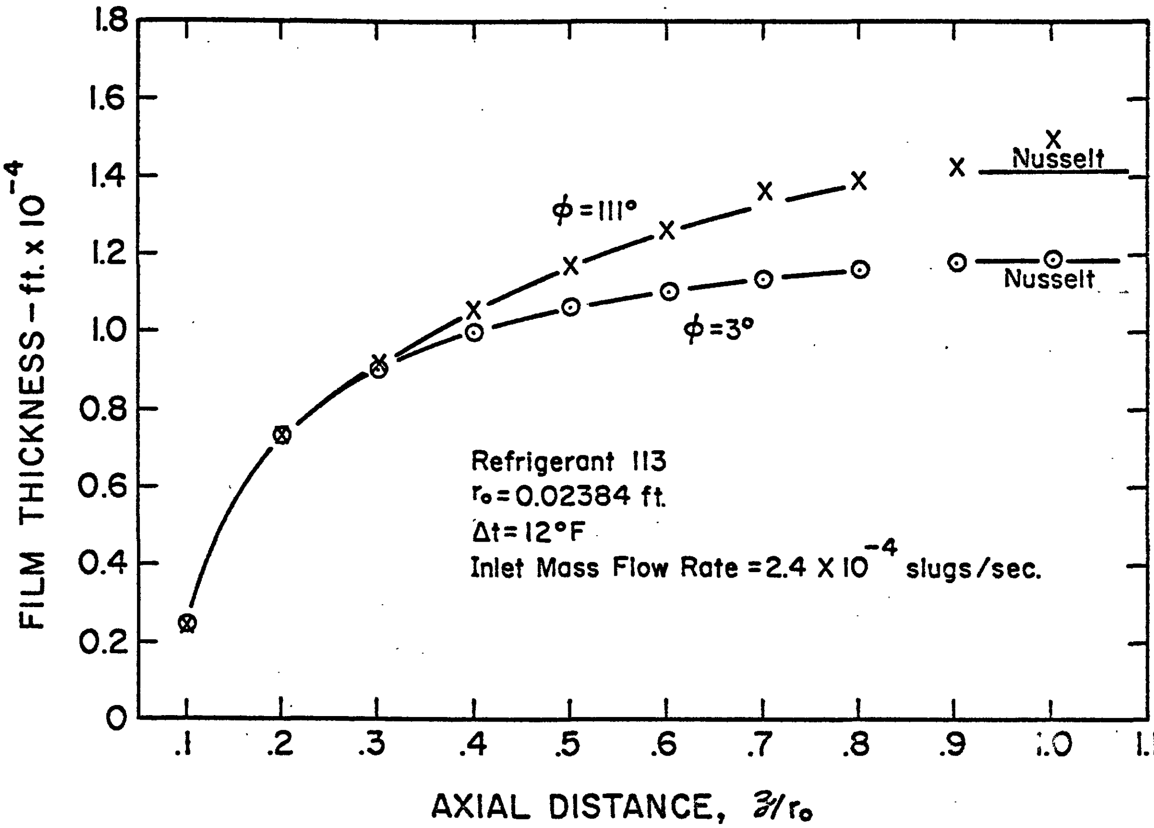

CALCULATED SURFACE PROFILES AT TUBE ENTRANCE
FIG. 5.1

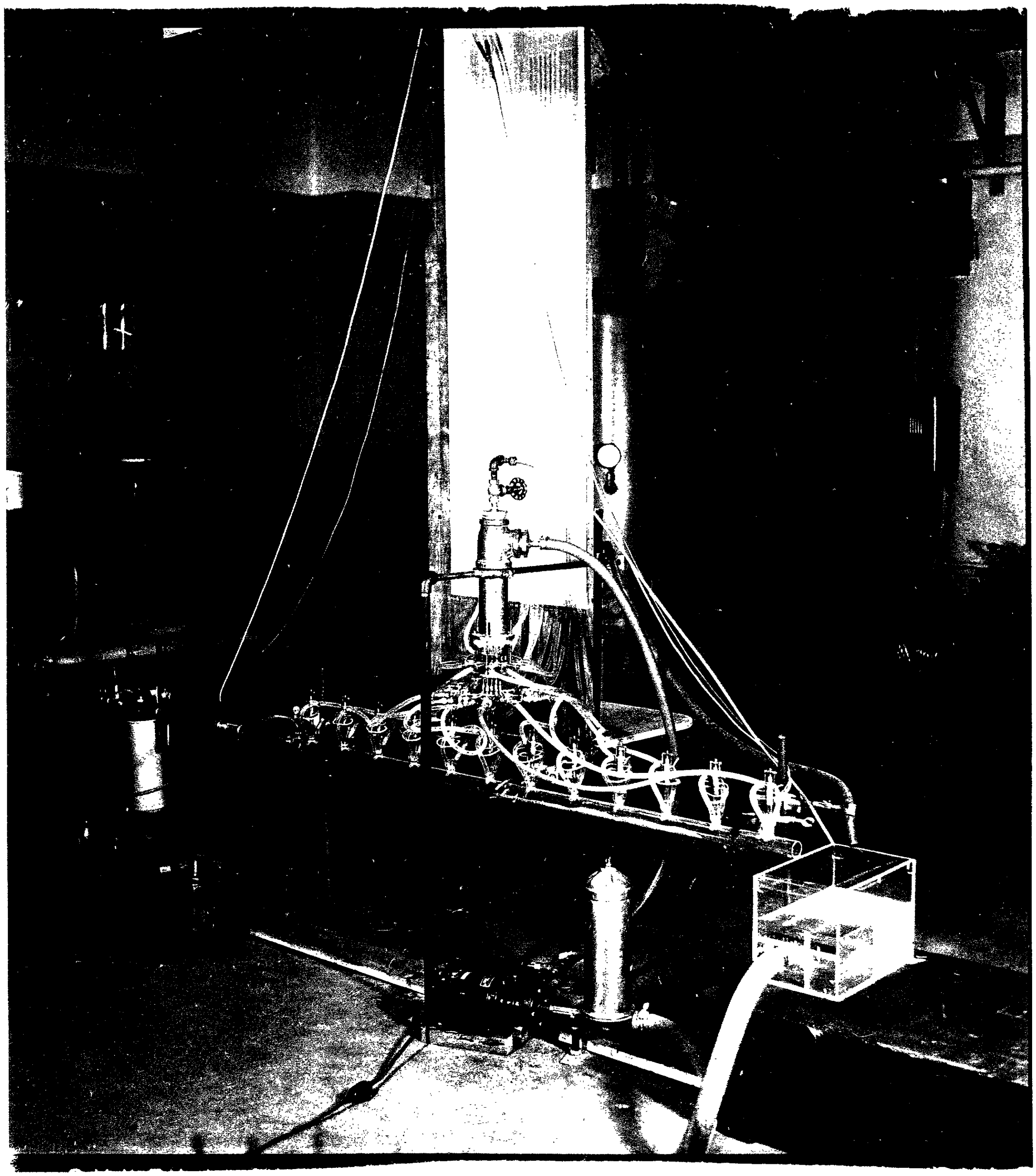

FLUID MECHANICS ANALOGY APPARATUS

FIG. 6.1

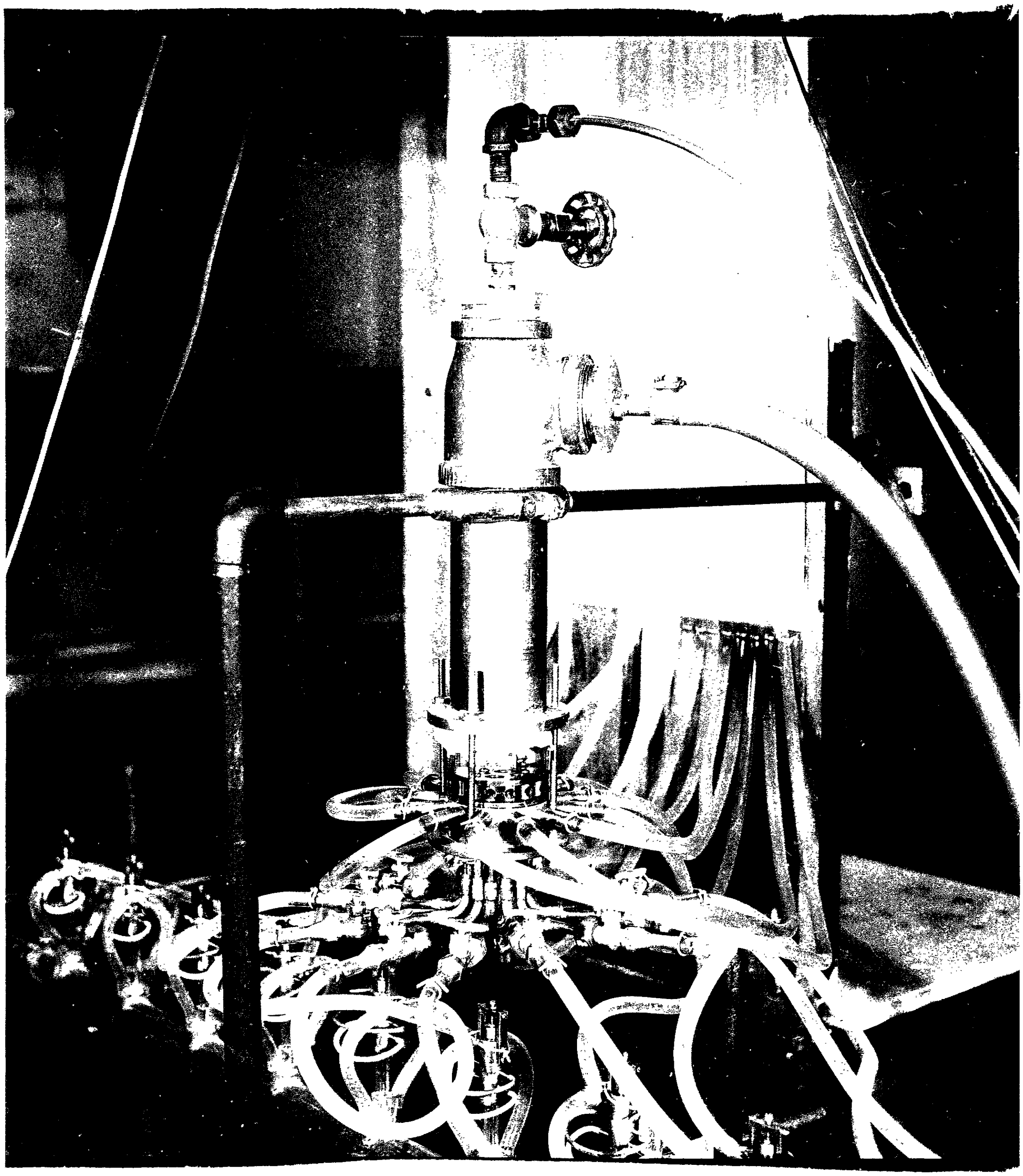

LIQUID DISTRIBUTOR

FLUID MECHANICS ANALOGY APPARATUS

FIG. 6.2

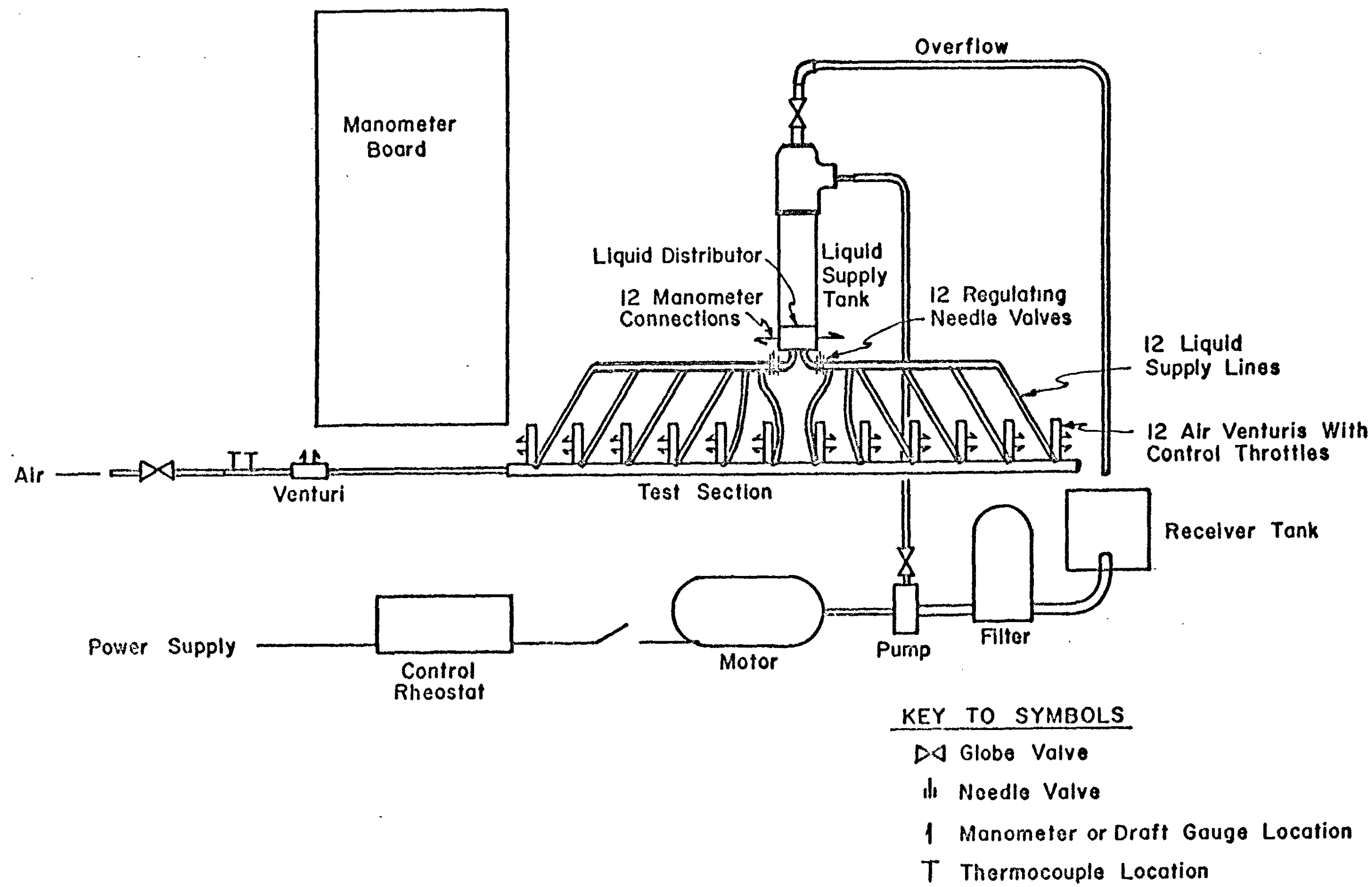

SCHEMATIC DIAGRAM OF SETUP FOR FLUID MECHANICS ANALOGY EXPERIMENTS
FIG. 6.3

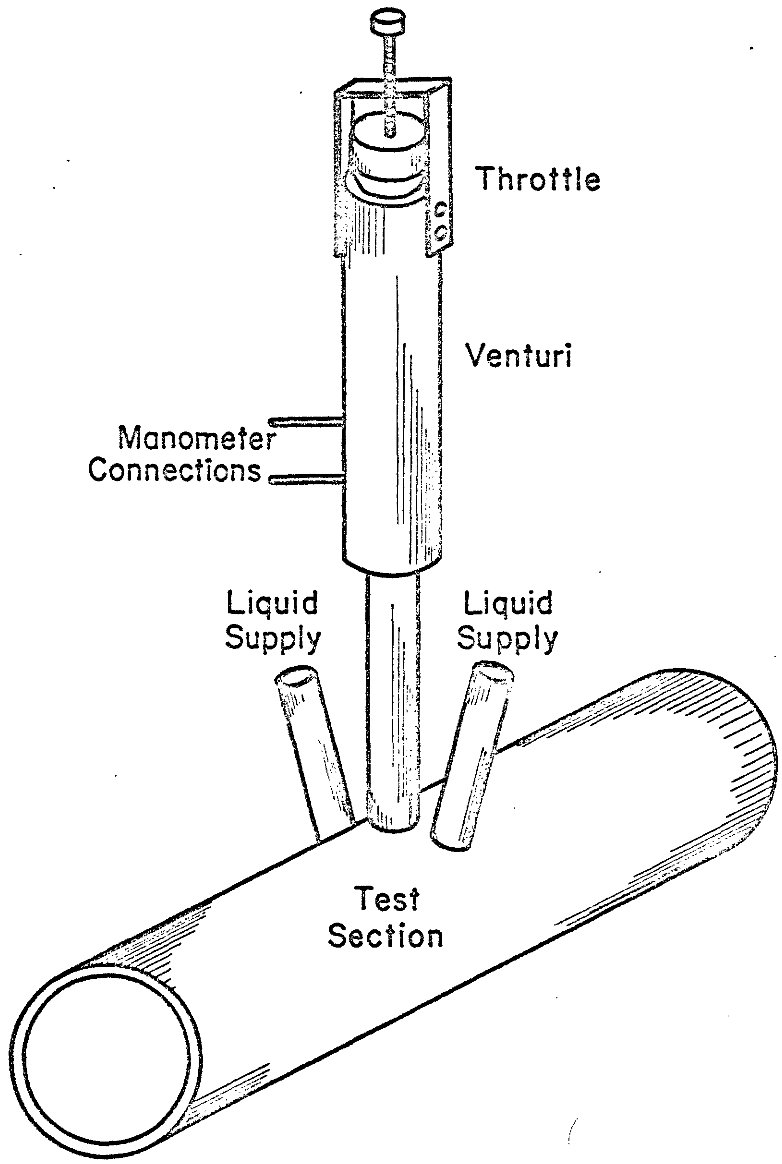

DETAIL OF TEST SECTION
FOR FLUID MECHANICS ANALOGY EXPERIMENTS
FIG. 6.4

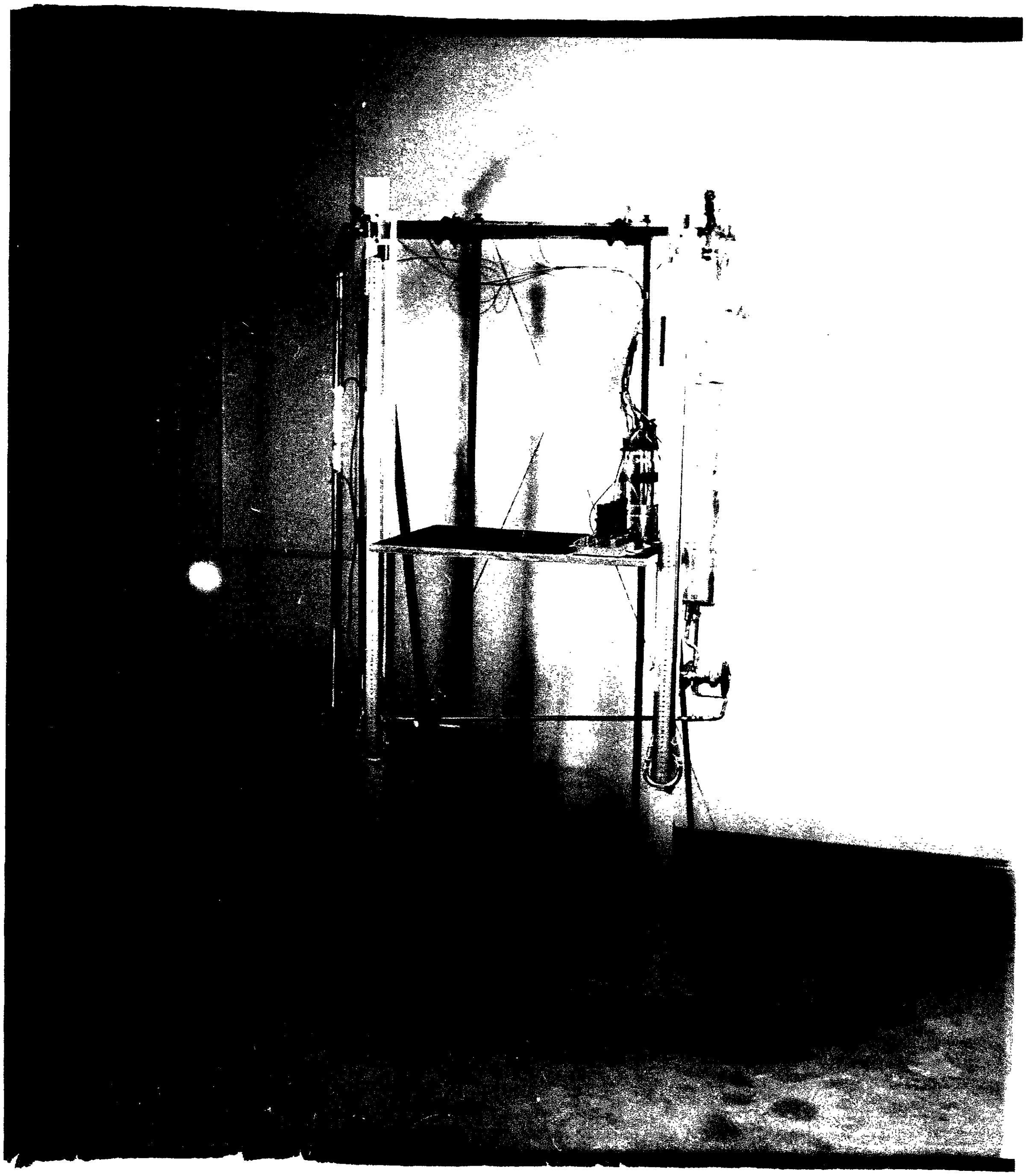

CONDENSER SETUP

FIG. 6.5

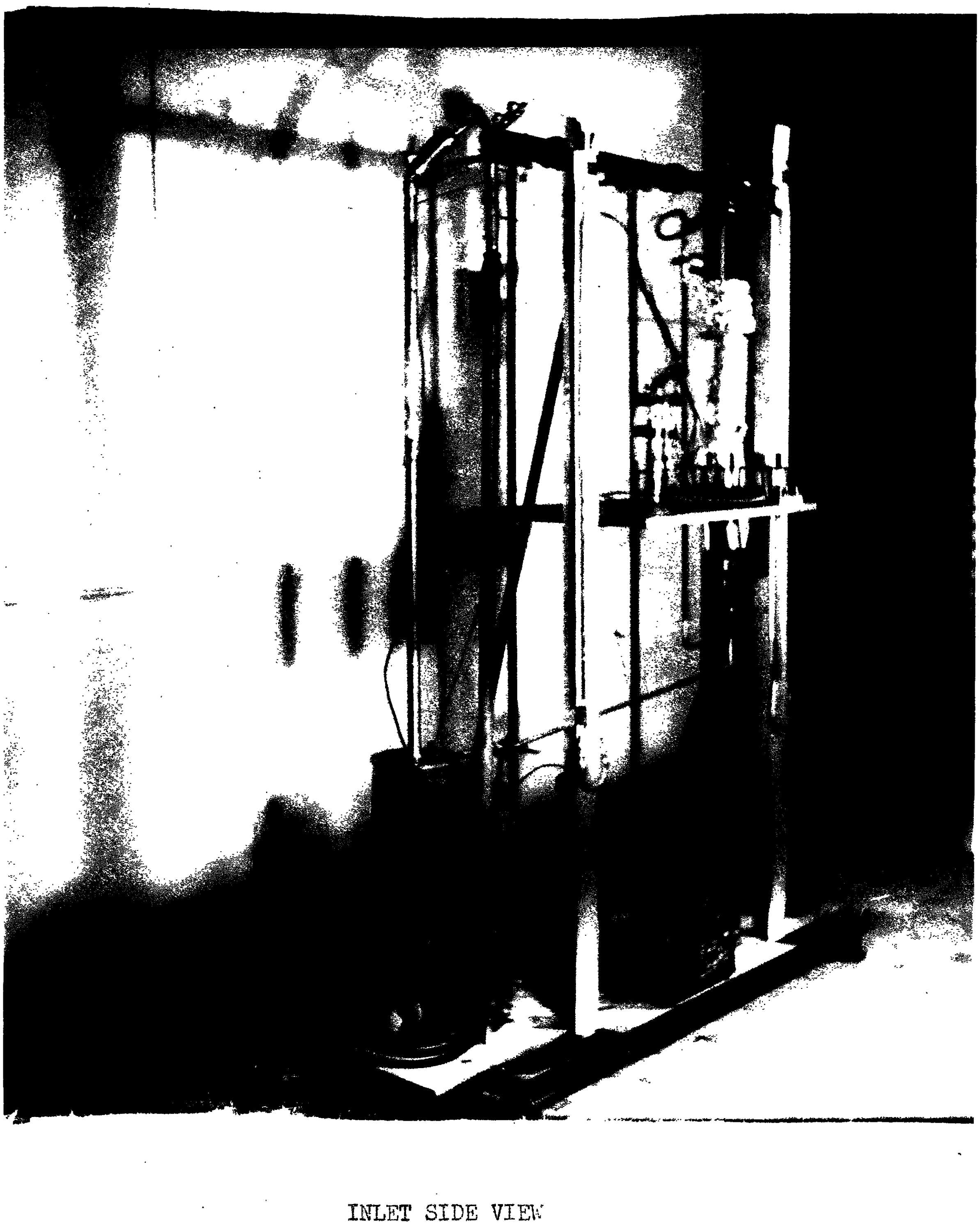

INLET SIDE VIEW
CONDENSER SETUP

FIG. 6.6

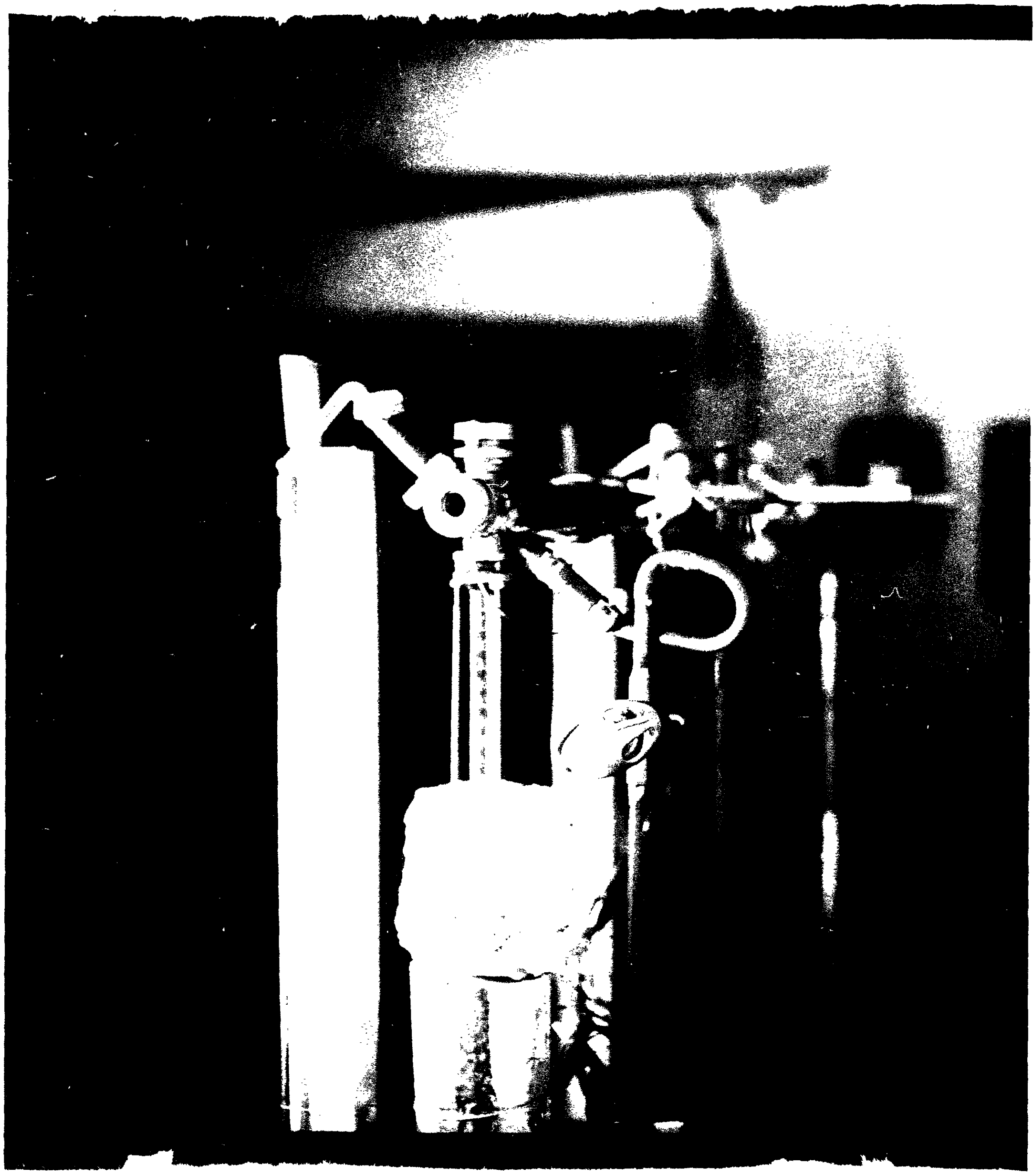

DISCHARGE SIDE VIEW
CONDENSER SETUP

FIG. 6.7

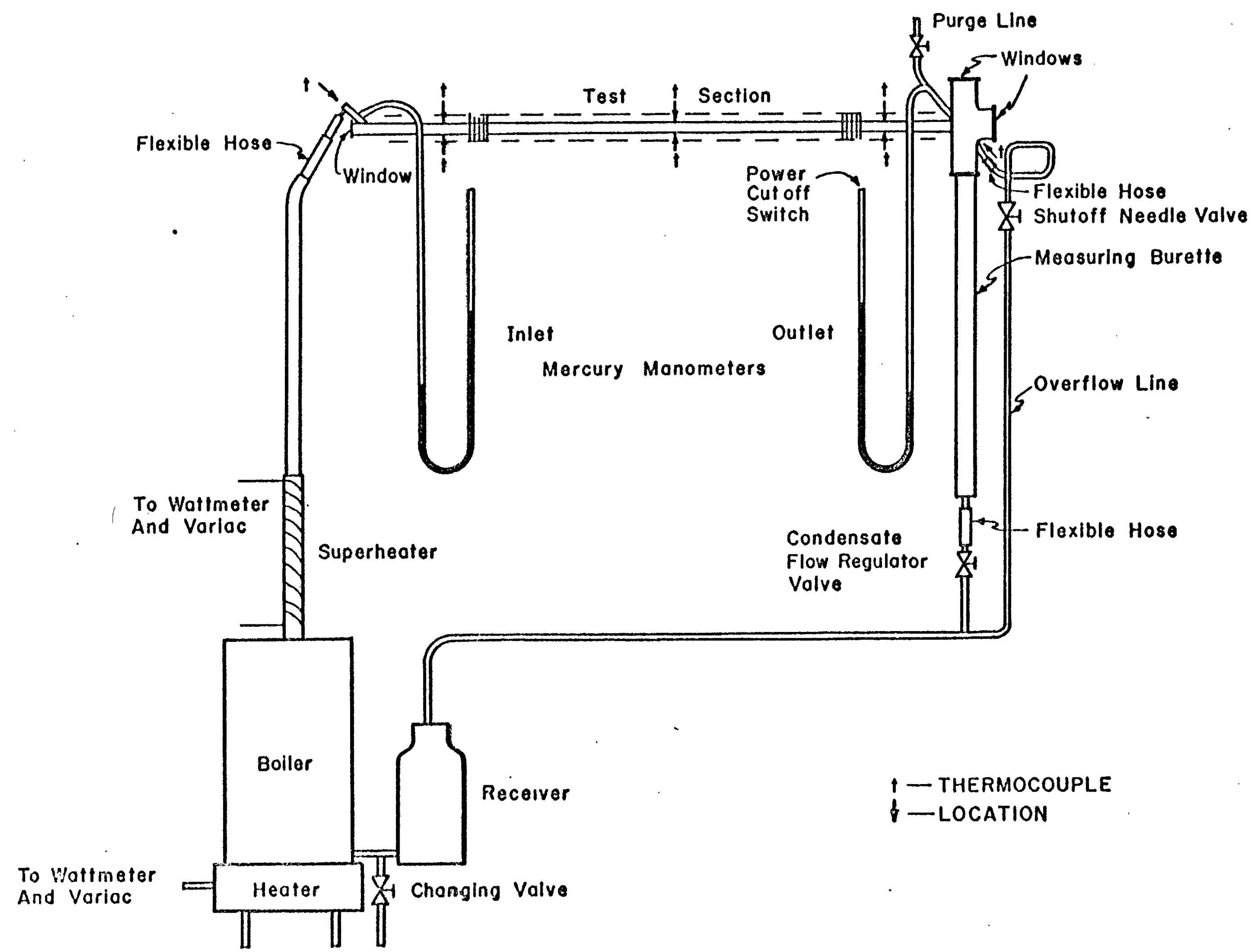

SCHEMATIC DIAGRAM OF SETUP FOR CONDENSATION EXPERIMENTS
FIG. 6.8

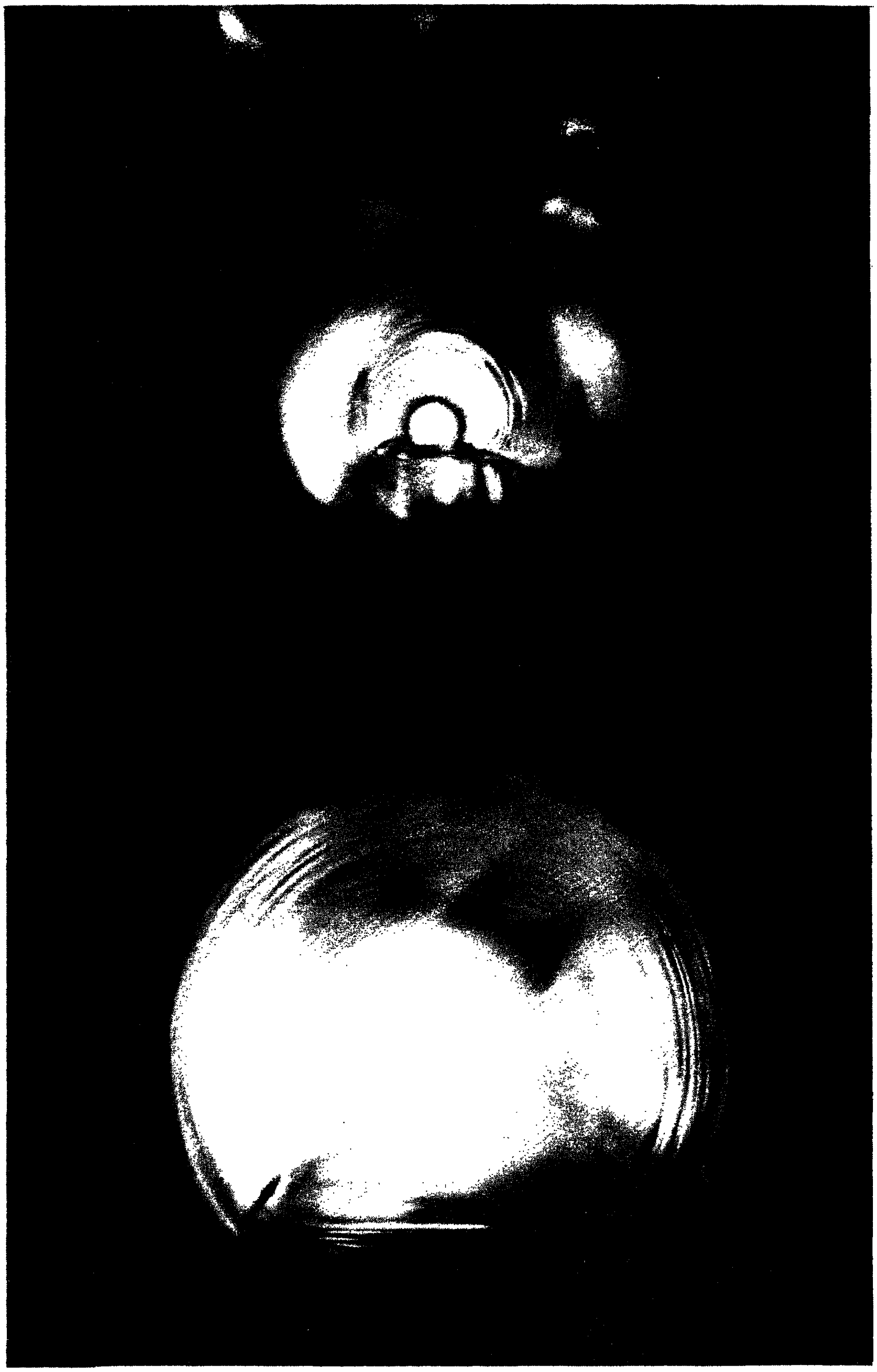

TYPICAL PHOTOGRAPHS SHOWING FLOW PATTERNS
IN THE CONDENSER TUBE

UPSTREAM END ON TOP

DOWNSTREAM END ON BOTTOM

FIG. 6.9

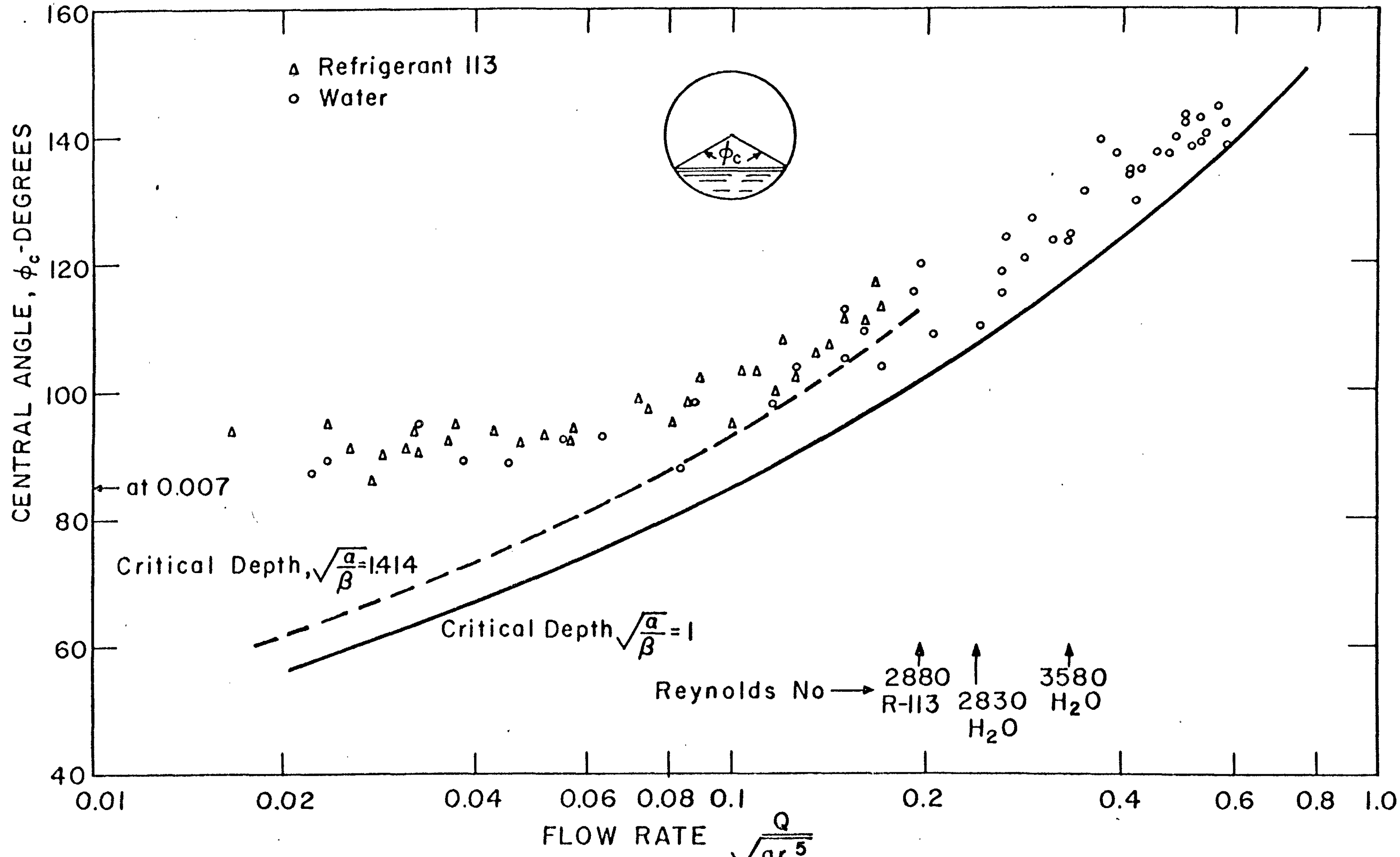

DISCHARGE DEPTH VS. FLOW RATE IN HORIZONTAL TUBES

FIG. 7.1

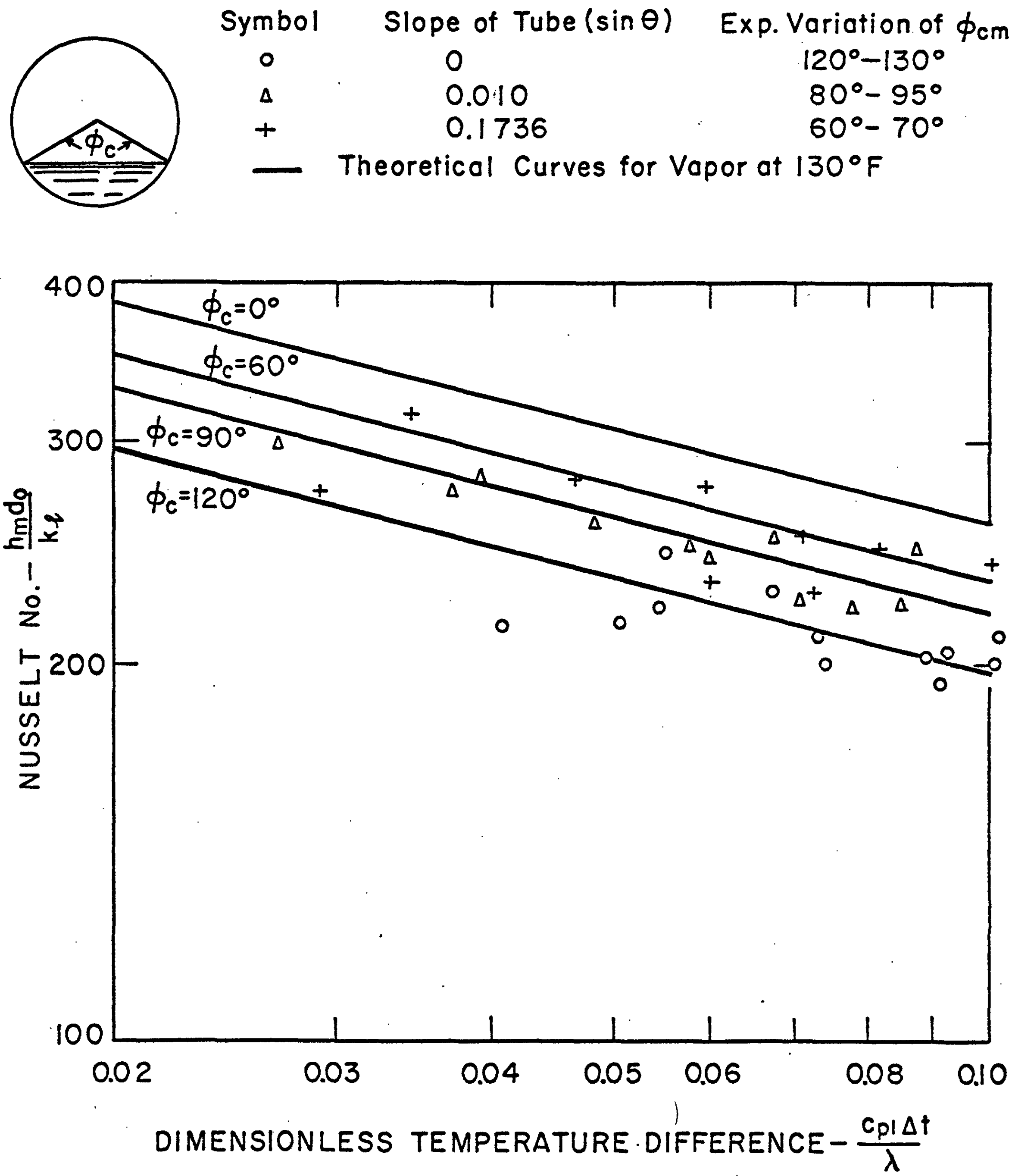

CONDENSATION OF REFRIGERANT 113
SELECTED HEAT TRANSFER RESULTS
FIG. 7.2 a

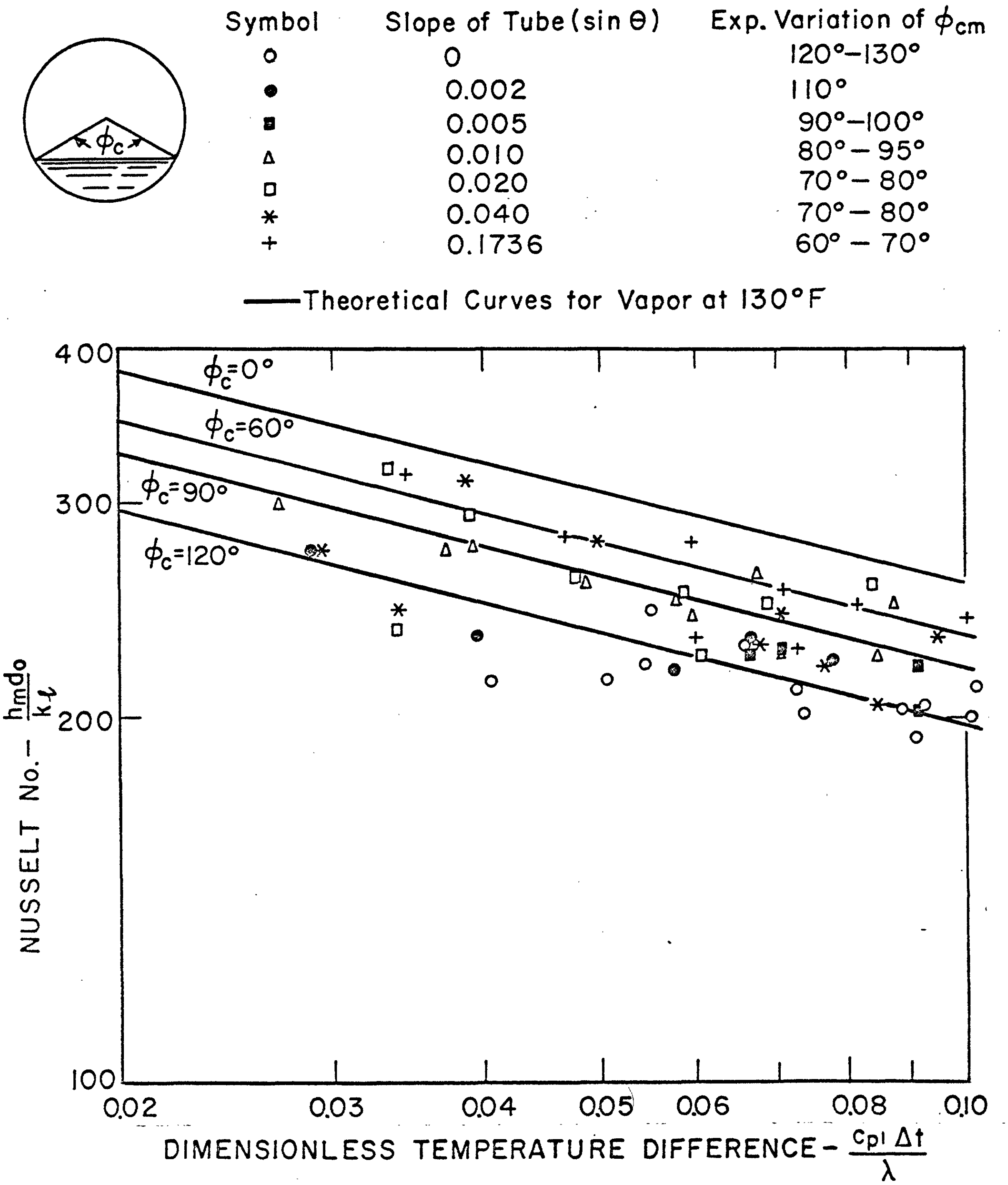

CONDENSATION OF REFRIGERANT 113
HEAT TRANSFER RESULTS
FIG. 7.2 b

APPENDIX I

DETERMINATION OF THE INTERFACE BOUNDARY CONDITIONS

DETERMINATION OF THE INTERFACE BOUNDARY CONDITIONS

To find the interface boundary conditions, the vapor velocity profile has to be established at least approximately. The momentum equation for an element of the vapor phase between $y > y_s$ and $y \to \infty$ is,

$$\mu_v \frac{\partial u_v}{\partial y} + u_v \frac{d}{dx}\left[\int_0^{y_s} \rho_\ell u_\ell \, dy + \int_{y_s}^{y} \rho_v u_v \, dy \right] + \frac{d}{dx}\int_y^{\infty} \rho_v u_v^2 \, dy = 0 \tag{A.1}$$

In dimensionless form, using the same development that led to equation (3.8),

$$\frac{\mu_v}{\mu_\ell} \frac{\partial u_v^+}{\partial y^+} + \frac{\rho_\ell}{\mu_\ell} y_s \frac{df}{dx}\left\{ u_v^+ \left[1 + \frac{\rho_v}{\rho_\ell}\int_0^{y^+} u_v^+ \, dy^+ \right] + \frac{\rho_v}{\rho_\ell}\left[2 - \frac{f \frac{dy_s}{dx}}{y_s \frac{df}{dx}} \right] \int_{y^+}^{\infty} u_v^{+2} \, dy^+ = 0 \tag{A.2}$$

If $\rho_v / \rho_\ell << 1$, terms containing this ratio may be neglected. Using equation (3.6) yields:

$$\frac{\mu_v}{\mu_\ell} \frac{\partial u_v^+}{\partial y^+} = - \frac{k_\ell \Delta t \, D}{\mu_\ell \lambda (1 + C\xi)} u_v^+ = - \mathcal{K} u_v^+ \tag{A.3}$$

The solution of this equation is:

$$u_v^+ = u_s^+ \, e^{\frac{\mu_l}{\mu_v} \mathcal{K}(1-y^+)} \tag{A.4}$$

Now write the momentum equation for an element starting in the liquid surface

$$\mu_l \frac{\partial u_l}{\partial y}\bigg|_s + u_s \frac{d}{dx}\int_0^{y_s} \rho_l u_l \, dy + \rho_v \frac{d}{dx}\int_{y_s}^{\infty} u_v^2 \, dy = 0 \tag{A.5}$$

$$\frac{\partial u_l^+}{\partial y^+}\bigg|_s + \mathcal{K} u_s^+ = -\mathcal{K} \frac{\rho_v}{\rho_l}\left[2 - \frac{f \frac{dy_s}{dx}}{y_s \frac{df}{dx}}\right] \int_{y_s}^{\infty} u_v^{+2} \, dy^+$$

$$= u_s^{+2}\left[1 - \frac{f \frac{dy_s}{dx}}{2 y_s \frac{df}{dx}}\right] \frac{\mu_v \rho_v}{\mu_l \rho_l} \approx \frac{\mu_v \rho_v}{\mu_l \rho_l} \tag{A.6}$$

APPENDIX II

SAMPLE CALCULATIONS

HORIZONTAL TUBE

RUN NO. 82

Given Data:

$r_o = 0.02384$ ft.

$L = 2.354$ ft.

$\sigma = 0$

$t_i = 141.8$ °F

$\Delta t = 23.2$ °F

Comparative Experimental Data:

$t_o = 129.1$ °F

$Q_{\ell o} = 0.750 \times 10^{-4}$ ft^3/sec

$\frac{Q_{\ell o}}{\sqrt{g r_o^5}} = 0.1507$

$\phi_{cm} \simeq 115°$

Fluid: Refrigerant-113

Properties

$\rho_\ell g = 92.17$ lb/ft^3

$\rho_v g = 0.6904$ lb/ft^3

$\lambda/g = 61.15$ Btu/lb

$\varsigma = 0.0890$

$k_\ell = 1.293 \times 10^{-5}$ Btu/sec ft °F

$\mu_\ell = 0.9150 \times 10^{-5}$ lbf sec/ft^2

$h_{in}/g = 99.62$ Btu/lb

$h_{out}/g = 35.54$ Btu/lb

$(\rho_\ell g)_{out} = 93.30$ lbf/ft^3

Assume $\phi_{cm} = 120°$, $\theta_c = 60°$, $\phi = 120°$

From equation (4.36):

$$\Omega = 2\left[\frac{91.48 \times (1.293)^3 \times 10^{-15} \times (0.02384)^3 \times (23.2)^3}{3 \times 0.9150 \times 10^{-5} \times (92.17 \times 61.15 \times 1.0605)^3}\right]^{\frac{1}{4}} \times 1.240 \times 1.564$$

$$= 0.3375 \times 10^{-4} \text{ ft}^3/\text{sec ft}$$

$$\frac{\Omega L}{\sqrt{g r_o^5}} = \frac{0.3375 \times 10^{-4} \times 2.354}{\sqrt{32.17 \times (0.02384)^5}} = 0.1596$$

$$\frac{\Omega^2 L^2}{g r_o^5} = 0.02545 \qquad \frac{\mu_\ell}{\rho_\ell \Omega} = 0.0946$$

From Figure 7.1: $\phi_c = 106°$, $\theta_c = 53°$, $\phi = 127°$

Integrating equation (4.42) from $z^+ = 1$ to $z^+ = 0.8$ yields on the right hand side the terms of equation (4.43):

I $\sigma = 0$

II $-0.001417 \times 133.4 \times 0.02545 \times 98.7 \times \frac{0.79864}{(2.6972)^2} \times (0.008) = -0.000417$

III $-1.125 \times 0.02545 \times 0.0946 \times \frac{1}{(0.240)^2} \times (0.64 - 1) = 0.01690$

IV $133.4 \times 0.02545 \times \frac{0.4444}{(2.6972)^2}\left[0.04 - 0.001417 \times 98.7 \times \frac{0.008}{0.4473}\right]$

$= 0.00779$

V $-2.67 \times \frac{1}{0.4444} \times 0.02545(0.64 - 1) = 0.05505$

The left hand side becomes:

$$\left[\frac{A_\ell s_c}{r_o^3}\right]_1^2 = \left.\frac{A_\ell s_c}{r_o^3}\right|_2 - 0.07214$$

Equating the two sides

$$\left.\frac{A_\ell s_c}{r_o^3}\right|_2 = 0.07214 - 0.000417 + 0.01690 + 0.00779 + 0.05505$$

$$= 0.1514$$

Correspondingly, $\phi_c \simeq 125°$, $\theta_c = 62.5°$, $\phi = 117.5°$

Following the same procedure yields:

from $z^+ = 0.8$ to $z^+ = 0.5$ $\phi_c = 142°$, $\theta_c = 71°$, $\phi = 109°$

from $z^+ = 0.5$ to $z^+ = 0.2$ $\phi_c = 158°$, $\theta_c = 79°$, $\phi = 101°$

$\phi_m \simeq 113$ ϕ_m assumed $= 120°$

Assumed value of ϕ_m is satisfactory.

The heat transfer coefficient can be calculated from equation (3.23) or by the following equivalent relation:

$$h_m = \frac{\Omega \rho_\ell \lambda (1 + 0.68\,\xi)}{2\pi r_o \Delta t} = \frac{0.3375 \times 10^{-4} \times 92.17 \times 61.15 \times 1.0605}{2\pi \times 0.02384 \times 23.2}$$

$$= 0.0580 \text{ Btu/sec ft}^2\ °\text{F}$$

$$= 208.8 \text{ Btu/sec ft}^2\ °\text{F}$$

$$h_{m(\text{experimental})} = \frac{Q_{\ell o}\, \rho_{\ell out}\, (h_{in} - h_{out})}{2\pi r_o L\, \Delta t}$$

$$= \frac{0.750 \times 10^{-4} \times 93.30 \times (99.62 - 35.54)}{2\pi \times 0.02384 \times 2.354 \times 23.2}$$

$$= 0.0560 \text{ Btu/sec ft}^2\ °\text{F}$$

$$= 201.6 \text{ Btu/hr ft}^2\ °\text{F}$$

Difference between heat transfer coefficients is 3.6%

Nusselt Number based on diameter is:

$$\frac{h_m d_o}{k_\ell} = \frac{0.0560 \times 0.04768}{1.293 \times 10^{-5}}$$

$$= 206.4$$

INCLINED TUBE

RUN NO. 119

Given Data:

r_o = 0.02384 ft.

L = 2.354 ft.

σ = 0.1736

t_i = 127.8 °F

Δt = 9.4 °F

Comparative Experimental Data

t_o = 124.7 °F

$Q_{\ell o}$ = 0.4955×10^{-4} ft^3/sec

$$\frac{Q_{\ell o}}{\sqrt{g r_o^{5}}} = 0.0995$$

$\phi_{cm} \simeq 58°$

Fluid: Refrigerant 113

Properties:

$\rho_\ell g$ = 94.41 lb/ft^3

$\rho_v g$ = 0.5496 lb/ft^3

λ/g = 62.32 Btu/lb

ζ = 0.0347

k_ℓ = 1.332×10^{-5} Btu/sec-ft-°F

μ_ℓ = 0.9941×10^{-5} lbf/sec/ft^2

h_{in}/g = 97.56 Btu/lb

h_{out}/g = 34.54 Btu/lb

$(\rho_\ell g)_{out}$ = 93.68 lb/ft^3

Assume

$$\phi_{cm} \simeq 58°, \ \phi = 151°, \ \theta_c = 29°$$

$$\Omega = 2\left[\frac{92.86 \times (1.332)^3 \times 10^{-15} \times (0.02384)^3 \times (9.4)^3}{3 \times 0.9941 \times 10^{-5} \times (93.41 \times 62.32 \times 1.024)^3}\right]^{\frac{1}{4}} \times 1.240 \times 1.859$$

$$= 0.2057 \times 10^{-4} \ \text{ft}^3/\text{sec-ft}$$

$$\frac{\Omega L}{\sqrt{g r_o^{5}}} = \frac{0.2057 \times 10^{-4} \times 2.354}{\sqrt{32.17 \times (0.02384)^5}}$$

$$= 0.0970$$

$$\frac{\Omega^2 L^2}{g r_o^{5}} = 0.00943$$

$$\frac{\mu_\ell}{\rho_\ell \Omega} = 0.1664$$

Substitute the above quantities together with the angle functions corresponding to the assumed depth into equation (4.43), and set the limits at $z_1^+ = 0.5$ and $z_2^+ = 1$.

$$\text{I} \quad 98.7 \times 0.08212 \times \sigma \times (0.5) = 4.050\,\sigma$$

$$\text{II} \quad -0.001417 \times 170.0 \times 0.00943 \times \frac{98.7}{(3.060)^2} \times 0.48481 \times (-0.125)$$

$$= 0.00145$$

$$\text{III} \quad -1.125 \times 0.00943 \times \frac{0.1664}{(0.0811)^2}\,(1 - 0.25)$$

$$= -0.2013$$

$$\text{IV} \quad 170 \times 0.00943 \times \frac{0.08212}{(3.060)^2}\left(-0.25 + 0.001417 \times \frac{98.7}{0.490} \times 0.125\right)$$

$$= -0.00301$$

$$\text{V} \quad -2.67 \times \frac{0.00943}{0.08212}\,(1 - 0.25)$$

$$= -0.2300$$

$$4.050\,\sigma + 0.00145 - 0.2013 - 0.00301 - 0.2300 = 0$$

$$\sigma = 0.1069$$

Following the same procedure yields:

$\theta_c = 30°, \ \phi = 150° \qquad \sigma = 0.0824$

$\theta_c = 27°, \ \phi = 153° \qquad \sigma = 0.1620$

$\theta_c = 25°, \ \phi = 155° \qquad \sigma = 0.2658$

$\theta_c = 23°, \ \phi = 157° \qquad \sigma = 0.454$

Plot on chart of Figure (4.3) and read $\phi = 153.3°$ corresponding to

$\sigma = 0.1736$

Assumed value of ϕ satisfactory

A maximum product of the other two coordinates (relation 4.44) is

1.874, and it occurs at about

$\sigma_{opt} = 0.2$

The heat transfer coefficient can be calculated from equation (3.23) or by the following, equivalent relation:

$$h_m = \frac{\Omega \rho_\ell \lambda (1 + 0.68 \zeta)}{2\pi r_o \; \Delta t} = \frac{0.2057 \times 93.41 \times 62.32 \times 1.024}{2\pi \times 0.02384 \times 9.4}$$

$$= 0.0870 \text{ Btu/sec-ft}^2\text{-}^\circ\text{F}$$

$$= 313.2 \text{ Btu/hr-ft}^2\text{-}^\circ\text{F}$$

$$h_{m(\text{experimental})} = \frac{Q_{\ell o} \rho_{\ell out} (h_{in} - h_{out})}{2\pi r_o \, L \, \Delta t}$$

$$= \frac{0.4955 \times 10^{-4} \times 93.68 \times (97.56 - 34.54)}{2\pi \times 0.02384 \times 2.354 \times 9.4}$$

$$= 0.0883 \text{ Btu/sec-ft}^2\text{-}^\circ\text{F}$$

$$= 317.9 \text{ Btu/hr-ft}^2\text{-}^\circ\text{F}$$

Difference between heat transfer coefficients is 1.5%

Nusselt Number based on diameter is:

$$\frac{h_m d_o}{k} = \frac{0.0883 \times 0.04768}{1.332 \times 10\text{-}5}$$

$$= 316.0$$

APPENDIX III

EXPERIMENTAL DATA

TABLE A-1

EQUIPMENT DATA

WATER ANALOGY EXPERIMENTS

Test Section

Material: Methacrylate plastic

Length: 54 in.

Mean internal diameter: 1.101 in.

Number of liquid feed locations: 12, equally spaced

Number of air bleed locations: 12, equally spaced

Pump

Eastern Industries, Model E-7, Monel Metal Pump with Ohmite Control Rheostat

Liquid used was distilled water

Note on all experimental data

There were a number of exploratory tests made both before and between actual test runs. Also, in some of the experiments errors or other difficulties were discovered. Each of these runs had an assigned number. In the following tables only those data are included which have direct and meaningful relation to the topics covered in the text.

TABLE A-2

FLOW DEPTH DATA

WATER ANALOGY EXPERIMENTS

Run No.	Flow Rate Q_{ℓ} ml/sec	Flow Rate $\frac{Q_{\ell}}{\sqrt{g r_o^5}}$	Angle Subtended by Liquid $2\theta_c$, Degrees	Location $\frac{L-z}{d_o}$ Distance from Outlet	Comments
2	11.70	0.1616	109.3	1.5	
3	21.28	0.2938	127.1	1.5	
4	39.26	0.5419	139.6	1.5	
5	30.18	0.4166	133.5	1.5	
6	25.45	0.3514	131.0	1.5	Water temp.: 83.6 °F
7	37.45	0.5170	138.0	1.5	
8	36.72	0.5069	142.2	1.5	
9	34.54	0.4768	136.8	1.5	
10	31.25	0.4314	134.7	1.5	Water temp.: 85.8 °F
11	6.093	0.0841	88.0	1.5	
12	8.508	0.1175	98.1	1.5	
13	12.48	0.1722	103.9	1.5	
14	17.66	0.2437	120.0	1.5	
15	19.45	0.2685	123.9	1.5	Water temp.: 80.8 °F
16	10.90	0.1505	104.7	1.5	
17	15.04	0.2076	108.7	1.5	
18	19.13	0.2641	115.0	1.5	Water temp.: 82.5 °F
19	28.60	0.3948	137.0	1.5	
20	33.04	0.4561	137.1	1.5	
21	36.57	0.5048	143.2	1.5	
22	41.17	0.5684	144.0	1.5	
23	38.88	0.5367	142.5	1.5	
24	31.19	0.4305	134.5	1.5	
25	23.09	0.3188	123.7	1.5	
26	19.11	0.2638	118.7	1.5	
27	14.33	0.1978	120.2	1.5	
28	10.90	0.1505	112.5	1.5	Water temp.: 83.0 °F
29	3.296	0.0454	89.0	1.5	
30	4.015	0.0554	92.5	1.5	
31	1.591	0.0220	87.8	1.5	
32	1.709	0.0236	89.6	1.5	
33	2.810	0.0388	89.3	1.5	
34	4.600	0.0635	93.0	1.5	
35	24.10	0.3324	123.0	1.5	Water temp.: 80.4 °F

TABLE A-2

(continued)

Run No.	Flow Rate $Q_{\ell o}$ ml/sec	$\frac{Q_{\ell o}}{\sqrt{g r_o^5}}$	Angle Subtended by Liquid $2\theta_c$, Degrees	Location $\frac{L-z}{d_o}$ Distance from Outlet	Comments
36	2.380	0.0328	95.0	1.5	
	"	"	97.4	8.17	
	"	"	97.4	16.33	
	"	"	105.6	32.67	
	"	"	119.1	40.83	
	"	"	121.0	48.5	
37	6.340	0.0875	98.5	1.5	Flow is laminar although streamlines are wavy.
	"	"	102.2	8.17	
	"	"	104.3	16.33	
	"	"	102.9	24.5	
	"	"	111.0	32.67	
	"	"	122.2	40.83	
	"	"	131.0	48.5	
38	9.200	0.1270	104.1	1.5	Flow is laminar although streamlines are wavy
	"	"	114.5	8.17	
	"	"	115.1	16.33	
	"	"	111.7	24.5	
	"	"	124.0	32.67	
	"	"	135.0	40.83	
	"	"	140.0	48.5	
39	13.96	0.1927	115.8	1.5	Flow is predominantly turbulent
	"	"	127.0	8.17	
	"	"	129.8	16.33	
	"	"	131.0	24.5	
	"	"	140.1	32.67	
	"	"	151.8	40.83	
	"	"	158.0	48.5	
40	20.67	0.2855	120.3	1.5	Flow is turbulent
	"	"	136.3	8.17	
	"	"	143.4	16.33	
	"	"	144.3	24.5	
	"	"	157.0	32.67	
	"	"	166.0	40.83	
	"	"	171.5	48.5	
41	24.53	0.3382	124.2	1.5	
	"	"	144.9	8.17	
	"	"	152.1	16.33	
	"	"	154.3	24.5	
	"	"	165.9	32.67	
	"	"	176.7	40.83	
	"	"	179.0	48.5	

TABLE A-2

(continued)

Run No.	Flow Rate Q_{lo} ml/sec	$\frac{Q_{lo}}{\sqrt{gr_o^5}}$	Angle Subtended by Liquid $2\theta_c$, Degrees	Location $\frac{L-z}{d_o}$ Distance from Outlet	Comments
42	30.80	0.4250	129.5	1.5	
	"	"	157.0	8.17	
	"	"	165.0	16.33	
	"	"	169.6	24.5	
	"	"	179.0	32.67	
	"	"	188.3	40.83	
	"	"	189.4	48.5	
43	42.45	0.5855	141.8	1.5	
	"	"	179.0	8.17	
	"	"	187.5	16.33	
	"	"	190.5	24.5	
	"	"	201.9	32.67	
	"	"	211.7	40.83	
	"	"	216.4	48.5	
45	42.60	0.588	138.0	1.5	In the following experiments the water was observed to cling to the tube rather strongly. Consequently all observed angles are somewhat high.
	"	"	174.8	8.17	
	"	"	187.8	16.33	
	"	"	197.2	24.5	
	"	"	209.3	32.67	
	"	"	214.2	40.83	
	"	"	216.7	48.5	
46	38.87	0.5365	138.7	1.5	
	"	"	173.0	8.17	
	"	"	187.0	16.33	
	"	"	191.7	24.5	
	"	"	202.1	32.67	
	"	"	208.0	40.83	
	"	"	211.7	48.5	
47	35.53	0.4905	139.9	1.5	
	"	"	171.4	8.17	
	"	"	186.0	16.33	
	"	"	186.3	24.5	
	"	"	200.0	32.67	
	"	"	206.2	40.83	
	"	"	206.3	48.5	
48	26.94	0.3720	139.6	1.5	
	"	"	162.0	8.17	
	"	"	170.2	16.33	
	"	"	174.0	24.5	
	"	"	180.9	32.67	
	"	"	190.7	40.83	
	"	"	195.2	48.5	

TABLE A-2

(continued)

Run No.	Flow Rate Q_l ml/sec	Flow Rate $\frac{Q_l}{\sqrt{gr_o^5}}$	Angle Subtended by Liquid $2\theta_c$, Degrees	Location $\frac{L-z}{d_o}$ Distance from Outlet	Comments
49	18.10	0.2500	132.0	1.5	
	"	"	145.3	8.17	
	"	"	153.2	16.33	
	"	"	159.1	24.5	
	"	"	165.4	32.67	
	"	"	172.8	40.83	
	"	"	174.0	48.5	
50	8.925	0.1231	119.1	1.5	
	"	"	126.0	8.17	
	"	"	132.7	16.33	
	"	"	136.0	24.55	
	"	"	142.5	32.67	
	"	"	150.5	40.83	
	"	"	155.6	48.5	

TABLE A-3

CRITICAL FLOW DATA

WATER ANALOGY EXPERIMENTS

Flow Rate $Q_{\ell o}$ ml/sec	Flow Rate $\frac{Q_{\ell o}}{\sqrt{g r_o^5}}$	Description of Flow at Outlet	Comments
24.10	0.3324	Turbulent	Run No. 35
23.76	0.3280	Laminar	Liquid supply nearest to
23.80	0.3286	Laminar	outlet was closed in order
22.46	0.3101	Laminar	to reduce turbulence.
21.96	0.3032	Laminar	Water Temperature was 80.4 °F
22.56	0.3114	Laminar	
23.40	0.3230	Laminar	Transition point is at
23.78	0.3283	Laminar	
24.50	0.3382	Turbulent	
23.62	0.3260	Mostly Turbulent	$\frac{Q_{\ell o}}{\sqrt{g r_o^5}} = 0.33$
24.00	0.3313	Turbulent	Equivalent Critical Reynolds
			Number $Re_c = 3{,}580$
			Run No. 44
15.44	0.2131	Laminar but Disturbed	Liquid was supplied uniformly
17.35	0.2395	Partly Laminar	through all input locations,
19.84	0.2739	Turbulent	including the one nearest to
19.26	0.2659	Turbulent	outlet
18.50	0.2554	Turbulent	Water temperature was 80.2 °F
18.83	0.2602	Turbulent	
17.23	0.2379	Partly Laminar	Transition point is at
17.94	0.2477	Turbulent	
			$\frac{Q_{\ell o}}{\sqrt{g r_o^5}} = 0.24$
			Equivalent Critical Reynolds
			Number $Re_c = 2{,}330$

TABLE A-4

EQUIPMENT DATA
CONDENSATION EXPERIMENTS

Test Section

Material: Std. 5/8" o.d. Aerofin copper tubing

Length: 28.25 in.

Internal diameter: $0.571 \begin{smallmatrix} + 0.003 \\ - 0.000 \end{smallmatrix}$ in.

Internal heat transfer area: 0.3527 ft^2

Number of fins per inch: 8

Fin outside diameter: 1.375 in.

Fin thickness: 0.008 in.

Thermocouples

Materials: No. 30, Leeds & Northrup copper-constantan wires

Calibration: $$\frac{(\text{Emf})_{\text{std.}} - (\text{Emf})_{\text{obs.}}}{(\text{Emf})_{\text{obs.}}} = -0.00418$$

Locations: One in the vapor stream entering test section; three pairs soldered into slots at the top and bottom of the tube at 1/6 L, 1/2 L, and 5/6 L distance along the tube; one directly behind bottom point at outlet end in the condensate stream discharging from test section; two movable junctions.

Potentiometer: Leeds & Northrup Semiprecision Potentiometer

Variacs: General Radio Company, Type 100-R
General Radio Company, Type W5MT

Wattmeter: Weston Model 310, No. 3760

Leveling Instrument: Wild (Heerbrugg) Switzerland N2-59138

Liquid used was distilled Refrigerant-113

TABLE A-5

NOMENCLATURE FOR HEAT TRANSFER DATA

σ	slope of tube
t_r	room temperature, °F
t_i	vapor entering temperature, °F
t_o	condensate discharge temperature, °F
t_t	average temperature at top of tube, °F
t_b	average temperature at bottom of tube, °F
Δt	mean temperature difference between vapor and wall, °F
$Q_l/\sqrt{gr_o^5}$	dimensionless discharge flow rate
ϕ_{cm}	mean central angle subtended by condensate, degrees
$\zeta = \frac{c_{pl}\Delta t}{\lambda}$	dimensionless temperature difference
$\frac{hd_o}{k_l}$	Nusselt number

Run No.	σ	t_r	t_i	t_o	t_t	t_b	Δt	$Q_{1o}/\sqrt{gr_o^5}$	ϕ_{cm}	Liquid Ramp	Waves	Ripples on Wall	$\delta x10^3$	$\frac{hd_{mo}}{k_1}$
71	0.002	67	123.7	116.7	114.40	110.93	11.0	0.0844	110	0-3"	small		39.5	233
72	"	"	137.2	127.4	124.07	119.50	15.4	0.1090	120	0-1/4 L	0-1/4 L		57.5	218
73	"	"	149.3	139.7	134.13	129.20	17.6	0.1320	122	1.5"-1/4 L	0-1/3 L		66.8	232
74	"	"	156.0	144.8	139.50	132.70	19.9	0.1435	110	2" - 1/4 L	0-1/3 L		78.0	222
75	"	"	114.1	110.2	107.43	104.57	8.1	0.0737	112	0-1/4 L	0-1"		28.8	273
76	0.0	82	130.2	124.0	121.50	116.93	11.0	0.0774	120	0-2"	0-2"		40.7	213
77	"	67	130.1	122.2	119.13	113.93	13.6	0.0961	120	0-2"	0-1/4 L		50.3	215
78	"	"	137.0	129.2	125.23	119.63	14.6	0.1060	118	1.5"-1/5 L	0-1/4 L		54.4	221
79	"	"	143.5	135.1	130.60	127.20	14.6	0.1181	118	1.5"-1/5 L	0-1/3 L		55.0	245
80	"	"	150.1	140.1	135.87	129.87	17.2	0.1280	115	1.5"-1/5 L	0-1/3 L		66.9	228
81	"	43	128.4	114.4	112.70	104.17	20.0	0.1272	118	2"-1/3 L	0-2/3 L		73.8	200
82	"	"	141.8	129.1	122.30	114.97	23.2	0.1507	115	2"-1/3 L	0-1/2 L		89.0	202
83	"	"	154.7	142.2	131.83	125.50	26.0	0.1755	120	2"-1/3 L	0-2/3 L		101.9	210
84	"	"	130.4	119.6	113.97	107.40	19.7	0.1343	108	1.5"-1/4 L	0-1/2 L		73.0	210
85	"	"	148.0	136.8	127.57	120.60	23.9	0.1570	120	1.5"-1/4 L	0-1/2 L		92.7	204
86	"	"	151.9	140.0	130.70	121.10	26.0	0.1678	110	2"-1/4 L	0-2/3 L		101.3	200
87	"	"	149.4	135.2	128.73	121.97	24.0	0.1495	105	1.5"-1/4 L	0-1/2 L		91.5	192
88	0.005	"	149.6	137.8	130.23	121.73	23.6	0.1546	90	1"-1/4 L	0-1/4 L		91.0	203
89	"	"	131.7	121.3	116.03	111.70	17.8	0.1310	92	1.5"-1/4 L	none		66.1	226
90	"	"	136.3	125.8	120.80	114.03	18.9	0.1390	95	1.5"-1/5 L	"		70.5	227
91	"	"	154.2	143.0	135.50	125.47	23.7	0.1688	100	1.5"-1/4 L	0-1/3 L		92.7	220
92	0.010	"	127.7	116.2	114.07	110.10	15.6	0.1256	80	1"-1/4 L	none		57.6	248
93	"	"	132.3	121.7	115.93	110.67	19.0	0.1380	85	1"-1/3 L	"		70.5	224
94	"	"	138.7	126.7	121.13	114.70	20.8	0.1480	88	1"-1/4 L	0-1/4 L	0-2.5"	77.8	221
95	"	"	145.0	113.2	126.33	119.07	22.3	0.1603	88	1"-1/4 L	none	0-2.5"	85.0	223
96	"	"	153.4	141.4	134.07	127.93	22.4	0.1790	95	0.5"-1/4 L	"	0-2.5"	87.5	246
97	"	72	118.5	113.1	111.80	110.10	7.6	0.0750	78	0-1/3 L	"	0-2.5"	27.0	298
98	"	"	127.6	121.2	119.53	115.50	10.1	0.0915	80	0-1/3 L	"	none	37.2	274
99	"	"	132.5	126.0	123.27	120.60	10.6	0.0980	80	0-1/3 L	"	"	39.2	281
100	"	"	139.4	132.3	129.23	123.80	12.9	0.1098	82	0-1/4 L	"	"	48.2	258
101	"	"	147.0	139.0	133.40	129.93	15.3	0.1219	90	0-1/4 L	0-1/5 L	"	59.4	242
102	"	"	157.4	146.9	143.50	137.10	17.1	0.1405	85	0-1/4 L	0-1/4 L	"	67.2	261
103	0.020	"	119.0	113.5	111.40	107.63	9.5	0.0743	70	0-1/5 L	none	"	33.8	236
104	"	"	129.1	123.9	121.93	118.30	9.0	0.0955	75	0-1/4 L	0-2"	"	33.2	319
105	"	"	137.6	131.1	127.03	122.83	12.7	0.1087	80	0-1/3 L	0-2.5"	"	47.3	260
106	"	"	149.1	142.1	136.30	131.17	15.4	0.1274	80	0-1/3 L	0-3"	0-1.5"	58.3	252
107	"	43	124.2	114.6	109.63	105.20	16.8	0.1228	75	0-1/3 L	0-2.5"	some	60.3	225
108	"	"	133.8	124.4	117.53	113.17	18.4	0.1496	80	1"-1/3 L	0-2.5"	0-2.5"	68.5	249
109	"	"	149.8	138.4	130.27	125.13	22.1	0.1828	80	1"-1/3 L	0-3"	0-3"	84.0	256
110	0.040	"	151.8	143.0	131.03	123.73	24.4	0.1858	80	0-1/3 L	gravity from 1/3 L	0-4"	95.1	232
111	"	"	141.5	129.8	122.67	116.17	22.1	0.1554	78	0-1/3 L	" " " "	0-2"	84.9	203
112	"	"	130.5	121.3	115.07	109.73	18.1	0.1350	75	0-1/3 L	none	0-2"	67.0	229
113	"	"	122.5	117.6	114.47	111.60	9.5	0.0768	68	very gradual to 1/2 L	ripples	none	33.9	245
114	"	"	135.4	130.0	126.87	123.10	10.4	0.1028	68	0-1/3 L	"	"	38.8	297

Run No.	σ	t_r	t_i	t_o	t_t	t_b	Δt	$\omega_1/\sqrt{gr_o^5}$	ϕ_{cm}	Liquid Ramp	Waves	Ripples on Wall	$\xi \times 10^3$	$\frac{hd_{mo}}{k_1}$
115	0.040	72	143.2	136.7	132.23	127.80	13.2	0.1217	75	0-1/3 L	0-2", ripples	0-2"	49.6	278.4
116	"	"	157.1	149.2	142.30	135.90	18.0	0.1503	77	0-1/3 L	gravity from 1/3 L	0-2"	70.6	205.0
117	"	"	134.7	129.6	126.23	122.43	10.4	0.1082	72	0-1/3 L	ripples	0-2"	38.7	312.8
118	0.1736	"	115.2	111.8	108.60	105.33	8.2	0.0745	60	0-3"	"	none	29.1	272.2
119	"	"	127.8	124.7	119.67	117.13	9.4	0.0995	58	0-3"	"	"	34.7	316.0
120	"	"	140.0	136.8	129.50	126.03	12.2	0.1142	60	0-3"	"	0-2"	46.7	280.2
121	"	"	153.4	148.5	140.10	136.30	15.2	0.1401	62	0-3"	"	0-2"	59.3	276.6
122	"	39	118.5	112.6	103.97	99.33	16.8	0.1310	63	0-3"	"	0-3"	59.9	232.2
123	"	"	128.8	121.7	110.97	107.37	19.6	0.1458	65	1.5"-4"	0-5", ripples	0-5"	72.3	226.2
124	"	"	140.1	134.2	121.27	116.40	21.3	0.1739	65	2"-4"	0-5", "	0-5"	81.6	146.2
125	"	"	153.5	149.2	131.23	124.37	25.7	0.2060	70	2"-1/4 L	gravity from 1/4 L	0-3"	100.5	239.6
126	"	"	131.7	125.8	114.80	110.50	19.0	0.1590	62	1.5"-4"	0-5", ripples	0-5"	70.7	252.6

TABLE A-6

DEFINITIONS OF SYMBOLS

Q_{to}	condensate discharge rate, ml/sec
$Q_{to}/\sqrt{g r_o^5}$	dimensionless flow rate
$2\theta_c = \phi_c$	angle subtended by condensate, degrees
$\frac{L-z}{L}$	approximate dimensionless distance from outlet end, fraction of tube length

TABLE A-6

FLOW DEPTH DATA

CONDENSATION EXPERIMENTS

HORIZONTAL POSITION

Run No.	Q_{lo}	$\frac{Q_{lo}}{\sqrt{gr_o^5}}$	$2\theta_c$	$\frac{L-z}{L}$	Comments
2	0.1000	0.00709	85	Near Outlet	
4	0.2360	0.01672	94	" "	
6	0.3066	0.02174	95	" "	
8	0.3607	0.02558	91	" "	
9	0.4077	0.0289	90	" "	
10	0.464	0.0329	90	" "	
11	0.3930	0.02786	86	" "	
12	0.440	0.0312	91	" "	
13	0.518	0.0367	92	" "	
14	0.664	0.0471	92	" "	
15	0.730	0.0518	93	" "	
16	0.798	0.0566	92	" "	
17	0.805	0.0571	94	" "	
18	1.019	0.0723	99	" "	
19	1.055	0.0748	97	" "	
20	1.158	0.0820	95	" "	
21	1.268	0.0898	102	" "	
22	1.463	0.1038	103	" "	
23	1.670	0.1183	100	" "	
24	1.785	0.1265	102	" "	
25	1.922	0.1362	106	" "	
26	1.569	0.1111	103	" "	
27	2.368	0.1680	117	" "	
28	2.145	0.1520	111	" "	
31	0.607	0.0431	94	" "	
	"	"	115	0.95	Dubious
32	0.981	0.0695	114	0.95	"
33	1.439	0.1020	95	Near Outlet	"
	"	"	108	0.3	
	"	"	112	0.7	
	"	"	117	0.95	
34	1.724	0.1222	108	Near Outlet	
	"	"	114	0.3	
	"	"	124	0.7	
	"	"	124	0.95	

TABLE A-6

(continued)

Run No.	$Q_{\ell o}$	$\frac{Q_{\ell o}}{\sqrt{g r_o^5}}$	$2\theta_c$	$\frac{L-z}{L}$	Comments
35	2.020	0.1432	107	Near Outlet	
	"	"	118	0.3	
	"	"	123	0.7	
	"	"	120	0.95	
36	2.307	0.1637	110.5	Near Outlet	
	"	"	121	0.3	
	"	"	122	0.7	
	"	"	130	0.95	
37	0.470	0.0333	94	Near Outlet	
	"	"	97	0.3	
	"	"	118	0.7	
	"	"	115	0.95	Dubious
38	0.526	0.0373	95	Near Outlet	
	"	"	99	0.3	
	"	"	118	0.7	
	"	"	120	0.95	
39	0.733	0.0519	93	Near Outlet	
	"	"	103	0.3	
	"	"	106	0.7	
	"	"	109	0.95	
40	1.224	0.0868	98	Near Outlet	
	"	"	102	0.3	
	"	"	102	0.7	
	"	"	101	0.95	
41	2.414	0.1711	113	Near Outlet	
	"	"	122	0.3	
	"	"	120	0.7	
42	2.816	0.1996	113	Near Outlet	
	"	"	117	0.3	
	"	"	112	0.7	

APPENDIX IV

COMPUTER PROGRAMS

NOMENCLATURE FOR COMPUTER PROGRAM No. M 931-3

(In order of appearance)

P	$\bar{p} = y_s^{\,3}$
DPZ	$\Delta \bar{p}$ in z direction
DPX	$\Delta \bar{p}$ in ϕ (or x) direction
X	ϕ
Y	y_s
GRAV	$\frac{g(\rho_\ell - \rho_v)}{r_o}\left[\sin\phi\, \bar{p}_n^{\,1/3} \left(\frac{\partial \bar{p}}{\partial \phi}\right)_n + p_n^{\,4/3}\cos\phi\right]$
SHEAR	$1.5\, \bar{p}_n \frac{\partial \tau_v}{\partial z}$
R	r_o
DTEMP	Δt
GAMV	Γ_v
DZ	Δz
DPHI	$\Delta \phi$
M,N	constants to determine total arc and numbers to be printed
G	$g(\rho_\ell - \rho_v)$
VISLI	$3\,\frac{\mu_\ell}{\rho_\ell}$
VISVA	μ_v
COND	k_ℓ
EVAP	λ'
HYD	$\frac{d_{hv} r_o}{A_v}$

Q	$\dfrac{2\rho_v A_v^2}{r_o^4}$
F	K
MORE	code for indicating last set of input data
GAMIN	Γ_{in}
START, COUNT	codes for determining printing sequence
REV	$\overline{Re}_v$
A	a_i
B	b_i
GAMEXP	$\Gamma_v^{2+b_i}$
HYDEXP	$\left(\dfrac{d_{nv}}{A_v}\right)^{b_i}$
VISEXP	$\mu_v^{b_i}$
TAU	τ_v
DRIVE	$\dfrac{3\mu_\ell k_\ell \Delta t}{\rho_\ell \lambda'}$
CONST	initial y_s of condensate layer
SUM	$\sum_1^M \dfrac{1}{y_s}$
DEGAM	$-\dfrac{d\Gamma_v}{dz}$
HEATL	$\Gamma_{in}\lambda'/2\pi r_o \Delta t = h_m L$
DNUSSL	$\dfrac{h_m L}{k_\ell}$

```
 M 931-3
 JOHN CHATO 763
 CONDENSATION IN A HORIZONTAL TUBE
 DIMENSION P(70),DPZ(70),DPX(70),X(70),Y(70),GRAV(70),SHEAR(7 )
10 READ 12,FLUID,R,DTEMP,GAMV
 READ 14,DZ,DPHI,M,N,G
 READ 19,VISLI,VISVA,COND,EVAP
 READ 18,HYD,Q,F,MORE
12  FORMAT(7H FLUID=I4,3H R=E15.8,7H DTEMP=E10.4,6H GAMV=E15.8)
14  FORMAT(4H DZ=E15.8,6H DPHI=E15.8,3H M=I3,3H N=I3,3H G=E15.8)
16  FORMAT(7H VISLI=E15.8,7H VISVA=E15.8,6H COND=E15.8,6H EVAP=E15.8)
18  FORMAT(5H HYD=E15.8,3H Q=E15.8,3H F=E15.8,I2)
19  FORMAT(4E15.8)
 WRITE OUTPUT TAPE 2,12,FLUID,R,DTEMP,GAMV
 WRITE OUTPUT TAPE 2,14,DZ,DPHI,M,N,G
 WRITE OUTPUT TAPE 2,16,VISLI,VISVA,COND,EVAP
 WRITE OUTPUT TAPE 2,18,HYD,Q,F
 GAMIN=GAMV
 START=0.0
 DO 68 I=1,M
 S=I
68  X(I)=S*DPHI-DPHI/2.
20 REV=GAMV*HYD/(R*VISVA)
 IF (REV-3000.) 21,23,23
21 A=18.
 B=-1.
 GO TO 25
23 A=0.072
 B=-0.243
25 GAMEXP=EXPF((2.+B)*LOGF(GAMV))
 HYDEXP=EXPF(B*LOGF(HYD/R))
 VISEXP=EXPF(B*LOGF(VISVA))
 TAU=A*HYDEXP*GAMEXP/(VISEXP*Q*(R**4))
 IF (START) 27,27,30
27 DRIVE=VISLI*COND*DTEMP/EVAP
 CONST=F*EXPF((LOGF(DRIVE*R/G))/4.)
 DO 29 I=1,M
 Y(I)=CONST
29 P(I)=CONST**3
 WRITE OUTPUT TAPE 2,62,(Y(I),I=1,M,N)
 START=1.
 COUNT=2.
30 DO 32 I=1,2
32 DPX(I)=-3.*P(I)+4.*P(I+1)-P(I+2)
 DO 34 I=3,M
34 DPX(I)=3.*P(I)-4.*P(I-1)+P(I-2)
 SUM=0.0
 DO 40 J=1,M
40 SUM=SUM+1./Y(J)
 DEGAM=2.*COND*DTEMP*R*DPHI*SUM/EVAP
36 DO 38 I=1,M
 GRAV(I)=(G/R)*((SINF(X(I)))*Y(I)*DPX(I)/(2.*DPHI)
1          +P(I)*Y(I)*COSF(X(I)))
 SHEAR(I)=1.5*P(I)*TAU*(2.+P)*DEGAM/GAMV
38 DPZ(I)=(DRIVE-GRAV(I)+SHEAR(I))*DZ/TAU
 DO 41 I=1,M
 P(I)=P(I)+DPZ(I)
 IF(P(I)) 57,57,39
```

```
39    Y(I)=EXPF((LOGF(P(I)))/3.)
      IF(Y(I)-R) 41,45,45
41    CONTINUE
      GAMV=GAMV-DEGAM*DZ
      IF(1.5*TAU/(G*Y(I)*SINF(X(I)))-0.01) 47,47,42
42    IF (SENSE SWITCH 1) 43,50
43    IF(GAMV) 47,47,46
46    IF(COUNT-R/DZ) 48,48,49
48    WRITE OUTPUT TAPE 2,62,(Y(I),I=1,M,N)
      GO TO 52
49    IF(COUNT-26.*R/DZ) 52,54,54
52    COUNT=COUNT+1.
      GO TO 20
50    IF (COUNT-3.) 52,47,47
45    WRITE OUTPUT TAPE 2,56,Y(I),I,COUNT
56     FORMAT(3H Y=F15.8,3H I=I3,7H COUNT=F11.4)
      GO TO 58
57    WRITE OUTPUT TAPE 2,59,P(I),I
59     FORMAT(3H P=F15.8,3H I=I3)
47    HEATL=GAMIN*EVAP/(6.2831853*R*DTEMP)
      DNUSSL=GAMIN*EVAP/(3.1415927*COND*DTEMP)
      WRITE OUTPUT TAPE 2,60,COUNT,GAMV,HEATL,DNUSSL
      WRITE OUTPUT TAPE 2,62,(Y(I),I=1,M,N)
60     FORMAT(7H COUNT=F11.4,6H GAMV=F15.8,7H HEATL=F15.8,
     1          8H DNUSSL=F15.8)
62     FORMAT(3F15.8)
      IF (SENSE SWITCH 1) 58,66
54    WRITE OUTPUT TAPE 2,60,COUNT,GAMV
      WRITE OUTPUT TAPE 2,62,(Y(I),I=1,M,N)
      COUNT=1.+R/DZ
      GO TO 20
58    IF (MORE) 66,66,10
66    END FILE 2
      STOP 77777
      END (0,1,0,0,0)
```

NOMENCLATURE FOR COMPUTER PROGRAM No. M 931-5

(In order of appearance)

ANG, THE	central half angle, θ_c for liquid, ϕ for vapor
AREA	$\frac{A_\ell}{r_o^2}$ or $\frac{A_v}{r_o^2}$
RHL	$r_{h\ell}/r_o$
RHV	r_{hv}/r_o
PRE	$A_\ell\, s_c/r_o^3$
FRO	$\sqrt{b/A_\ell^{\;3}}$
TEG	$\int_0^\phi \sin^{1/3}\phi\, d\phi$
EXTEG	$(TEG)^{3/4}$

All numbers are to be multiplied by 10^E

Example: 0.12345678E - 01 = 0.012345678

```
C     M 931-5
C     JOHN CHATO
C     ANGLE FUNCTIONS
      DIMENSION ANG(1440),THE(1440),AREA(1440),RHL(1440),RHV(1440),
     1PRE(1440),FRO(1440),TEG(180),EXTEG(360)
      REWIND 7
   10 READ 12, ARC, M
   12 FORMAT (5H ARC=E15.8,3H M=I4)
      DO 14 I=1, M
      S=I
      ANG(I)=S*180./ARC
      THE(I)=S*3.14159265/ARC
      AREA(I)=THE(I)-0.5*SINF(2.*THE(I))
      RHL(I)=AREA(I)/(2.*THE(I))
      RHV(I)=AREA(I)/(2.*(THE(I)+SINF(THE(I))))
      PRE(I)=0.66666667*(SINF(THE(I)))**3.-AREA(I)*COSF(THE(I))
   14 FRO(I)=SQRTF(2.*SINF(THE(I))/((AREA(I))**3.))
      DO 24 J=1, 90
      READ 22, TEG(J)
   22 FORMAT (4E15.8)
   24 EXTEG(J)=EXPF(0.75*LOGF(TEG(J)))
      DO 26 J=91, 179
      K=180-J
   26 EXTEG(J)=EXPF(0.75*LOGF(2.58710956-TEG(K)))
      EXTEG(180)=EXPF(0.75*LOGF(2.58710956))
      WRITE OUTPUT TAPE 7, 28,((ANG(I),AREA(I),I=1,M),
     1(ANG(I),RHL(I),I=1,M),(ANG(I),RHV(I),I=1,M),
     1(ANG(I),PRE(I),I=1,M),(ANG(I),FRO(I),I=1,M))
   28 FORMAT (3(F8.3,E14.7))
      WRITE OUTPUT TAPE 7, 30, (J,EXTEG(J),J=1,180)
   30 FORMAT (4(I4,E14.7))
      END FILE 7
      REWIND 7
      STOP 77777
      END (0,1,0,0,0)
```

APPENDIX V

ANGLE FUNCTIONS

All numbers are to multiplied by 10^E

Example: 0.12345678E - 01 = 0.012345678

ANGLE	EXTEG	ANGLE	EXTEG	ANGLE	EXTEG	ANGLE	EXTEG
1	0.1406602E-01	2	0.2813159E-01	3	0.4219634E-01	4	0.5625978E-01
5	0.7032150E-01	6	0.8438111E-01	7	0.9843812E-01	8	0.1124921E-00
9	0.1265427E-00	10	0.1405895E-00	11	0.1546319E-00	12	0.1686696E-00
13	0.1827022E-00	14	0.1967292E-00	15	0.2107502E-00	16	0.2247648E-00
17	0.2387724E-00	18	0.2527728E-00	19	0.2667655E-00	20	0.2807500E-00
21	0.2947259E-00	22	0.3086928E-00	23	0.3226502E-00	24	0.3365978E-00
25	0.3505350E-00	26	0.3644615E-00	27	0.3783768E-00	28	0.3922804E-00
29	0.4061720E-00	30	0.4200511E-00	31	0.4339173E-00	32	0.4477701E-00
33	0.4616091E-00	34	0.4754339E-00	35	0.4892439E-00	36	0.5030389E 00
37	0.5168183E 00	38	0.5305817E 00	39	0.5443286E 00	40	0.5580587E 00
41	0.5717715E 00	42	0.5854664E 00	43	0.5991432E 00	44	0.6128013E 00
45	0.6264403E 00	46	0.6400598E 00	47	0.6536592E 00	48	0.6672383E 00
49	0.6807964E 00	50	0.6943331E 00	51	0.7078481E 00	52	0.7213408E 00
53	0.7348108E 00	54	0.7482576E 00	55	0.7616808E 00	56	0.7750799E 00
57	0.7884546E 00	58	0.8018041E 00	59	0.8151283E 00	60	0.8284265E 00
61	0.8416983E 00	62	0.8549432E 00	63	0.8681608E 00	64	0.8813506E 00
65	0.8945122E 00	66	0.9076450E 00	67	0.9207486E 00	68	0.9338224E 00
69	0.9468662E 00	70	0.9598792E 00	71	0.9728611E 00	72	0.9858114E 00
73	0.9987295E 00	74	0.1011615E 01	75	0.1024467E 01	76	0.1037286E 01
77	0.1050071E 01	78	0.1062821E 01	79	0.1075536E 01	80	0.1088216E 01
81	0.1100859E 01	82	0.1113466E 01	83	0.1126035E 01	84	0.1138567E 01
85	0.1151061E 01	86	0.1163516E 01	87	0.1175932E 01	88	0.1188308E 01
89	0.1200643E 01	90	0.1212938E 01	91	0.1225191E 01	92	0.1237403E 01
93	0.1249572E 01	94	0.1261698E 01	95	0.1273780E 01	96	0.1285818E 01
97	0.1297811E 01	98	0.1309759E 01	99	0.1321661E 01	100	0.1333516E 01
101	0.1345325E 01	102	0.1357085E 01	103	0.1368797E 01	104	0.1380461E 01
105	0.1392074E 01	106	0.1403638E 01	107	0.1415150E 01	108	0.1426611E 01
109	0.1438020E 01	110	0.1449376E 01	111	0.1460679E 01	112	0.1471927E 01
113	0.1483120E 01	114	0.1494258E 01	115	0.1505340E 01	116	0.1516364E 01
117	0.1527331E 01	118	0.1538239E 01	119	0.1549088E 01	120	0.1559877E 01
121	0.1570605E 01	122	0.1581271E 01	123	0.1591875E 01	124	0.1602415E 01
125	0.1612892E 01	126	0.1623303E 01	127	0.1633648E 01	128	0.1643926E 01
129	0.1654136E 01	130	0.1664278E 01	131	0.1674350E 01	132	0.1684351E 01
133	0.1694280E 01	134	0.1704136E 01	135	0.1713918E 01	136	0.1723625E 01
137	0.1733256E 01	138	0.1742809E 01	139	0.1752283E 01	140	0.1761677E 01
141	0.1770990E 01	142	0.1780220E 01	143	0.1789366E 01	144	0.1798426E 01
145	0.1807399E 01	146	0.1816283E 01	147	0.1825076E 01	148	0.1833777E 01
149	0.1842384E 01	150	0.1850894E 01	151	0.1859307E 01	152	0.1867619E 01
153	0.1875829E 01	154	0.1883933E 01	155	0.1891930E 01	156	0.1899817E 01
157	0.1907591E 01	158	0.1915248E 01	159	0.1922786E 01	160	0.1930201E 01
161	0.1937490E 01	162	0.1944647E 01	163	0.1951668E 01	164	0.1958549E 01
165	0.1965284E 01	166	0.1971867E 01	167	0.1978290E 01	168	0.1984547E 01
169	0.1990629E 01	170	0.1996525E 01	171	0.2002224E 01	172	0.2007712E 01
173	0.2012972E 01	174	0.2017984E 01	175	0.2022721E 01	176	0.2027149E 01
177	0.2031217E 01	178	0.2034849E 01	179	0.2037902E 01	180	0.2039910E 01

ANGLE	AREA	ANGLE	AREA	ANGLE	AREA
0.500	0.4431931E-06	1.000	0.3544561E-05	1.500	0.1196098E-04
2.000	0.2834853E-04	2.500	0.5536014E-04	3.000	0.9564636E-04
3.500	0.1518526E-03	4.000	0.2266206E-03	4.500	0.3223641E-03
5.000	0.4423749E-03	5.500	0.5886117E-03	6.000	0.7639108E-03
6.500	0.9706749E-03	7.000	0.1212100E-02	7.500	0.1490172E-02
8.000	0.1807664E-02	8.500	0.2167135E-02	9.000	0.2571138E-02
9.500	0.3022201E-02	10.000	0.3522854E-02	10.500	0.4075598E-02
11.000	0.4682923E-02	11.500	0.5347500E-02	12.000	0.6071189E-02
12.500	0.6857026E-02	13.000	0.7707231E-02	13.500	0.8624200E-02
14.000	0.9610316E-02	14.500	0.1066795E-01	15.000	0.1179939E-01
15.500	0.1300700E-01	16.000	0.1429305E-01	16.500	0.1565981E-01
17.000	0.1710952E-01	17.500	0.1864440E-01	18.000	0.2026664E-01
18.500	0.2197840E-01	19.000	0.2378182E-01	19.500	0.2567901E-01
20.000	0.2767204E-01	20.500	0.2976298E-01	21.000	0.3195384E-01
21.500	0.3424661E-01	22.000	0.3664325E-01	22.500	0.3914569E-01
23.000	0.4175583E-01	23.500	0.4447552E-01	24.000	0.4730661E-01
24.500	0.5025088E-01	25.000	0.5331009E-01	25.500	0.5640599E-01
26.000	0.5978023E-01	26.500	0.6319449E-01	27.000	0.6673040E-01
27.500	0.7038992E-01	28.000	0.7417540E-01	28.500	0.7808395E-01
29.000	0.8212143E-01	29.500	0.8628347E-01	30.000	0.9058007E-01
30.500	0.9501556E-01	31.000	0.9957027E-01	31.500	0.1042754E-00
32.000	0.1091083E-00	32.500	0.1140761E-00	33.000	[illegible]
33.500	0.1244329E-00	34.000	0.1298200E-00	34.500	0.1353484E-00
35.000	0.1410189E-00	35.500	0.1468328E-00	36.000	0.1527903E-00
36.500	0.1588928E-00	37.000	0.1651410E-00	37.500	0.1715356E-00
38.000	0.1780772E-00	38.500	0.1847667E-00	39.000	0.1916046E-00
39.500	0.1985915E-00	40.000	0.2057276E-00	40.500	0.2130142E-00
41.000	0.2204509E-00	41.500	0.2280386E-00	42.000	0.2357775E-00
42.500	0.2436676E-00	43.000	0.2517095E-00	43.500	0.2599034E-00
44.000	0.2682494E-00	44.500	0.2767477E-00	45.000	0.2853982E-00
45.500	0.2942009E-00	46.000	0.3031560E-00	46.500	0.3122635E-00
47.000	0.3215227E-00	47.500	0.3309340E-00	48.000	0.3404971E-00
48.500	0.3502116E-00	49.000	0.3600773E-00	49.500	0.3700936E-00
50.000	0.3802607E-00	50.500	0.3905777E-00	51.000	0.4010441E-00
51.500	0.4116595E-00	52.000	0.4224235E-00	52.500	0.4333549E-00
53.000	0.4443936E-00	53.500	0.4555957E-00	54.000	0.4669498E-00
54.500	0.4784451E-00	55.000	0.4900846E-00	55.500	0.5018671E 00
56.000	0.5137924E 00	56.500	0.5258556E 00	57.000	0.5380549E 00
57.500	0.5504104E 00	58.000	0.5628939E 00	58.500	0.5755149E 00
59.000	0.5882704E 00	59.500	0.6011558E 00	60.000	[illegible]

ANGLE	AREA	ANGLE	AREA	ANGLE	AREA
60.500	0.6273405E 00	61.000	0.6406266E 00	61.500	0.6540422E 00
62.000	0.6675853E 00	62.500	0.6812547E 00	63.000	0.6950489E 00
63.500	0.7089663E 00	64.000	0.7230053E 00	64.500	0.7371643E 00
65.000	0.7514417E 00	65.500	0.7658358E 00	66.000	0.7803449E 00
66.500	0.7949671E 00	67.000	0.8097006E 00	67.500	0.8245438E 00
68.000	0.8394947E 00	68.500	0.8545513E 00	69.000	0.8697118E 00
69.500	0.8849743E 00	70.000	0.9003366E 00	70.500	0.9157969E 00
71.000	0.9313530E 00	71.500	0.9470029E 00	72.000	0.9627444E 00
72.500	0.9785754E 00	73.000	0.9944939E 00	73.500	0.1010497E 01
74.000	0.1026584E 01	74.500	0.1042751E 01	75.000	0.1058997E 01
75.500	0.1075319E 01	76.000	0.1091714E 01	76.500	0.1108182E 01
77.000	0.1124718E 01	77.500	0.1141321E 01	78.000	0.1157985E 01
78.500	0.1174718E 01	79.000	0.1191507E 01	79.500	0.1208355E 01
80.000	0.1225253E 01	80.500	0.1242206E 01	81.000	0.1259208E 01
81.500	0.1276257E 01	82.000	0.1293351E 01	82.500	0.1310487E 01
83.000	0.1327662E 01	83.500	0.1344874E 01	84.000	0.1362121E 01
84.500	0.1379399E 01	85.000	0.1396706E 01	85.500	0.1414039E 01
86.000	0.1431397E 01	86.500	0.1448775E 01	87.000	0.1466172E 01
87.500	0.1483585E 01	88.000	0.1501011E 01	88.500	0.1518446E 01
89.000	0.1535893E 01	89.500	0.1553343E 01	90.000	0.1570796E 01
90.500	0.1588249E 01	91.000	0.1605699E 01	91.500	0.1623144E 01
92.000	0.1640581E 01	92.500	0.1658007E 01	93.000	0.1675420E 01
93.500	0.1692817E 01	94.000	0.1710196E 01	94.500	0.1727553E 01
95.000	0.1744887E 01	95.500	0.1762194E 01	96.000	0.1779472E 01
96.500	0.1796718E 01	97.000	0.1813930E 01	97.500	0.1831105E 01
98.000	0.1848241E 01	98.500	0.1865335E 01	99.000	0.1882384E 01
99.500	0.1899387E 01	100.000	0.1916339E 01	100.500	0.1933240E 01
101.000	0.1950086E 01	101.500	0.1966875E 01	102.000	0.1983604E 01
102.500	0.2000272E 01	103.000	0.2016875E 01	103.500	0.2033411E 01
104.000	0.2049878E 01	104.500	0.2066274E 01	105.000	0.2082596E 01
105.500	0.2098841E 01	106.000	0.2115009E 01	106.500	0.2131095E 01
107.000	0.2147099E 01	107.500	0.2163017E 01	108.000	0.2178848E 01
108.500	0.2194590E 01	109.000	0.2210239E 01	109.500	0.2225796E 01
110.000	0.2241256E 01	110.500	0.2256618E 01	111.000	0.2271881E 01
111.500	0.2287041E 01	112.000	0.2302098E 01	112.500	0.2317049E 01
113.000	0.2331892E 01	113.500	0.2346625E 01	114.000	0.2361248E 01
114.500	0.2375757E 01	115.000	0.2390151E 01	115.500	0.2404428E 01
116.000	0.2418587E 01	116.500	0.2432626E 01	117.000	0.2446544E 01
117.500	0.2460338E 01	118.000	0.2474007E 01	118.500	0.2487550E 01
119.000	0.2500966E 01	119.500	0.2514252E 01	120.000	0.2527408E 01

ANGLE	AREA	ANGLE	AREA	ANGLE	AREA
120.500	0.2540431E 01	121.000	0.2553322E 01	121.500	0.2566076E 01
122.000	0.2578699E 01	122.500	0.2591182E 01	123.000	0.2603528E 01
123.500	0.2615734E 01	124.000	0.2627600E 01	124.500	0.2639725E 01
125.000	0.2651508E 01	125.500	0.2663147E 01	126.000	0.2674643E 01
126.500	0.2685994E 01	127.000	0.2697199E 01	127.500	0.2708258E 01
128.000	0.2719169E 01	128.500	0.2729933E 01	129.000	0.2740548E 01
129.500	0.2751015E 01	130.000	0.2761332E 01	130.500	0.2771499E 01
131.000	0.2781515E 01	131.500	0.2791381E 01	132.000	0.2801095E 01
132.500	0.2810659E 01	133.000	0.2820070E 01	133.500	0.2829329E 01
134.000	0.2838437E 01	134.500	0.2847392E 01	135.000	0.2856194E 01
135.500	0.2864845E 01	136.000	0.2873343E 01	136.500	0.2881689E 01
137.000	0.2889883E 01	137.500	0.2897925E 01	138.000	0.2905815E 01
138.500	0.2913554E 01	139.000	0.2921142E 01	139.500	0.2928578E 01
140.000	0.2935865E 01	140.500	0.2943001E 01	141.000	0.2949986E 01
141.500	0.2956826E 01	142.000	0.2963515E 01	142.500	0.2970057E 01
143.000	0.2976452E 01	143.500	0.2982700E 01	144.000	0.2988802E 01
144.500	0.2994760E 01	145.000	0.3000574E 01	145.500	0.3006244E 01
146.000	0.3011773E 01	146.500	0.3017160E 01	147.000	0.3022407E 01
147.500	0.3027514E 01	148.000	0.3032484E 01	148.500	0.3037317E 01
149.000	0.3042014E 01	149.500	0.3046577E 01	150.000	0.3051006E 01
150.500	0.3055304E 01	151.000	0.3059471E 01	151.500	0.3063509E 01
152.000	0.3067419E 01	152.500	0.3071203E 01	153.000	0.3074862E 01
153.500	0.3078398E 01	154.000	0.3081812E 01	154.500	0.3085107E 01
155.000	0.3088282E 01	155.500	0.3091342E 01	156.000	0.3094286E 01
156.500	0.3097117E 01	157.000	0.3099837E 01	157.500	0.3102447E 01
158.000	0.3104949E 01	158.500	0.3107346E 01	159.000	0.3109639E 01
159.500	0.3111830E 01	160.000	0.3113921E 01	160.500	0.3115914E 01
161.000	0.3117811E 01	161.500	0.3119614E 01	162.000	0.3121326E 01
162.500	0.3122948E 01	163.000	0.3124483E 01	163.500	0.3125933E 01
164.000	0.3127300E 01	164.500	0.3128586E 01	165.000	0.3129793E 01
165.500	0.3130925E 01	166.000	0.3131982E 01	166.500	0.3132968E 01
167.000	0.3133885E 01	167.500	0.3134736E 01	168.000	0.3135521E 01
168.500	0.3136245E 01	169.000	0.3136910E 01	169.500	0.3137517E 01
170.000	0.3138070E 01	170.500	0.3138570E 01	171.000	0.3139021E 01
171.500	0.3139425E 01	172.000	0.3139785E 01	172.500	0.3140102E 01
173.000	0.3140381E 01	173.500	0.3140622E 01	174.000	0.3140829E 01
174.500	0.3141004E 01	175.000	0.3141150E 01	175.500	0.3141270E 01
176.000	0.3141366E 01	176.500	0.3141441E 01	177.000	0.3141497E 01
177.500	0.3141537E 01	178.000	0.3141564E 01	178.500	0.3141581E 01
179.000	0.3141589E 01	179.500	0.3141592E 01	180.000	0.3141593E 01

ANGLE	RHL	ANGLE	RHL	ANGLE	RHL
0.500	0.2539310E-04	1.000	0.1015396E-03	1.500	0.2284378E-03
2.000	0.4060628E-03	2.500	0.6343805E-03	3.000	0.9133555E-03
3.500	0.1242931E-02	4.000	0.1623050E-02	4.500	0.2053634E-02
5.000	0.2534619E-02	5.500	0.3065906E-02	6.000	0.3647406E-02
6.500	0.4279003E-02	7.000	0.4960589E-02	7.500	0.5692038E-02
8.000	0.6473218E-02	8.500	0.7303983E-02	9.000	0.8184185E-02
9.500	0.9113652E-02	10.000	0.1009223E-01	10.500	0.1111974E-01
11.000	0.1219599E-01	11.500	0.1332077E-01	12.000	0.1449390E-01
12.500	0.1571515E-01	13.000	0.1698430E-01	13.500	0.1830112E-01
14.000	0.1966538E-01	14.500	0.2107681E-01	15.000	0.2253517E-01
15.500	0.2404019E-01	16.000	0.2559161E-01	16.500	0.2718912E-01
17.000	0.2883246E-01	17.500	0.3052130E-01	18.000	0.3225536E-01
18.500	0.3403431E-01	19.000	0.3585784E-01	19.500	0.3772561E-01
20.000	0.3963728E-01	20.500	0.4159252E-01	21.000	0.4359095E-01
21.500	0.4563224E-01	22.000	0.4771599E-01	22.500	0.4984184E-01
23.000	0.5200941E-01	23.500	0.5421829E-01	24.000	0.5646810E-01
24.500	0.5875843E-01	25.000	0.6108886E-01	25.500	0.6345898E-01
26.000	0.6586836E-01	26.500	0.6831656E-01	27.000	0.7080315E-01
27.500	0.7332768E-01	28.000	0.7588970E-01	28.500	0.7848874E-01
29.000	0.8112433E-01	29.500	0.8379603E-01	30.000	0.8650333E-01
30.500	0.8924575E-01	31.000	0.9202282E-01	31.500	0.9483402E-01
32.000	0.9767686E-01	32.500	0.1005568E-00	33.000	0.1034674E-00
33.500	0.1064101E-00	34.000	0.1093844E-00	34.500	0.1123897E-00
35.000	0.1154256E-00	35.500	0.1184914E-00	36.000	0.1215866E-00
36.500	0.1247108E-00	37.000	0.1278633E-00	37.500	0.1310435E-00
38.000	0.1342510E-00	38.500	0.1374851E-00	39.000	0.1407453E-00
39.500	0.1440310E-00	40.000	0.1473417E-00	40.500	0.1506767E-00
41.000	0.1540355E-00	41.500	0.1574174E-00	42.000	0.1608220E-00
42.500	0.1642485E-00	43.000	0.1676964E-00	43.500	0.1711652E-00
44.000	0.1746541E-00	44.500	0.1781626E-00	45.000	0.1816901E-00
45.500	0.1852360E-00	46.000	0.1887996E-00	46.500	0.1923803E-00
47.000	0.1959776E-00	47.500	0.1995908E-00	48.000	0.2032192E-00
48.500	0.2068623E-00	49.000	0.2105195E-00	49.500	0.2141900E-00
50.000	0.2178733E-00	50.500	0.2215688E-00	51.000	0.2252758E-00
51.500	0.2289937E-00	52.000	0.2327219E-00	52.500	0.2364596E-00
53.000	0.2402064E-00	53.500	0.2439616E-00	54.000	0.2477244E-00
54.500	0.2514944E-00	55.000	0.2552708E-00	55.500	0.2590531E-00
56.000	0.2628405E-00	56.500	0.2666325E-00	57.000	0.2704285E-00
57.500	0.2742278E-00	58.000	0.2780297E-00	58.500	0.2818337E-00
59.000	0.2856391E-00	59.500	0.2894453E-00	60.000	0.2932517E-00

ANGLE	RHL	ANGLE	RHL	ANGLE	RHL
60.500	0.2970576E-00	61.000	0.3008624E-00	61.500	0.3046655E-00
62.000	0.3084663E-00	62.500	0.3122642E-00	63.000	0.3160585E-00
63.500	0.3198486E-00	64.000	0.3236340E-00	64.500	0.3274140E-00
65.000	0.3311880E-00	65.500	0.3349554E-00	66.000	0.3387157E-00
66.500	0.3424681E-00	67.000	0.3462122E-00	67.500	0.3499473E-00
68.000	0.3536723E-00	68.500	0.3573882E-00	69.000	0.3610929E-00
69.500	0.3647863E-00	70.000	0.3684678E-00	70.500	0.3721369E-00
71.000	0.3757929E-00	71.500	0.3794354E-00	72.000	0.3830638E-00
72.500	0.3866775E-00	73.000	0.3902760E-00	73.500	0.3938588E-00
74.000	0.3974232E-00	74.500	0.4009748E-00	75.000	0.4045070E-00
75.500	0.4080214E-00	76.000	0.4115173E-00	76.500	0.4149943E-00
77.000	0.4184519E-00	77.500	0.4218895E-00	78.000	0.4253067E-00
78.500	0.4287030E-00	79.000	0.4320779E-00	79.500	0.4354309E-00
80.000	0.4387615E-00	80.500	0.4420693E-00	81.000	0.4453538E-00
81.500	0.4486145E-00	82.000	0.4518510E-00	82.500	0.4550629E-00
83.000	0.4582497E-00	83.500	0.4614109E-00	84.000	0.4645462E-00
84.500	0.4676552E-00	85.000	0.4707373E-00	85.500	0.4737923E-00
86.000	0.4768197E-00	86.500	0.4798191E-00	87.000	0.4827901E-00
87.500	0.4857324E-00	88.000	0.4886456E-00	88.500	0.4915293E-00
89.000	0.4943832E-00	89.500	0.4972068E-00	90.000	0.5000000E 00
90.500	0.5027623E 00	91.000	0.5054934E 00	91.500	0.5081930E 00
92.000	0.5108607E 00	92.500	0.5134964E 00	93.000	0.5160996E 00
93.500	0.5186700E 00	94.000	0.5212075E 00	94.500	0.5237117E 00
95.000	0.5261824E 00	95.500	0.5286192E 00	96.000	0.5310220E 00
96.500	0.5333905E 00	97.000	0.5357245E 00	97.500	0.5380237E 00
98.000	0.5402879E 00	98.500	0.5425169E 00	99.000	0.5447105E 00
99.500	0.5468685E 00	100.000	0.5489908E 00	100.500	0.5510770E 00
101.000	0.5531272E 00	101.500	0.5551410E 00	102.000	0.55711[illegible]E 00
102.500	0.5590591E 00	103.000	0.5609631E 00	103.500	0.5628303E 00
104.000	0.5646604E 00	104.500	0.5664534E 00	105.000	0.56820[illegible]E 00
105.500	0.5699277E 00	106.000	0.5716088E 00	106.500	0.5732524E 00
107.000	0.5748584E 00	107.500	0.5764268E 00	108.000	0.5779574E 00
108.500	0.5794504E 00	109.000	0.5809055E 00	109.500	0.5823228E 00
110.000	0.5837023E 00	110.500	0.5850439E 00	111.000	0.5863476E 00
111.500	0.5876135E 00	112.000	0.5888415E 00	112.500	0.5900316E 00
113.000	0.5911639E 00	113.500	0.5922984E 00	114.000	0.5933751E 00
114.500	0.5944141E 00	115.000	0.5954155E 00	115.500	0.5963792E 00
116.000	0.5973054E 00	116.500	0.5981941E 00	117.000	0.5990454E 00
117.500	0.5998595E 00	118.000	0.6006363E 00	118.500	0.6013761E 00
119.000	0.6020789E 00	119.500	0.6027449E 00	120.000	0.6033742E 00

ANGLE	RHL	ANGLE	RHL	ANGLE	RHL
120.500	0.6039668E 00	121.000	0.6045231E 00	121.500	0.6050430E 00
122.000	0.6055268E 00	122.500	0.6059747E 00	123.000	0.6063868E 00
123.500	0.6067632E 00	124.000	0.6071043E 00	124.500	0.6074101E 00
125.000	0.6076808E 00	125.500	0.6079168E 00	126.000	0.6081181E 00
126.500	0.6082850E 00	127.000	0.6084178E 00	127.500	0.6085166E 00
128.000	0.6085817E 00	128.500	0.6086134E 00	129.000	0.6086119E 00
129.500	0.6085774E 00	130.000	0.6085102E 00	130.500	0.6084107E 00
131.000	0.6082790E 00	131.500	0.6081154E 00	132.000	0.6079203E 00
132.500	0.6076939E 00	133.000	0.6074365E 00	133.500	0.6071484E 00
134.000	0.6068300E 00	134.500	0.6064815E 00	135.000	0.6061033E 00
135.500	0.6056957E 00	136.000	0.6052590E 00	136.500	0.6047935E 00
137.000	0.6042996E 00	137.500	0.6037777E 00	138.000	0.6032281E 00
138.500	0.6026511E 00	139.000	0.6020471E 00	139.500	0.6014164E 00
140.000	0.6007595E 00	140.500	0.6000767E 00	141.000	0.5993683E 00
141.500	0.5986348E 00	142.000	0.5978765E 00	142.500	0.5970938E 00
143.000	0.5962871E 00	143.500	0.5954568E 00	144.000	0.5946033E 00
144.500	0.5937270E 00	145.000	0.5928283E 00	145.500	0.5919076E 00
146.000	0.5909653E 00	146.500	0.5900018E 00	147.000	0.5890175E 00
147.500	0.5880129E 00	148.000	0.5869884E 00	148.500	0.5859443E 00
149.000	0.5848812E 00	149.500	0.5837994E 00	150.000	0.5826993E 00
150.500	0.5815815E 00	151.000	0.5804463E 00	151.500	0.5792942E 00
152.000	0.5781256E 00	152.500	0.5769409E 00	153.000	0.5757406E 00
153.500	0.5745252E 00	154.000	0.5732950E 00	154.500	0.5720505E 00
155.000	0.5707921E 00	155.500	0.5695204E 00	156.000	0.5682357E 00
156.500	0.5669385E 00	157.000	0.5656292E 00	157.500	0.5643083E 00
158.000	0.5629762E 00	158.500	0.5616335E 00	159.000	0.5602804E 00
159.500	0.5589176E 00	160.000	0.5575453E 00	160.500	0.5561642E 00
161.000	0.5547745E 00	161.500	0.5533769E 00	162.000	0.5519716E 00
162.500	0.5505592E 00	163.000	0.5491402E 00	163.500	0.5477149E 00
164.000	0.5462838E 00	164.500	0.5448473E 00	165.000	0.5434059E 00
165.500	0.5419600E 00	166.000	0.5405101E 00	166.500	0.5390567E 00
167.000	0.5376000E 00	167.500	0.5361407E 00	168.000	0.5346790E 00
168.500	0.5332155E 00	169.000	0.5317506E 00	169.500	0.5302846E 00
170.000	0.5288181E 00	170.500	0.5273514E 00	171.000	0.5258850E 00
171.500	0.5244193E 00	172.000	0.5229547E 00	172.500	0.5214917E 00
173.000	0.5200305E 00	173.500	0.5185717E 00	174.000	0.5171156E 00
174.500	0.5156627E 00	175.000	0.5142133E 00	175.500	0.5127679E 00
176.000	0.5113266E 00	176.500	0.5098904E 00	177.000	0.5084591E 00
177.500	0.5070333E 00	178.000	0.5056134E 00	178.500	0.5041998E 00
179.000	0.5027927E 00	179.500	0.5013927E 00	180.000	0.5000000E 00

ANGLE	RHV	ANGLE	RHV	ANGLE	RHV
0.500	0.1269663E-04	1.000	0.5077061E-04	1.500	0.1142254E-03
2.000	0.2030520E-03	2.500	0.3172406E-03	3.000	0.4567821E-03
3.500	0.6216586E-03	4.000	0.8118549E-03	4.500	0.1027345E-02
5.000	0.1268114E-02	5.500	0.1534130E-02	6.000	0.1825370E-02
6.500	0.2141797E-02	7.000	0.2483381E-02	7.500	0.2850085E-02
8.000	0.3241871E-02	8.500	0.3658695E-02	9.000	0.4100514E-02
9.500	0.4567275E-02	10.000	0.5058940E-02	10.500	0.5575448E-02
11.000	0.6116747E-02	11.500	0.6682776E-02	12.000	0.7273476E-02
12.500	0.7888789E-02	13.000	0.8528644E-02	13.500	0.9192973E-02
14.000	0.9881707E-02	14.500	0.1059477E-01	15.000	0.1133209E-01
15.500	0.1209358E-01	16.000	0.1287917E-01	16.500	0.1368877E-01
17.000	0.1452230E-01	17.500	0.1537966E-01	18.000	0.1626078E-01
18.500	0.1716551E-01	19.000	0.1809382E-01	19.500	0.1904556E-01
20.000	0.2002070E-01	20.500	0.2101906E-01	21.000	0.2204036E-01
21.500	0.2308510E-01	22.000	0.2415256E-01	22.500	0.2524282E-01
23.000	0.2635578E-01	23.500	0.2749131E-01	24.000	0.2864929E-01
24.500	0.2982960E-01	25.000	0.3103211E-01	25.500	0.3225669E-01
26.000	0.3350321E-01	26.500	0.3477154E-01	27.000	0.3606154E-01
27.500	0.3737306E-01	28.000	0.3870602E-01	28.500	0.4006020E-01
29.000	0.4143549E-01	29.500	0.4283175E-01	30.000	0.4424882E-01
30.500	0.4568654E-01	31.000	0.4714478E-01	31.500	0.4862336E-01
32.000	0.5012214E-01	32.500	0.5164094E-01	33.000	0.5317962E-01
33.500	0.5473800E-01	34.000	0.5631592E-01	34.500	0.5791321E-01
35.000	0.5952970E-01	35.500	0.6116522E-01	36.000	0.6281959E-01
36.500	0.6449262E-01	37.000	0.6618416E-01	37.500	0.6789401E-01
38.000	0.6962198E-01	38.500	0.7136791E-01	39.000	0.7313159E-01
39.500	0.7491285E-01	40.000	0.7671148E-01	40.500	0.7852731E-01
41.000	0.8036012E-01	41.500	0.8220973E-01	42.000	0.8407594E-01
42.500	0.8595855E-01	43.000	0.8785735E-01	43.500	0.8977215E-01
44.000	0.9170274E-01	44.500	0.9364891E-01	45.000	0.9561046E-01
45.500	0.9758717E-01	46.000	0.9957883E-01	46.500	0.1015852E-00
47.000	0.1036061E-00	47.500	0.1056414E-00	48.000	0.1076907E-00
48.500	0.1097539E-00	49.000	0.1118307E-00	49.500	0.1139210E-00
50.000	0.1160245E-00	50.500	0.1181409E-00	51.000	0.1202701E-00
51.500	0.1224119E-00	52.000	0.1245659E-00	52.500	0.1267320E-00
53.000	0.1289099E-00	53.500	0.1310994E-00	54.000	0.1333003E-00
54.500	0.1355123E-00	55.000	0.1377352E-00	55.500	0.1399688E-00
56.000	0.1422127E-00	56.500	0.1444669E-00	57.000	0.1467310E-00
57.500	0.1490048E-00	58.000	0.1512880E-00	58.500	0.1535604E-00
59.000	0.1558818E-00	59.500	0.1581919E-00	60.000	0.1605105E-00

ANGLE	RHV	ANGLE	RHV	ANGLE	RHV
60.500	0.1628379E-00	61.000	0.1651721E-00	61.500	0.1675146E-00
62.000	0.1698640E-00	62.500	0.1722216E-00	63.000	0.1745869E-00
63.500	0.1769568E-00	64.000	0.1793342E-00	64.500	0.1817177E-00
65.000	0.1841072E-00	65.500	0.1865025E-00	66.000	0.1889032E-00
66.500	0.1913090E-00	67.000	0.1937198E-00	67.500	0.1961355E-00
68.000	0.1985553E-00	68.500	0.2009793E-00	69.000	0.2034073E-00
69.500	0.2058390E-00	70.000	0.2082740E-00	70.500	0.2107122E-00
71.000	0.2131533E-00	71.500	0.2155970E-00	72.000	0.2180430E-00
72.500	0.2204912E-00	73.000	0.2229412E-00	73.500	0.2253928E-00
74.000	0.2278457E-00	74.500	0.2302997E-00	75.000	0.2327545E-00
75.500	0.2352098E-00	76.000	0.2376655E-00	76.500	0.2401211E-00
77.000	0.2425766E-00	77.500	0.2450316E-00	78.000	0.2474858E-00
78.500	0.2499391E-00	79.000	0.2523911E-00	79.500	0.2548416E-00
80.000	0.2572904E-00	80.500	0.2597371E-00	81.000	0.2621815E-00
81.500	0.2646235E-00	82.000	0.2670626E-00	82.500	0.2694986E-00
83.000	0.2719316E-00	83.500	0.2743609E-00	84.000	0.2767865E-00
84.500	0.2792080E-00	85.000	0.2816252E-00	85.500	0.2840379E-00
86.000	0.2864458E-00	86.500	0.2888487E-00	87.000	0.2912463E-00
87.500	0.2936384E-00	88.000	0.2960247E-00	88.500	0.2984051E-00
89.000	0.3007792E-00	89.500	0.3031468E-00	90.000	0.3055077E-00
90.500	0.3078617E-00	91.000	0.3102085E-00	91.500	0.3125476E-00
92.000	0.3148795E-00	92.500	0.3172035E-00	93.000	0.3195189E-00
93.500	0.3218263E-00	94.000	0.3241250E-00	94.500	0.3264149E-00
95.000	0.3286956E-00	95.500	0.3309675E-00	96.000	0.3332297E-00
96.500	0.3354822E-00	97.000	0.3377248E-00	97.500	0.3399572E-00
98.000	0.3421794E-00	98.500	0.3443909E-00	99.000	0.3465916E-00
99.500	0.3487816E-00	100.000	0.3509603E-00	100.500	0.3531276E-00
101.000	0.3552833E-00	101.500	0.3574272E-00	102.000	0.3595592E-00
102.500	0.3616789E-00	103.000	0.3637864E-00	103.500	0.3658812E-00
104.000	0.3679633E-00	104.500	0.3700325E-00	105.000	0.3720886E-00
105.500	0.3741313E-00	106.000	0.3761606E-00	106.500	0.3781762E-00
107.000	0.3801780E-00	107.500	0.3821658E-00	108.000	0.3841394E-00
108.500	0.3860987E-00	109.000	0.3880435E-00	109.500	0.3899736E-00
110.000	0.3918890E-00	110.500	0.3937893E-00	111.000	0.3956745E-00
111.500	0.3975445E-00	112.000	0.3993990E-00	112.500	0.4012379E-00
113.000	0.4030612E-00	113.500	0.4048686E-00	114.000	0.4066600E-00
114.500	0.4084354E-00	115.000	0.4101944E-00	115.500	0.4119372E-00
116.000	0.4136634E-00	116.500	0.4153730E-00	117.000	0.4170659E-00
117.500	0.4187420E-00	118.000	0.4204012E-00	118.500	0.4220435E-00
119.000	0.4236683E-00	119.500	0.4252760E-00	120.000	0.4268663E-00

ANGLE	RHV	ANGLE	RHV	ANGLE	RHV
120.500	0.4284393E-00	121.000	0.4299947E-00	121.500	0.4315325E-00
122.000	0.4330527E-00	122.500	0.4345551E-00	123.000	0.4360396E-00
123.500	0.4375063E-00	124.000	0.4389549E-00	124.500	0.4403856E-00
125.000	0.4417982E-00	125.500	0.4431926E-00	126.000	0.4445688E-00
126.500	0.4459268E-00	127.000	0.4472665E-00	127.500	0.4485878E-00
128.000	0.4498908E-00	128.500	0.4511755E-00	129.000	0.4524417E-00
129.500	0.4536895E-00	130.000	0.4549188E-00	130.500	0.4561296E-00
131.000	0.4573220E-00	131.500	0.4584958E-00	132.000	0.4596312E-00
132.500	0.4607881E-00	133.000	0.4619065E-00	133.500	0.4630064E-00
134.000	0.4640879E-00	134.500	0.4651509E-00	135.000	0.4661955E-00
135.500	0.4672217E-00	136.000	0.4682295E-00	136.500	0.4692191E-00
137.000	0.4701903E-00	137.500	0.4711433E-00	138.000	0.4720781E-00
138.500	0.4729947E-00	139.000	0.4738933E-00	139.500	0.4747739E-00
140.000	0.4756365E-00	140.500	0.4764812E-00	141.000	0.4773081E-00
141.500	0.4781173E-00	142.000	0.4789088E-00	142.500	0.4796828E-00
143.000	0.4804392E-00	143.500	0.4811784E-00	144.000	0.4819002E-00
144.500	0.4826049E-00	145.000	0.4832925E-00	145.500	0.4839632E-00
146.000	0.4846171E-00	146.500	0.4852342E-00	147.000	0.4858748E-00
147.500	0.4864790E-00	148.000	0.4870668E-00	148.500	0.4876385E-00
149.000	0.4881941E-00	149.500	0.4887339E-00	150.000	0.48[illegible]2579E-00
150.500	0.4897664E-00	151.000	0.4902595E-00	151.500	0.4907374E-00
152.000	0.4912001E-00	152.500	0.4916480E-00	153.000	0.4920812E-00
153.500	0.4924999E-00	154.000	0.4929041E-00	154.500	0.4932943E-00
155.000	0.4936705E-00	155.500	0.4940329E-00	156.000	0.49438[illegible]7E-00
156.500	0.4947172E-00	157.000	0.4950396E-00	157.500	0.4953490E-00
158.000	0.4956457E-00	158.500	0.4959299E-00	159.000	0.4962018E-00
159.500	0.4964617E-00	160.000	0.4967098E-00	160.500	0.4969464E-00
161.000	0.4971716E-00	161.500	0.4973857E-00	162.000	0.4975889E-00
162.500	0.4977816E-00	163.000	0.4979639E-00	163.500	0.4981362E-00
164.000	0.4982986E-00	164.500	0.4984515E-00	165.000	0.4985951E-00
165.500	0.4987296E-00	166.000	0.4988554E-00	166.500	0.4989727E-00
167.000	0.4990818E-00	167.500	0.4991830E-00	168.000	0.4992763E-00
168.500	0.4993627E-00	169.000	0.4994418E-00	169.500	0.4995142E-00
170.000	0.4995800E-00	170.500	0.4996397E-00	171.000	0.4996934E-00
171.500	0.4997416E-00	172.000	0.4997844E-00	172.500	0.4998223E-00
173.000	0.4998554E-00	173.500	0.4998842E-00	174.000	0.4999089E-00
174.500	0.4999298E-00	175.000	0.4999472E-00	175.500	0.4999615E-00
176.000	0.4999729E-00	176.500	0.4999819E-00	177.000	0.4999866E-00
177.500	0.4999934E-00	178.000	0.4999966E-00	178.500	0.4999986E-00
179.000	0.4999996E-00	179.500	0.4999999E-00	180.000	0.5000000E 00

ANGLE	PRE	ANGLE	PRE	ANGLE	PRE
0.500	-0.1449578E-09	1.000	0.4604317E-11	1.500	0.1321723E-08
2.000	0.6552455E-08	2.500	0.2086745E-07	3.000	0.5199672E-07
3.500	0.1128155E-06	4.000	0.2198885E-06	4.500	0.3975692E-06
5.000	0.6727641E-06	5.500	0.1083659E-05	6.000	0.1673143E-05
6.500	0.2496286E-05	7.000	0.3614419E-05	7.500	0.5100723E-05
8.000	0.7038703E-05	8.500	0.9525014E-05	9.000	0.1266669E-04
9.500	0.1658927E-04	10.000	0.2142126E-04	10.500	0.2731685E-04
11.000	0.3444147E-04	11.500	0.4297600E-04	12.000	0.5311693E-04
12.500	0.6508059E-04	13.000	0.7909967E-04	13.500	0.9542797E-04
14.000	0.1143322E-03	14.500	0.1361069E-03	15.000	0.1610594E-03
15.500	0.1895215E-03	16.000	0.2218471E-03	16.500	0.2584116E-03
17.000	0.2996069E-03	17.500	0.3458592E-03	18.000	0.3976095E-03
18.500	0.4553248E-03	19.000	0.5194941E-03	19.500	0.5906357E-03
20.000	0.6692866E-03	20.500	0.7560132E-03	21.000	0.8514095E-03
21.500	0.9560869E-03	22.000	0.1070693E-02	22.500	0.1195894E-02
23.000	0.1332385E-02	23.500	0.1480893E-02	24.000	0.1642163E-02
24.500	0.1816978E-02	25.000	0.2006141E-02	25.500	0.2210478E-02
26.000	0.2430854E-02	26.500	0.2668154E-02	27.000	0.2923299E-02
27.500	0.3197223E-02	28.000	0.3490902E-02	28.500	0.3805328E-02
29.000	0.4141535E-02	29.500	0.4500559E-02	30.000	0.4883489E-02
30.500	0.5291438E-02	31.000	0.5725541E-02	31.500	0.6186546E-02
32.000	0.6676859E-02	32.500	0.7196485E-02	33.000	0.7747070E-02
33.500	0.8329873E-02	34.000	0.8946183E-02	34.500	0.9597528E-02
35.000	0.1028464E-01	35.500	0.1100930E-01	36.000	0.1177329E-01
36.500	0.1257741E-01	37.000	0.1342333E-01	37.500	0.1431246E-01
38.000	0.1524636E-01	38.500	0.1622648E-01	39.000	0.1725436E-01
39.500	0.1833152E-01	40.000	0.1945958E-01	40.500	0.2064007E-01
41.000	0.2187462E-01	41.500	0.2316485E-01	42.000	0.2451241E-01
42.500	0.2591895E-01	43.000	0.2738613E-01	43.500	0.2891565E-01
44.000	0.3050920E-01	44.500	0.3216851E-01	45.000	0.3389529E-01
45.500	0.3569128E-01	46.000	0.3755825E-01	46.500	0.3949795E-01
47.000	0.4151216E-01	47.500	0.4360264E-01	48.000	0.4577116E-01
48.500	0.4801960E-01	49.000	0.5034966E-01	49.500	0.5276320E-01
50.000	0.5526201E-01	50.500	0.5784789E-01	51.000	0.6052267E-01
51.500	0.6328816E-01	52.000	0.6614617E-01	52.500	0.6909851E-01
53.000	0.7214699E-01	53.500	0.7529343E-01	54.000	0.7853960E-01
54.500	0.8188735E-01	55.000	0.8533841E-01	55.500	0.8889461E-01
56.000	0.9255772E-01	56.500	0.9632950E-01	57.000	0.1002117E-00
57.500	0.1042060E-00	58.000	0.1083143E-00	58.500	0.1125381E-00
59.000	0.1168795E-00	59.500	0.1213394E-00	60.000	0.1259202E-00

ANGLE	PRE	ANGLE	PRE	ANGLE	PRE
60.500	0.1306233E-00	61.000	0.1354504E-00	61.500	0.1404030E-00
62.000	0.1454828E-00	62.500	0.1506913E-00	63.000	0.1560300E-00
63.500	0.1615005E-00	64.000	0.1671042E-00	64.500	0.1728427E-00
65.000	0.1787173E-00	65.500	0.1847295E-00	66.000	0.1908806E-00
66.500	0.1971721E-00	67.000	0.2036051E-00	67.500	0.2101810E-00
68.000	0.2169011E-00	68.500	0.2237665E-00	69.000	0.2307784E-00
69.500	0.2379380E-00	70.000	0.2452464E-00	70.500	0.2527045E-00
71.000	0.2603136E-00	71.500	0.2680744E-00	72.000	0.2759881E-00
72.500	0.2840554E-00	73.000	0.2922772E-00	73.500	0.3006544E-00
74.000	0.3091877E-00	74.500	0.3178778E-00	75.000	0.3267254E-00
75.500	0.3357312E-00	76.000	0.3448957E-00	76.500	0.3542194E-00
77.000	0.3637029E-00	77.500	0.3733464E-00	78.000	0.3831506E-00
78.500	0.3931156E-00	79.000	0.4032416E-00	79.500	0.4135293E-00
80.000	0.4239784E-00	80.500	0.4345892E-00	81.000	0.4453617E-00
81.500	0.4562959E-00	82.000	0.4673919E-00	82.500	0.4786494E-00
83.000	0.4900684E-00	83.500	0.5016487E 00	84.000	0.5133899E 00
84.500	0.5252918E 00	85.000	0.5373540E 00	85.500	0.5495760E 00
86.000	0.5619574E 00	86.500	0.5744975E 00	87.000	0.5871959E 00
87.500	0.6000517E 00	88.000	0.6130644E 00	88.500	0.6262331E 00
89.000	0.6395570E 00	89.500	0.6530351E 00	90.000	0.6666666E 00
90.500	0.6804503E 00	91.000	0.6943853E 00	91.500	0.7084704E 00
92.000	0.7227044E 00	92.500	0.7370861E 00	93.000	0.7516141E 00
93.500	0.7662872E 00	94.000	0.7811038E 00	94.500	0.7960625E 00
95.000	0.8111618E 00	95.500	0.8264001E 00	96.000	0.8417758E 00
96.500	0.8572870E 00	97.000	0.8729322E 00	97.500	0.8887095E 00
98.000	0.9046170E 00	98.500	0.9206528E 00	99.000	0.9368[illegible]E 00
99.500	0.9531015E 00	100.000	0.9695102E 00	100.500	0.9860390E 00
101.000	0.1002686E 01	101.500	0.1019448E 01	102.000	0.1036324E 01
102.500	0.1053311E 01	103.000	0.1070407E 01	103.500	0.1087610E 01
104.000	0.1104916E 01	104.500	0.1122323E 01	105.000	0.1139829E 01
105.500	0.1157432E 01	106.000	0.1175128E 01	106.500	0.1192915E 01
107.000	0.1210790E 01	107.500	0.1228750E 01	108.000	0.1246793E 01
108.500	0.1264916E 01	109.000	0.1283116E 01	109.500	0.1301390E 01
110.000	0.1319734E 01	110.500	0.1338147E 01	111.000	0.1356624E 01
111.500	0.1375164E 01	112.000	0.1393762E 01	112.500	0.1412416E 01
113.000	0.1431123E 01	113.500	0.1449879E 01	114.000	0.1468681E 01
114.500	0.1487527E 01	115.000	0.1506412E 01	115.500	0.1525333E 01
116.000	0.1544288E 01	116.500	0.1563272E 01	117.000	0.1582283E 01
117.500	0.1601317E 01	118.000	0.1620371E 01	118.500	0.1639441E 01
119.000	0.1658525E 01	119.500	0.1677617E 01	120.000	0.1696716E 01

ANGLE	PRE	ANGLE	PRE	ANGLE	PRE
120.500	0.1715818E 01	121.000	0.1734919E 01	121.500	0.1754016E 01
122.000	0.1773105E 01	122.500	0.1792182E 01	123.000	0.1811245E 01
123.500	0.1830290E 01	124.000	0.1849314E 01	124.500	0.1868312E 01
125.000	0.1887282E 01	125.500	0.1906219E 01	126.000	0.1925121E 01
126.500	0.1943984E 01	127.000	0.1962804E 01	127.500	0.1981579E 01
128.000	0.2000304E 01	128.500	0.2018975E 01	129.000	0.2037591E 01
129.500	0.2056146E 01	130.000	0.2074639E 01	130.500	0.2093064E 01
131.000	0.2111420E 01	131.500	0.2129702E 01	132.000	0.2147907E 01
132.500	0.2166032E 01	133.000	0.2184073E 01	133.500	0.2202027E 01
134.000	0.2219892E 01	134.500	0.2237662E 01	135.000	0.2255337E 01
135.500	0.2272911E 01	136.000	0.2290382E 01	136.500	0.2307746E 01
137.000	0.2325001E 01	137.500	0.2342144E 01	138.000	0.2359171E 01
138.500	0.2376079E 01	139.000	0.2392865E 01	139.500	0.2409526E 01
140.000	0.2426059E 01	140.500	0.2442461E 01	141.000	0.2458730E 01
141.500	0.2474862E 01	142.000	0.2490855E 01	142.500	0.2506705E 01
143.000	0.2522411E 01	143.500	0.2537968E 01	144.000	0.2553375E 01
144.500	0.2568629E 01	145.000	0.2583726E 01	145.500	0.2598666E 01
146.000	0.2613444E 01	146.500	0.2628059E 01	147.000	0.2642508E 01
147.500	0.2656789E 01	148.000	0.2670898E 01	148.500	0.2684835E 01
149.000	0.2698596E 01	149.500	0.2712179E 01	150.000	0.2725582E 01
150.500	0.2738803E 01	151.000	0.2751840E 01	151.500	0.2764691E 01
152.000	0.2777352E 01	152.500	0.2789824E 01	153.000	0.2802103E 01
153.500	0.2814187E 01	154.000	0.2826075E 01	154.500	0.2837766E 01
155.000	0.2849256E 01	155.500	0.2860544E 01	156.000	0.2871630E 01
156.500	0.2882510E 01	157.000	0.2893184E 01	157.500	0.2903649E 01
158.000	0.2913904E 01	158.500	0.2923949E 01	159.000	0.2933781E 01
159.500	0.2943398E 01	160.000	0.2952801E 01	160.500	0.2961986E 01
161.000	0.2970954E 01	161.500	0.2979702E 01	162.000	0.2988230E 01
162.500	0.2996536E 01	163.000	0.3004619E 01	163.500	0.3012479E 01
164.000	0.3020114E 01	164.500	0.3027524E 01	165.000	0.3034706E 01
165.500	0.3041661E 01	166.000	0.3048388E 01	166.500	0.3054885E 01
167.000	0.3061153E 01	167.500	0.3067189E 01	168.000	0.3072994E 01
168.500	0.3078567E 01	169.000	0.3083907E 01	169.500	0.3089014E 01
170.000	0.3093886E 01	170.500	0.3098524E 01	171.000	0.3102927E 01
171.500	0.3107094E 01	172.000	0.3111026E 01	172.500	0.3114721E 01
173.000	0.3118179E 01	173.500	0.3121400E 01	174.000	0.3124384E 01
174.500	0.3127130E 01	175.000	0.3129639E 01	175.500	0.3131908E 01
176.000	0.3133940E 01	176.500	0.3135733E 01	177.000	0.3137287E 01
177.500	0.3138602E 01	178.000	0.3139679E 01	178.500	0.3140516E 01
179.000	0.3141114E 01	179.500	0.3141473E 01	180.000	0.3141593E 01

ANGLE	FRO	ANGLE	FRO	ANGLE	FRO
0.500	0.4477610E 09	1.000	0.2779692E 08	1.500	0.5531285E 07
2.000	0.1750565E 07	2.500	0.7170657E 06	3.000	0.3458695E 06
3.500	0.1867322E 06	4.000	0.1094639E 06	4.500	0.6657104E 05
5.000	0.4487226E 05	5.500	0.3065900E 05	6.000	0.2165580E 05
6.500	0.1572694E 05	7.000	0.1169915E 05	7.500	0.8831968E 04
8.000	0.6864615E 04	8.500	0.5369350E 04	9.000	0.4290354E 04
9.500	0.3450076E 04	10.000	0.2818435E 04	10.500	0.2320302E 04
11.000	0.1927677E 04	11.500	0.1614882E 04	12.000	0.1363150E 04
12.500	0.1158723E 04	13.000	0.9913144E 03	13.500	0.8531576E 03
14.000	0.7383224E 03	14.500	0.6422357E 03	15.000	0.5613572E 03
15.500	0.4928320E 03	16.000	0.4345069E 03	16.500	0.3845972E 03
17.000	0.3416848E 03	17.500	[illegible]	18.000	[illegible]
18.500	0.2444868E 03	19.000	0.2200231E 03	19.500	0.1985616E 03
20.000	0.1796714E 03	20.500	0.1629907E 03	21.000	[illegible]
21.500	0.1350910E 03	22.000	[illegible]	22.500	0.1129559E 03
23.000	0.1036044E 03	23.500	[illegible]	24.000	0.8765746E 02
24.500	0.8084665E 02	25.000	0.7469216E 02	25.500	0.6911880E 02
26.000	0.6405167E 02	26.500	0.5945478E 02	27.000	0.5527806E 02
27.500	0.5149653E 02	28.000	0.4796752E 02	28.500	0.4477206E 02
29.000	0.4184233E 02	29.500	0.3915211E 02	30.000	0.3667319E 02
30.500	0.3439991E 02	31.000	0.3229890E 02	31.500	0.3035879E 02
32.000	0.2856492E 02	32.500	0.2690416E 02	33.000	0.2536483E 02
33.500	0.2393630E 02	34.000	0.2260910E 02	34.500	0.2137467E 02
35.000	0.2022526E 02	35.500	[illegible]	36.000	[illegible]
36.500	0.1722077E 02	37.000	0.1634790E 02	37.500	0.1553120E 02
38.000	0.1476636E 02	38.500	0.1404926E 02	39.000	0.1337645E 02
39.500	0.1274469E 02	40.000	0.1215072E 02	40.500	0.1159243E 02
41.000	0.1106671E 02	41.500	0.1057146E 02	42.000	0.1010450E 02
42.500	0.9664069E 01	43.000	0.9248196E 01	43.500	0.8855295E 01
44.000	0.8483636E 01	44.500	0.8132423E 01	45.000	[illegible]
45.500	0.7464622E 01	46.000	0.7163925E 01	46.500	0.6902630E 01
47.000	0.6633783E 01	47.500	0.6378496E 01	48.000	0.6135947E 01
48.500	0.5905372E 01	49.000	0.5686056E 01	49.500	0.5477344E 01
50.000	0.5278612E 01	50.500	0.5089266E 01	51.000	0.4908831E 01
51.500	0.4736744E 01	52.000	0.4572558E 01	52.500	0.4415835E 01
53.000	0.4266164E 01	53.500	0.4123164E 01	54.000	0.3986474E 01
54.500	0.3855756E 01	55.000	0.3730701E 01	55.500	0.3611006E 01
56.000	0.3496395E 01	56.500	0.3386607E 01	57.000	[illegible]
57.500	0.3180551E 01	58.000	0.3083794E 01	58.500	0.2990981E 01
59.000	[illegible]	59.500	[illegible]	60.000	[illegible]

ANGLE	FRO	ANGLE	FRO	ANGLE	FRO
60.500	0.2655268E 01	61.000	0.2579390E 01	61.500	0.2506430E 01
62.000	0.2436252E 01	62.500	0.2368728E 01	63.000	0.2303734E 01
63.500	0.2241157E 01	64.000	0.2180885E 01	64.500	0.2122817E 01
65.000	0.2066894E 01	65.500	0.2012903E 01	66.000	0.1960876E 01
66.500	0.1910690E 01	67.000	0.1862264E 01	67.500	0.1815524E 01
68.000	0.1770398E 01	68.500	0.1726819E 01	69.000	0.1684720E 01
69.500	0.1644042E 01	70.000	0.1604725E 01	70.500	0.1566713E 01
71.000	0.1529955E 01	71.500	0.1494398E 01	72.000	0.1459996E 01
72.500	0.1426702E 01	73.000	0.1394473E 01	73.500	0.1363266E 01
74.000	0.1333043E 01	74.500	0.1303765E 01	75.000	0.1275395E 01
75.500	0.1247901E 01	76.000	0.1221247E 01	76.500	0.1195403E 01
77.000	0.1170339E 01	77.500	0.1146025E 01	78.000	0.1122434E 01
78.500	0.1099540E 01	79.000	0.1077317E 01	79.500	0.1055741E 01
80.000	0.1034789E 01	80.500	0.1014439E 01	81.000	0.9946632E 00
81.500	0.9754594E 00	82.000	0.9567901E 00	82.500	0.9386424E 00
83.000	0.9209985E 00	83.500	0.9038411E 00	84.000	0.8871536E 00
84.500	0.8709200E 00	85.000	0.8551253E 00	85.500	0.8397546E 00
86.000	0.8247939E 00	86.500	0.8102297E 00	87.000	0.7960489E 00
87.500	0.7822390E 00	88.000	0.7687881E 00	88.500	0.7556645E 00
89.000	0.7429171E 00	89.500	0.7304752E 00	90.000	0.7183485E 00
90.500	0.7065270E 00	91.000	0.6950012E 00	91.500	0.6837620E 00
92.000	0.6728002E 00	92.500	0.6621076E 00	93.000	0.6516757E 00
93.500	0.6414967E 00	94.000	0.6315629E 00	94.500	0.6218668E 00
95.000	0.6124015E 00	95.500	0.6031599E 00	96.000	0.5941355E 00
96.500	0.5853218E 00	97.000	0.5767127E 00	97.500	0.5683021E 00
98.000	0.5600843E 00	98.500	0.5520537E 00	99.000	0.5442050E 00
99.500	0.5365328E 00	100.000	0.5290322E 00	100.500	0.5216984E 00
101.000	0.5145265E 00	101.500	0.5075120E 00	102.000	0.5006506E 00
102.500	0.4939378E-00	103.000	0.4873698E-00	103.500	0.4809423E-00
104.000	0.4746517E-00	104.500	0.4684940E-00	105.000	0.4624656E-00
105.500	0.4565632E-00	106.000	0.4507831E-00	106.500	0.4451222E-00
107.000	0.4395772E-00	107.500	0.4341450E-00	108.000	0.4288227E-00
108.500	0.4236072E-00	109.000	0.4184957E-00	109.500	0.4134855E-00
110.000	0.4085740E-00	110.500	0.4037585E-00	111.000	0.3990365E-00
111.500	0.3944055E-00	112.000	0.3898632E-00	112.500	0.3854073E-00
113.000	0.3810355E-00	113.500	0.3767456E-00	114.000	0.3725356E-00
114.500	0.3684033E-00	115.000	0.3643468E-00	115.500	0.3603640E-00
116.000	0.3564532E-00	116.500	0.3526124E-00	117.000	0.3488398E-00
117.500	0.3451337E-00	118.000	0.3414924E-00	118.500	0.3379142E-00
119.000	0.3343975E-00	119.500	0.3309407E-00	120.000	0.3275423E-00

ANGLE	FRO	ANGLE	FRO	ANGLE	FRO
120.500	0.3242007E-00	121.000	0.3209145E-00	121.500	0.3176823E-00
122.000	0.3145027E-00	122.500	0.3113742E-00	123.000	0.3082957E-00
123.500	0.3052657E-00	124.000	0.3022829E-00	124.500	0.2993463E-00
125.000	0.2964544E-00	125.500	0.2936062E-00	126.000	0.2908005E-00
126.500	0.2880361E-00	127.000	0.2853119E-00	127.500	0.2826268E-00
128.000	0.2799798E-00	128.500	0.2773698E-00	129.000	0.2747958E-00
129.500	0.2722567E-00	130.000	0.2697516E-00	130.500	0.2672796E-00
131.000	0.2648395E-00	131.500	0.2624306E-00	132.000	0.2600518E-00
132.500	0.2577023E-00	133.000	0.2553812E-00	133.500	0.2530876E-00
134.000	0.2503206E-00	134.500	0.2485795E-00	135.000	0.2463632E-00
135.500	0.2441711E-00	136.000	0.2420022E-00	136.500	0.2398559E-00
137.000	0.2377313E-00	137.500	0.2356275E-00	138.000	0.2335439E-00
138.500	0.2314796E-00	139.000	0.2294339E-00	139.500	0.2274060E-00
140.000	0.2253952E-00	140.500	0.2234007E-00	141.000	0.2214219E-00
141.500	0.2194579E-00	142.000	0.2175080E-00	142.500	0.2155715E-00
143.000	0.2136477E-00	143.500	0.2117359E-00	144.000	0.2098353E-00
144.500	0.2079452E-00	145.000	0.2060650E-00	145.500	0.2041938E-00
146.000	0.2023311E-00	146.500	0.2004760E-00	147.000	0.1986278E-00
147.500	0.1967859E-00	148.000	0.1949495E-00	148.500	0.1931178E-00
149.000	0.1912902E-00	149.500	0.1894660E-00	150.000	0.1876443E-00
150.500	0.1858244E-00	151.000	0.1840056E-00	151.500	0.1821871E-00
152.000	0.1803682E-00	152.500	0.1785480E-00	153.000	0.1767258E-00
153.500	0.1749007E-00	154.000	0.1730720E-00	154.500	0.1712387E-00
155.000	0.1694001E-00	155.500	0.1675552E-00	156.000	0.1657032E-00
156.500	0.1638432E-00	157.000	0.1619742E-00	157.500	0.1600952E-00
158.000	0.1582053E-00	158.500	0.1563034E-00	159.000	0.1543884E-00
159.500	0.1524593E-00	160.000	0.1505149E-00	160.500	0.1485541E-00
161.000	0.1465755E-00	161.500	0.1445779E-00	162.000	0.1425599E-00
162.500	0.1405202E-00	163.000	0.1384572E-00	163.500	0.1363693E-00
164.000	0.1342548E-00	164.500	0.1321120E-00	165.000	0.1299390E-00
165.500	0.1277338E-00	166.000	0.1254942E-00	166.500	0.1232179E-00
167.000	0.1209022E-00	167.500	0.1185447E-00	168.000	0.1161421E-00
168.500	0.1136914E-00	169.000	0.1111889E-00	169.500	0.1086307E-00
170.000	0.1060123E-00	170.500	0.1033289E-00	171.000	0.1005750E-00
171.500	0.9774416E-01	172.000	0.9482956E-01	172.500	0.9182231E-01
173.000	0.8871333E-01	173.500	0.8549113E-01	174.000	0.8214214E-01
174.500	0.7865001E-01	175.000	0.7499462E-01	175.500	0.7115063E-01
176.000	0.6708564E-01	176.500	0.6275862E-01	177.000	0.5810457E-01
177.500	0.5304466E-01	178.000	0.4744670E-01	178.500	0.4109155E-01
179.000	0.3335208E-01	179.500	0.2372555E-01	180.000	0.3100275E-04

APPENDIX VI

EQUIPMENT DRAWINGS

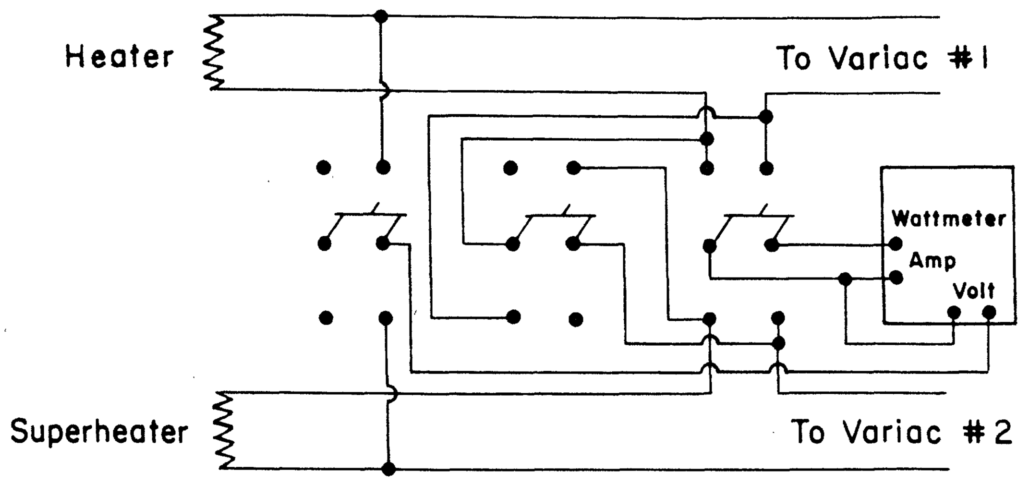

HEATER WIRING DIAGRAM
FIG. E.1

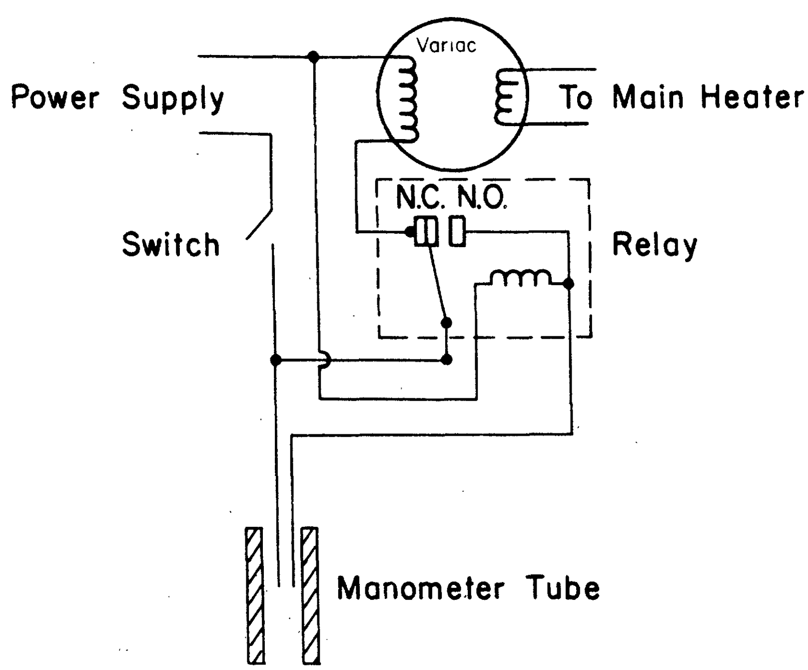

POWER SAFETY CUTOFF WIRING DIAGRAM
FIG. E.2

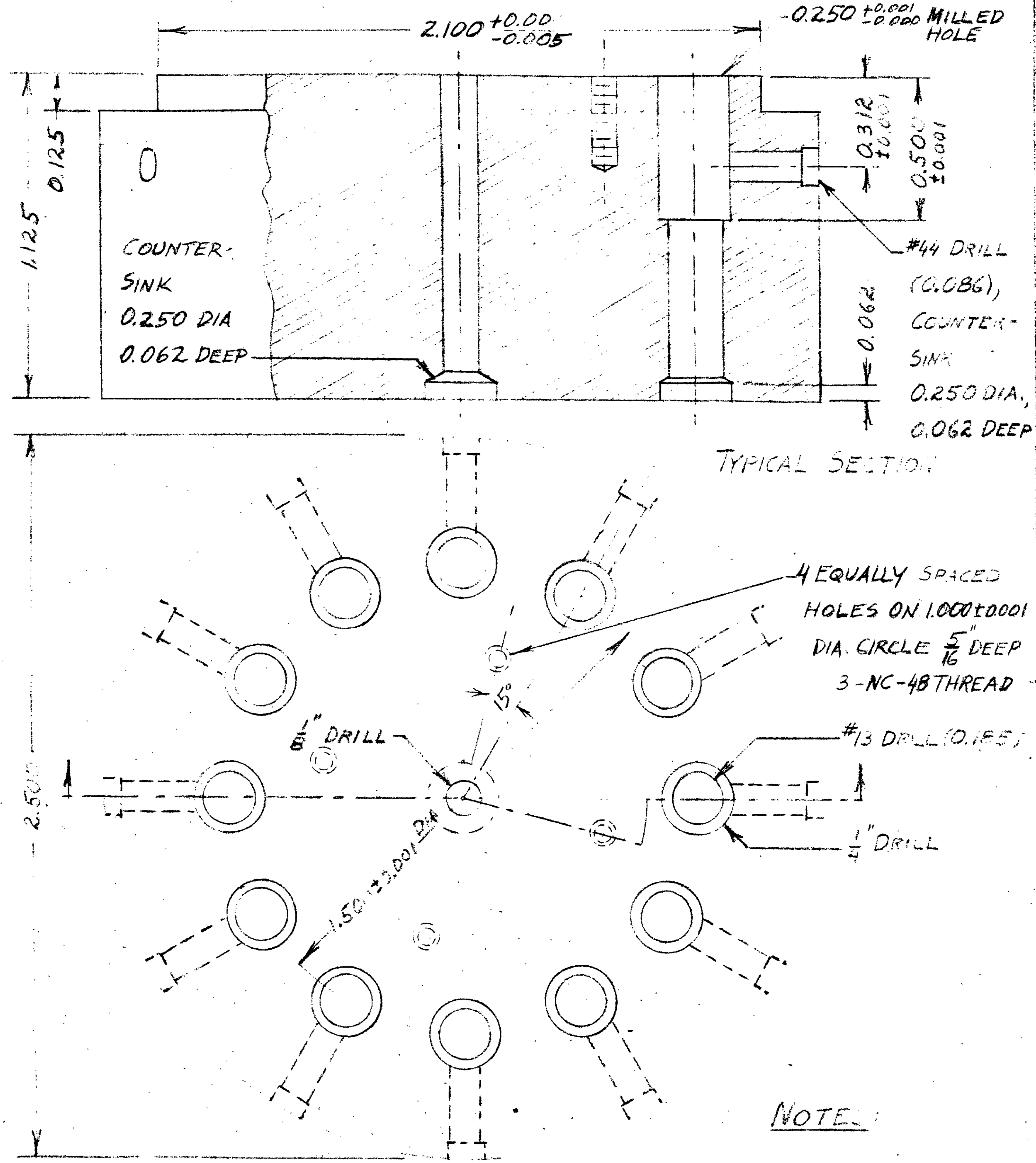

NOTE:

TOLERANCES ±0.003, EXCEPT AS NOTED
TWELVE SETS OF CIRCUMFERENTIAL HOLES REQ'D, EQUALLY SPACED
MATERIAL: BRASS

.I.T.	A.S.R.E. PROJECT	5
LOW DISTRIBUTOR BLOCK		
OUBLE SCALE		
PR. 17, 1957		
C.C.		

FIG. E.3

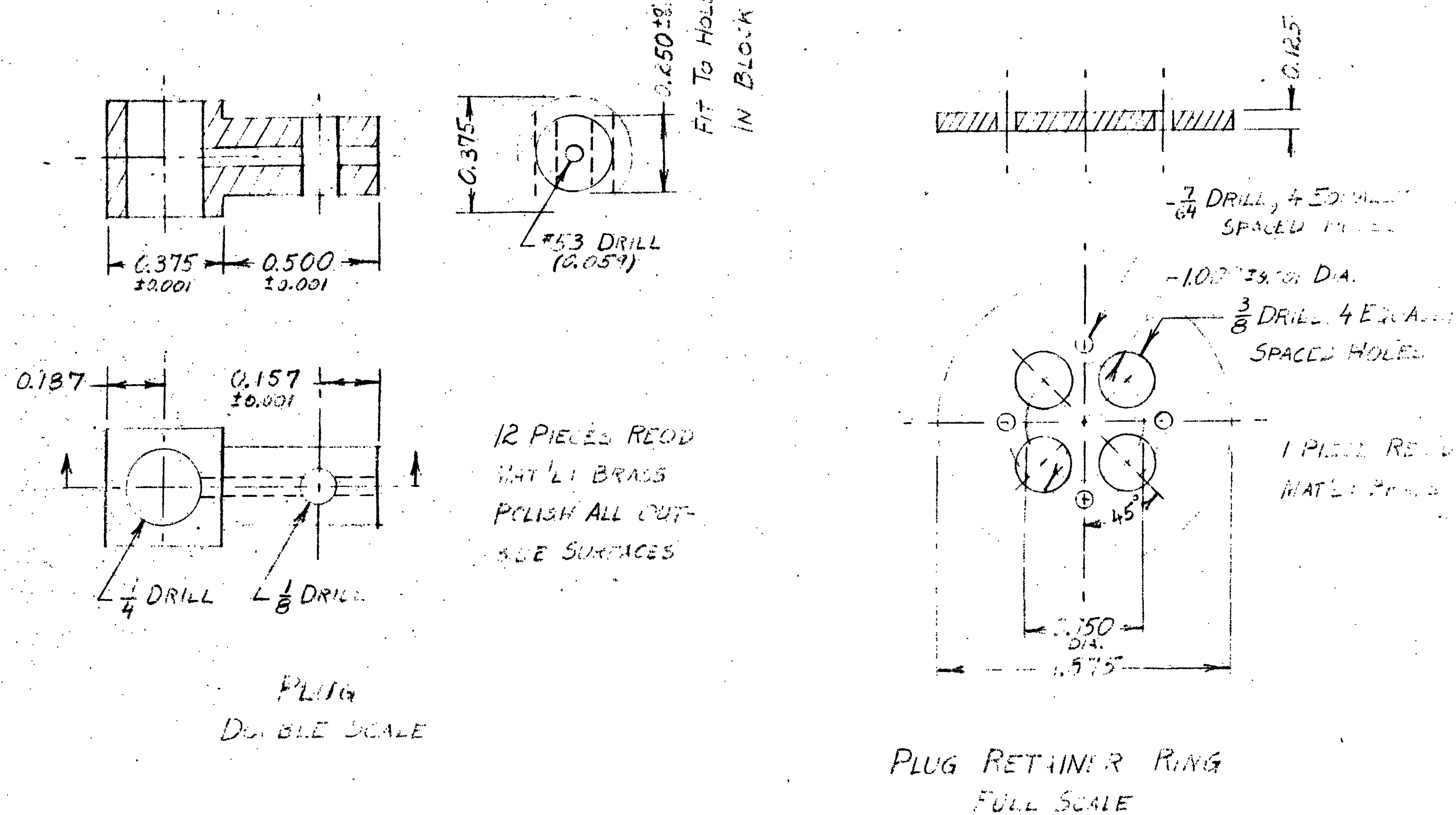

Note: Tolerances ±0.003, except as noted

M.I.T.	A.S.R.E. Project	6

Flow Distributor Parts
Scale As Noted
Apr. 18, 1957
J.C.C.

FIG. E.4

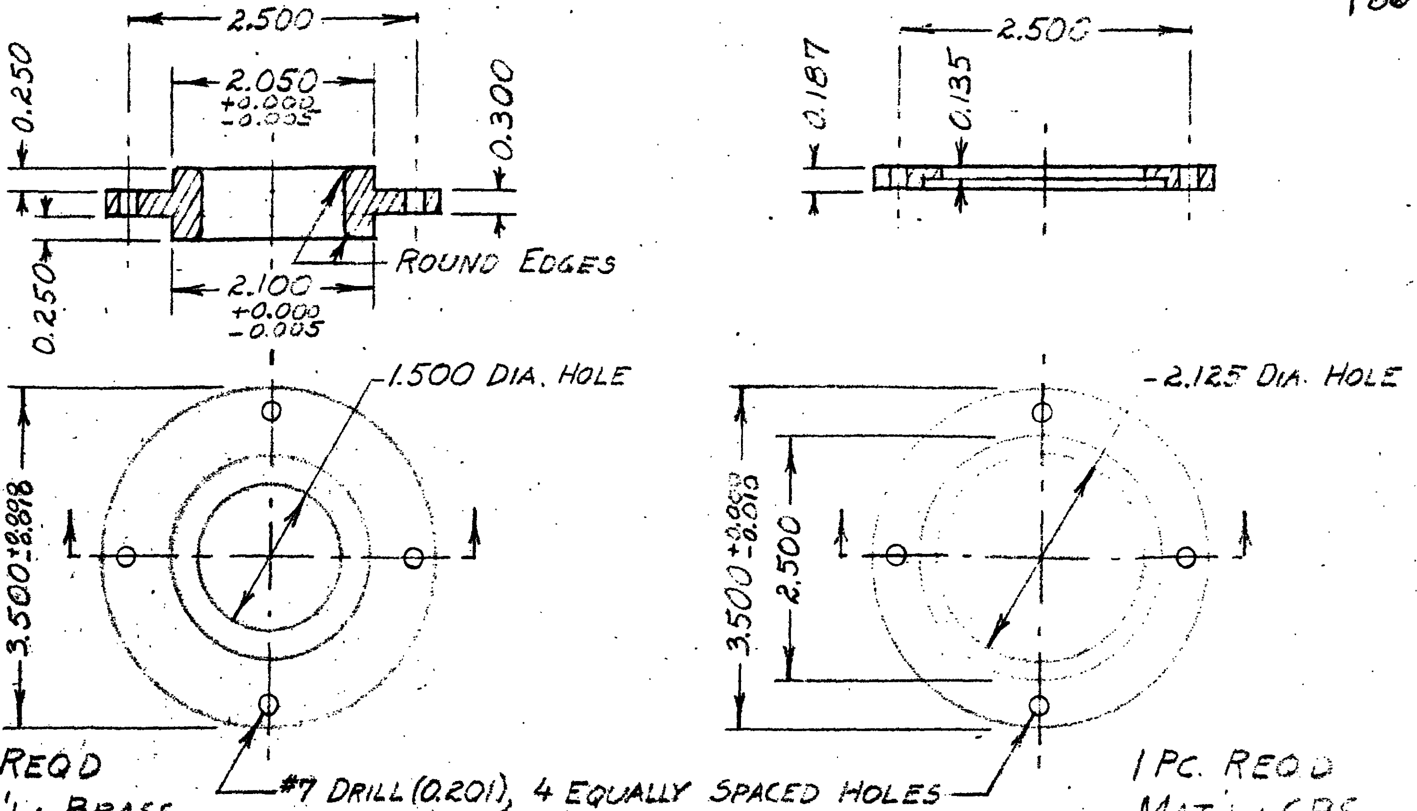

1 PC. REQ'D
MAT'L: BRASS

UPPER BRACKET
HALF SCALE

1 PC. REQ'D
MAT'L: C.R.S.

LOWER BRACKET
HALF SCALE

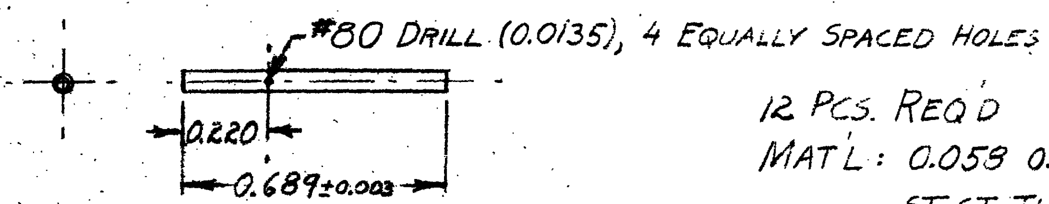

12 PCS. REQ'D
MAT'L: 0.058 O.D., 0.042 I.D.
ST. ST. TUBING

METERING TUBE
DOUBLE SCALE

NOTE:

TOLERANCES ±0.005, EXCEPT AS NOTED

M. I. T.	A. S. R. E. PROJECT	7

FLOW DISTRIBUTOR PARTS
SCALE AS NOTED
MAY 13, 1957
J. C. C.

FIG. E.5

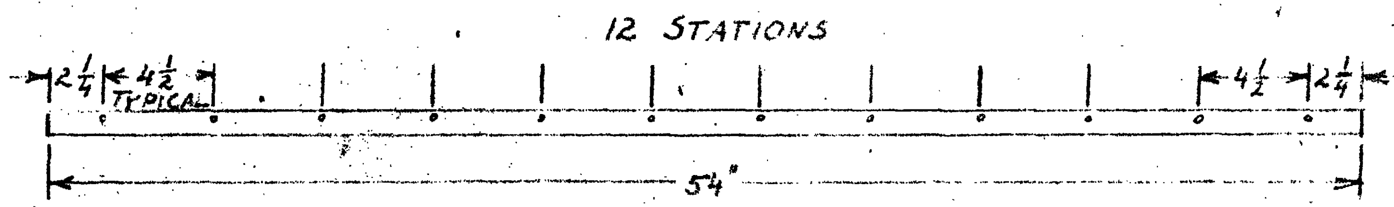

STATION LOCATIONS
SCALE: 1" = 8"

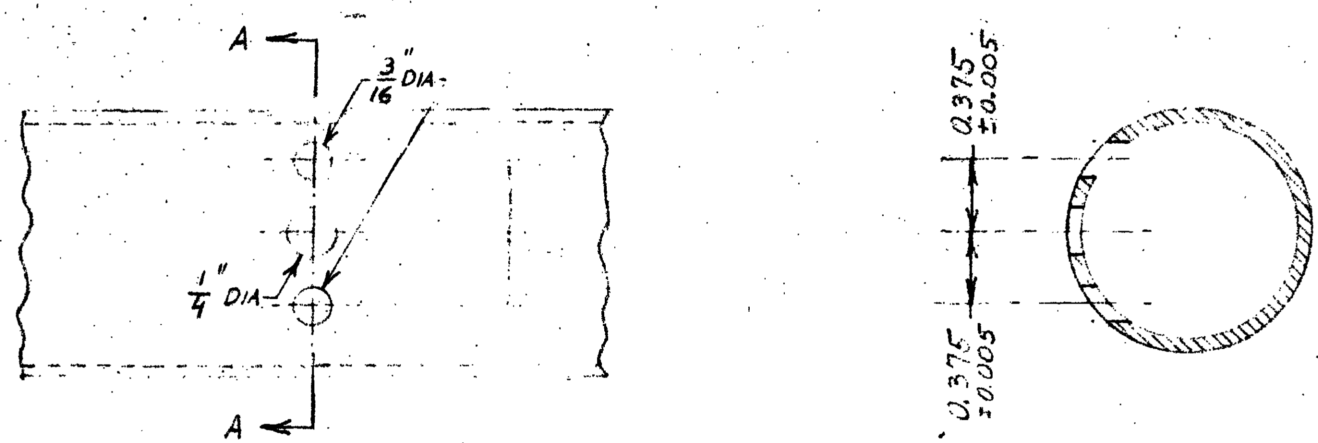

TYPICAL STATION
FULL SCALE

NOTES:
MATERIAL IS $1\frac{1}{8}$" I.D., $1\frac{1}{4}$" O.D. METHACRYLATE TUBING
THE HOLES OF ALL STATIONS SHOULD BE IN LINE WITHIN ±.005"

FIG. E.6

M. I. T.	A. S. R. E. PROJECT	8
TEST SECTION No. 1 SCALE AS NOTED SEPTEMBER 20, 1957 J. C. C.		

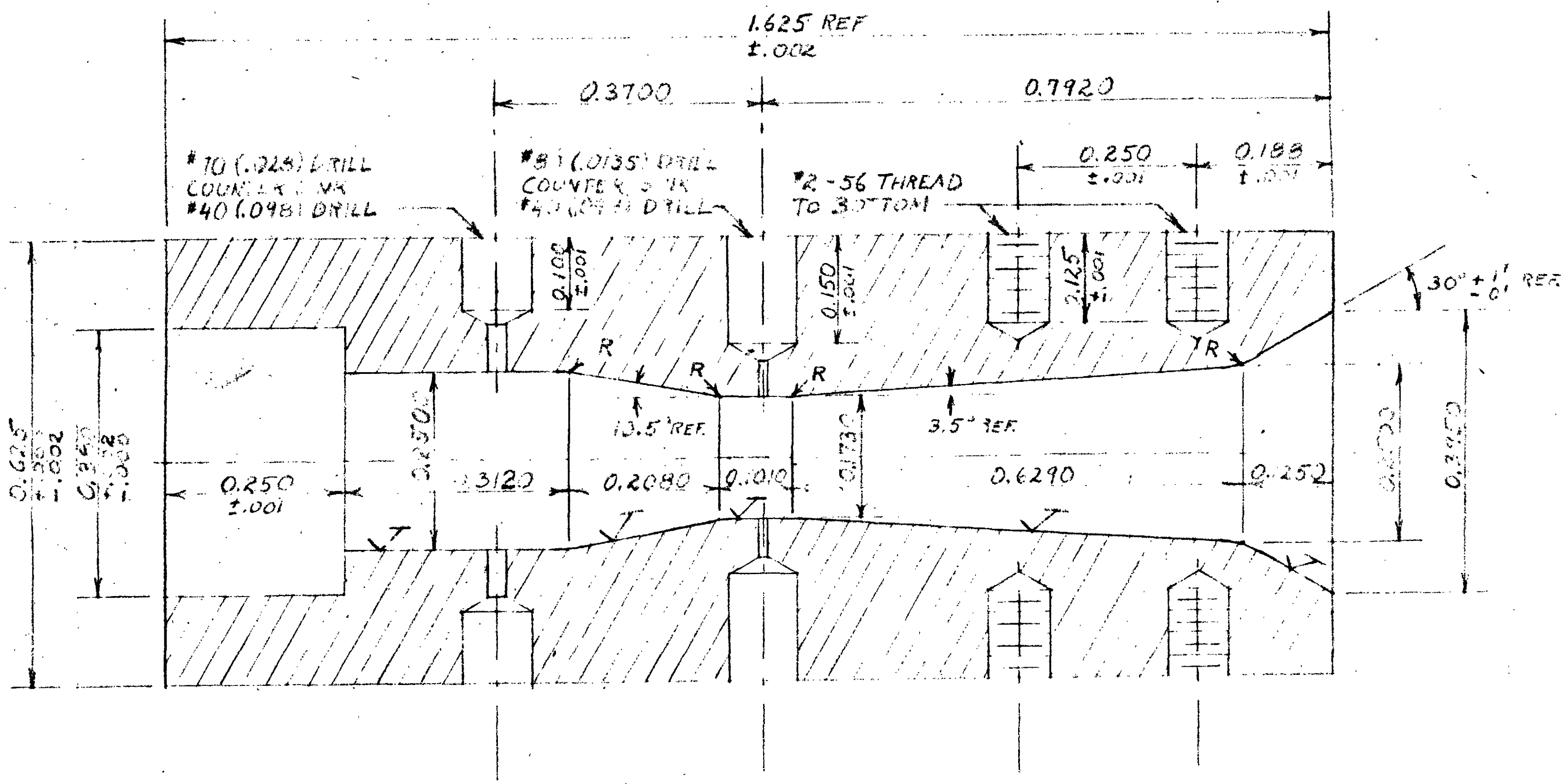

NOTES:

MATERIAL: BRASS

POLISH SURFACES MARKED

RADII, $R = \frac{1}{4}''$

TWO SETS OF 4 HOLES REQ'D AS SHOWN, 180° APART

ALL TOLERANCES ±.0005 EXCEPT AS NOTED

TWELVE PIECES REQ'D

FIG. E.7

M.I.T.	A.S.R.E PROJECT	9
SMALL VENTURI TUBE		
SCALE 4" = 1"		
OCTOBER 9, 1957		
J. C. C.		

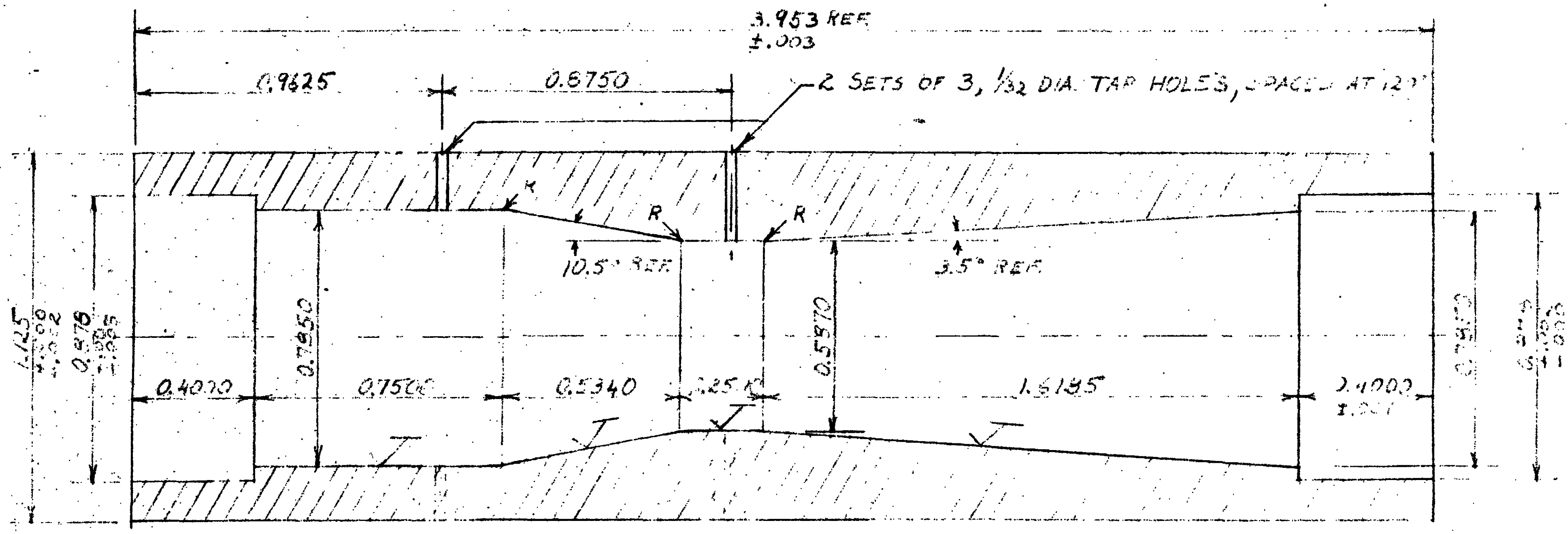

NOTES:

MATERIAL : BRASS

POLISH SURFACES MARKED ✓

RADII : R = 1/8

TOLERANCES ARE ±0.0005 EXCEPT AS NOTED

ONE PIECE REQ'D

M.I.T.	A.S.R.E. PROJECT	10

A - SUPPLY [illegible]

SCALE 2 : 1

OCTOBER 16, 1957

J.C.C.

FIG. E.8

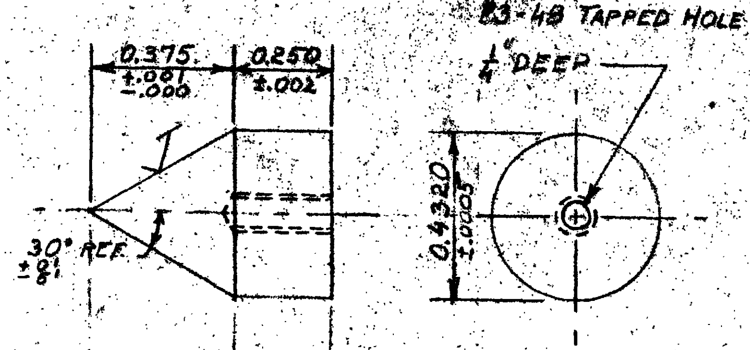

THROTTLING CONE
SCALE 2:1
12 PCS. REQ'D

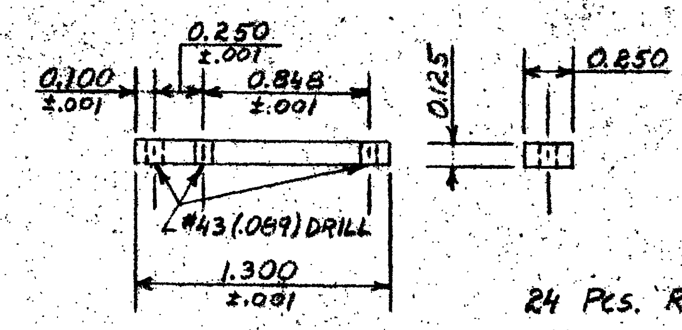

24 PCS. REQ'D

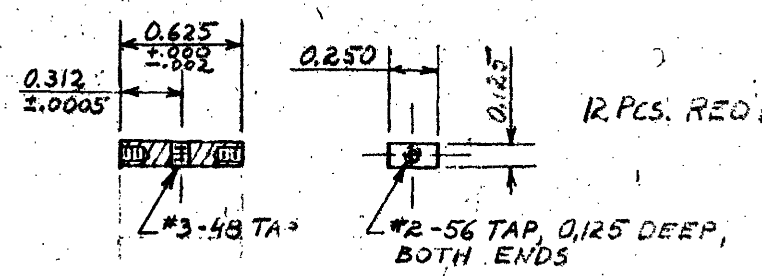

12 PCS. REQ'D

THROTTLE SUPPORTS
FULL SCALE

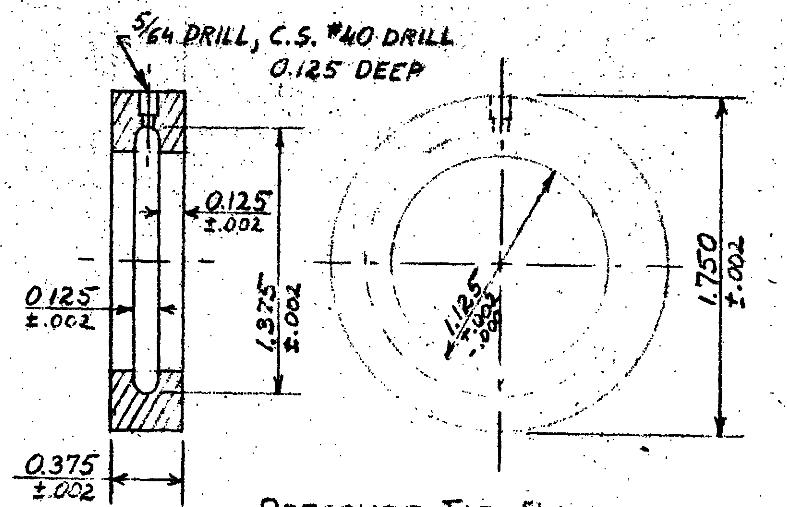

PRESSURE TAP RING
FULL SCALE
2 PCS. REQ'D

NOTES
MATERIAL : BRASS
POLISH SURFACE MARKED √

M. I. T.	A. S. R. E. PROJECT	11

VENTURI PARTS
SCALE AS NOTED
OCTOBER 17, 1957
J. C. C.

FIG. E.9

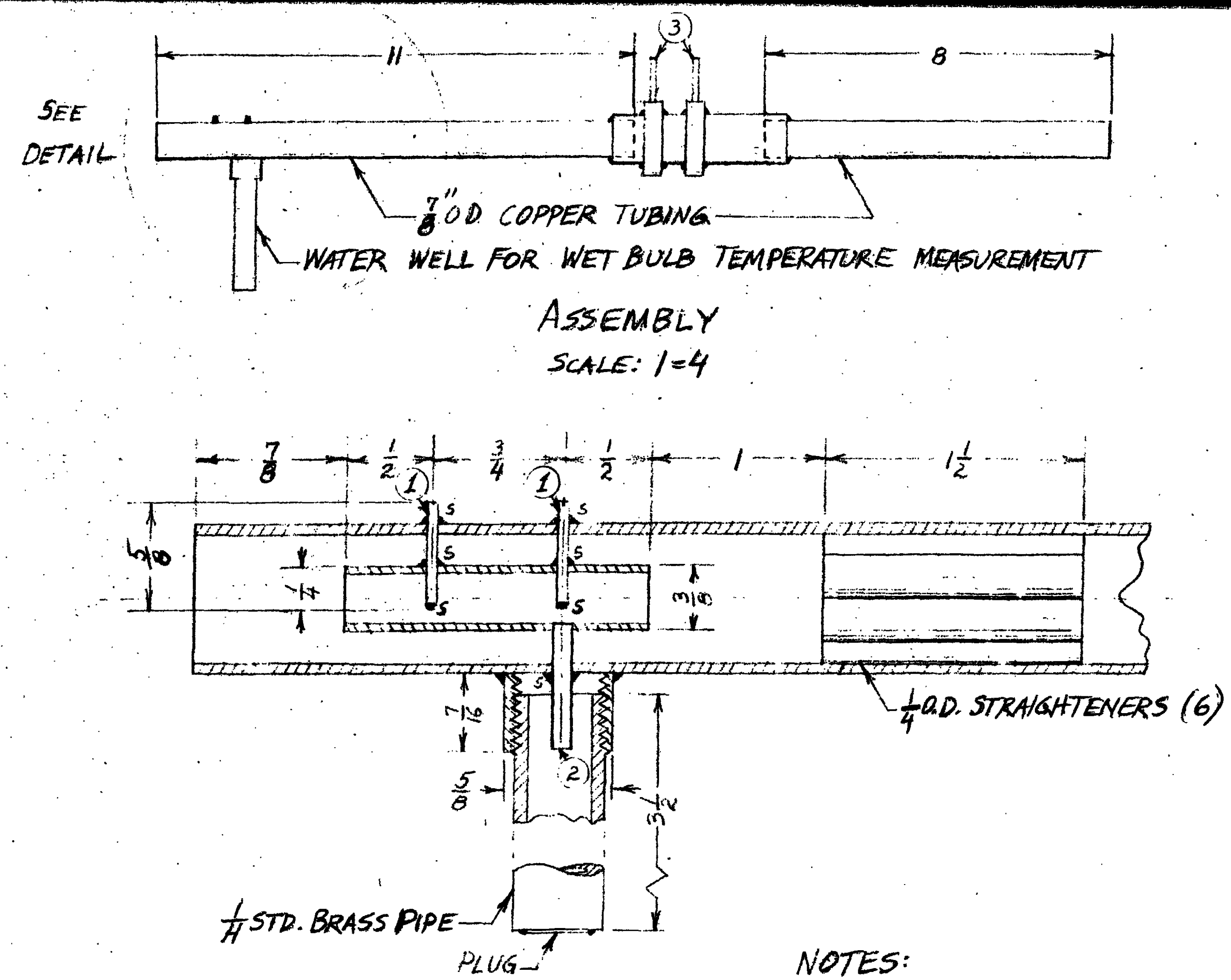

NOTES:

ALL MATERIALS ARE BRASS OR COPPER EXCEPT AS NOTED

INDICATES SOFT SOLDER

S INDICATES SILVER SOLDER

(1) 0.058 O.D. ST. ST. TUBING

(2) 0.109 O.D. ST. ST. TUBING

(3) 0.095 O.D. ST. ST. TUBING

M. I. T.	A.S.R.E. PROJECT	14

AIR SUPPLY VENTURI ASSEMBLY
SCALE AS SHOWN
DECEMBER 4, 1957
J. C. G.

FIG. E.10

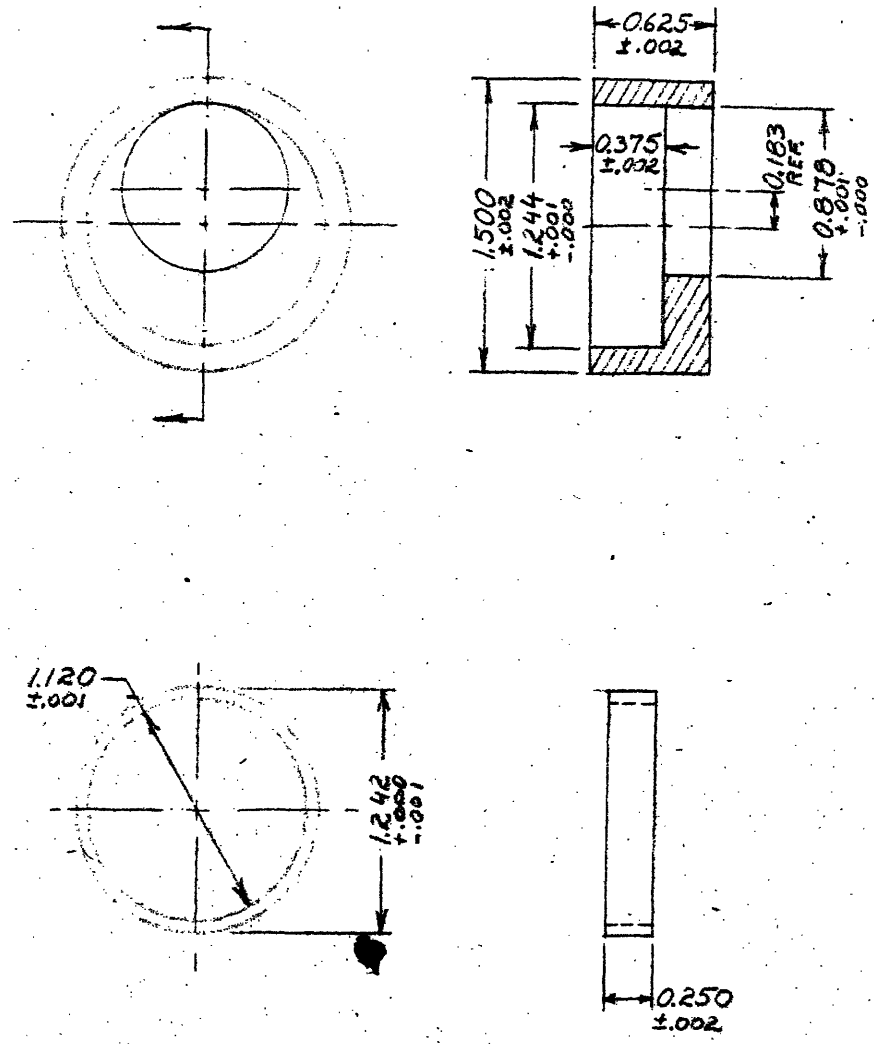

NOTES:

ALL MATERIALS ARE BRASS
ONE PIECE OF EACH REQ'D

M. I. T.	A.S.R.E. PROJECT	17

VENTURI ADAPTER
FULL SCALE
DECEMBER 13, 1957
J. C. C.

FIG. E.11

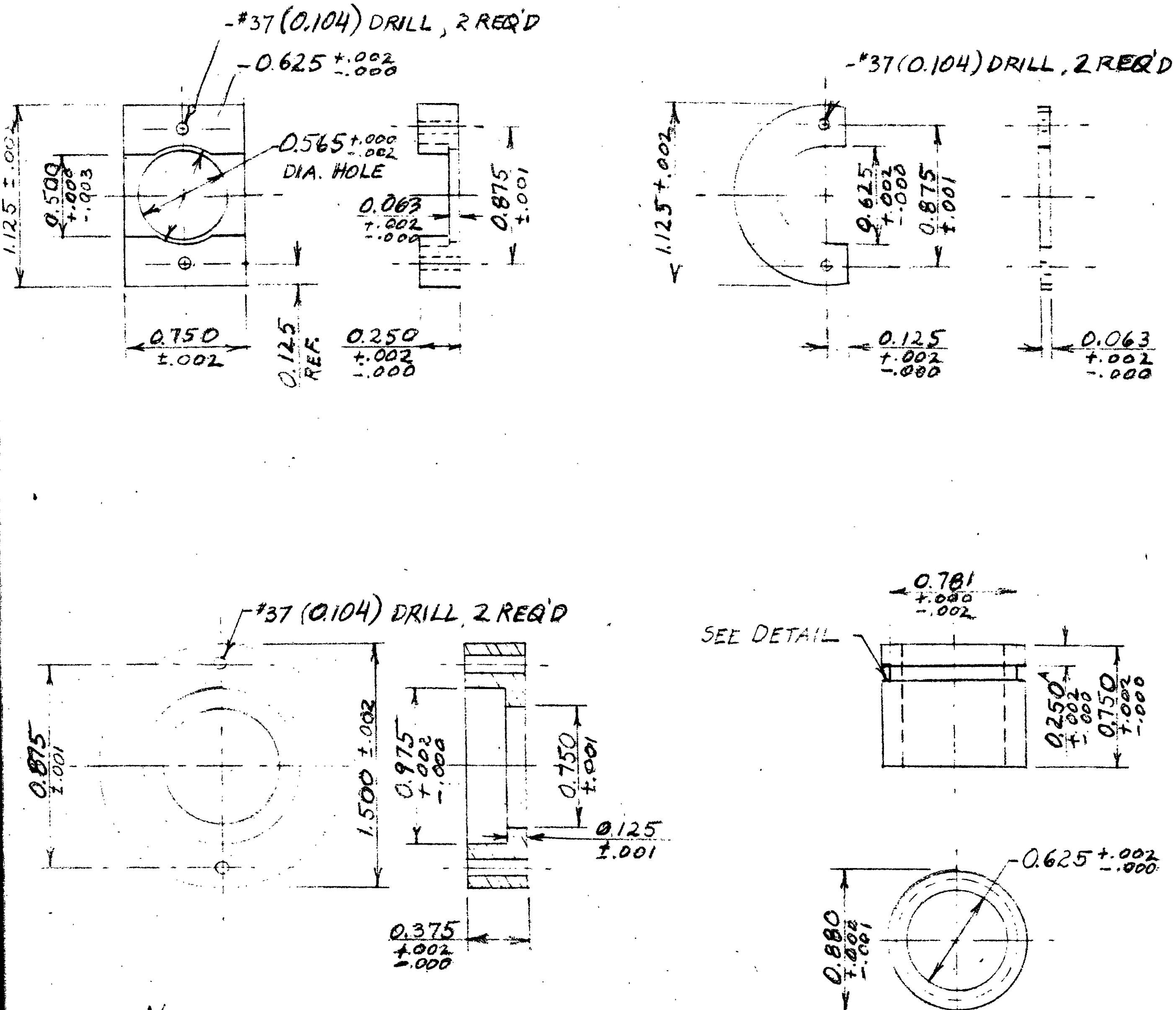

NOTES

MATERIAL BRASS

ONE OF EACH REQ'D

0^A DIMENSION NOT TO SCALE

GROOVE IS FOR PARKER NO 2-18 O-RING

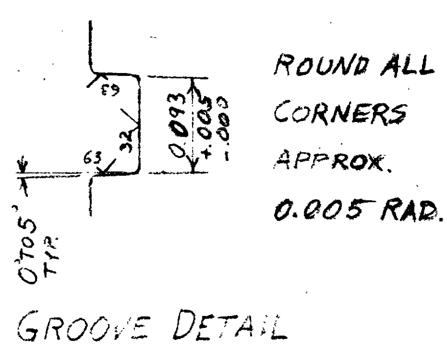

GROOVE DETAIL

M.I.T.	A.S.R.E. PROJECT	18

CONDENSER END FITTINGS
FULL SCALE
DECEMBER 9, 1958
J. C. C.

FIG. E.12

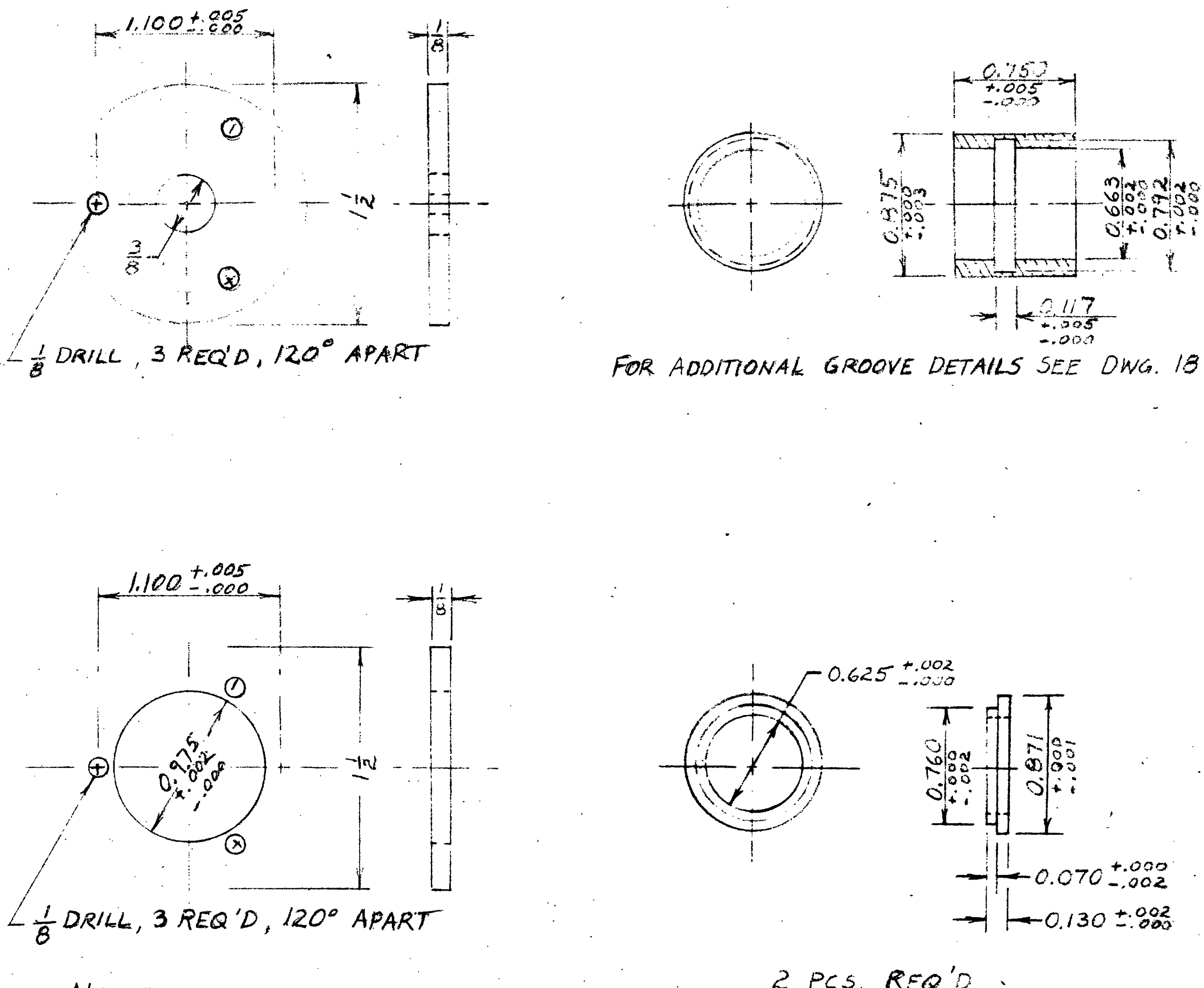

NOTES:

MATERIAL BRASS
ONE OF EACH REQ'D EXCEPT AS NOTED

M.I.T.	A.S.R.E. PROJECT	19

FIG. E.13